JOURNAL
OF
GEOMAGNETISM
AND
GEOELECTRICITY

VOL. V NO. 4

SOCIETY
OF
TERRESTRIAL MAGNETISM AND ELECTRICITY
OF
JAPAN

DEC. 1953
KYOTO

JOURNAL OF GEOMAGNETISM AND GEOELECTRICITY

EDITORIAL OFFICE: Society of Terrestrial Magnetism and Electricity of Japan, Geophysical Institute, Kyoto University, Kyoto, Japan

The fields of interest of this quarterly Journal are as follows:

Terrestrial Magnetism	Aurora and Night Sky
Atmospheric Electricity	The Ozone Layer
The Ionosphere	Physical States of the Upper Atmosphere
Radio Wave Propagation	Solar Phenomena relating to the above Subjects
Cosmic Rays	Electricity within the Earth

The text should be written in English, German or French. The price is provisionally set as 1 dollar per copy subject to change. We hope to exchange this Journal with periodical publications of any kind in the field of natural science.

The Editors

Ionospheric Variations Associated with Geomagnetic Disturbances*

I. Variations at Moderate Latitudes and the Equatorial Zone, and the Current System for the S_D Field

By Sadami MATSUSHITA

(Geophysical Institute, Kyoto University)

Abstract

Variations in the densities and heights of the ionospheric *Es* and *F*2 regions during magnetic storms are studied. At the moderate latitudes in *summer* solstice and at the equatorial zone, the disturbance variation of the *Es* in both local time (S_D) and storm time (*Dst*) is obtained by statistical examination, although the individual values of the *Es* data may not always be accurate.

The amplitude of the S_D variation of the *Es* at the moderate latitudes is about 0.5 Mc/s in frequency (15% for mean ionized density), and the phase of the variation seems to be *opposite* to that of the *F*2.

At the equatorial zone, the S_D variations of the *Es* and the *F*2 regions and the *Dst* variation for f_0F2 are rather peculiar for the phase, compared with those at the moderate latitudes. The geomagnetic S_D variation at this zone is also a little different from that in the moderate latitudes.

On the other hand, the current system for the S_D field is calculated by the dynamo theory, taking into consideration the anisotropic electrical-conductivity. A production mechanism of the *Es* is supposed, and the possibility that the ionospheric S_D variations are due to the effect of a drift by the earth's magnetic field and the electric field of the S_D current is discussed.

1. Introduction

The morphology of the *F*2 variations associated with magnetic disturbances has been studied by many researchers [1][2][3][4][5]. But these variations at the *E* region, which may be an important region for geomagnetic variations, are not yet obtained. For the Sporadic-*E* (*Es*) region, intense occurrence of the *Es* during geomagnetic storms or bay disturbances at the high latitudes is reported by a few

---

* Contribution to Geophysical Papers dedicated to Prof. M. Hasegawa on his sixtieth birthday

researchers [6][7][8]. At the moderate latitudes and the equatorial zone, however, results of the disturbance variations of the *Es* have been obtained by the present writer [9], from statistical examination, although the individual values of the *Es* data may not always be accurate. Further statistical studies are made in this report, and some peculiarities of the disturbance variations for the *Es* and *F*2 at the equatorial zone, and those of the geomagnetic variation, are described.

For the purpose of explaning the ionospheric disturbance variations in local time, the S_D current-system must be considered. The idealized current-system for

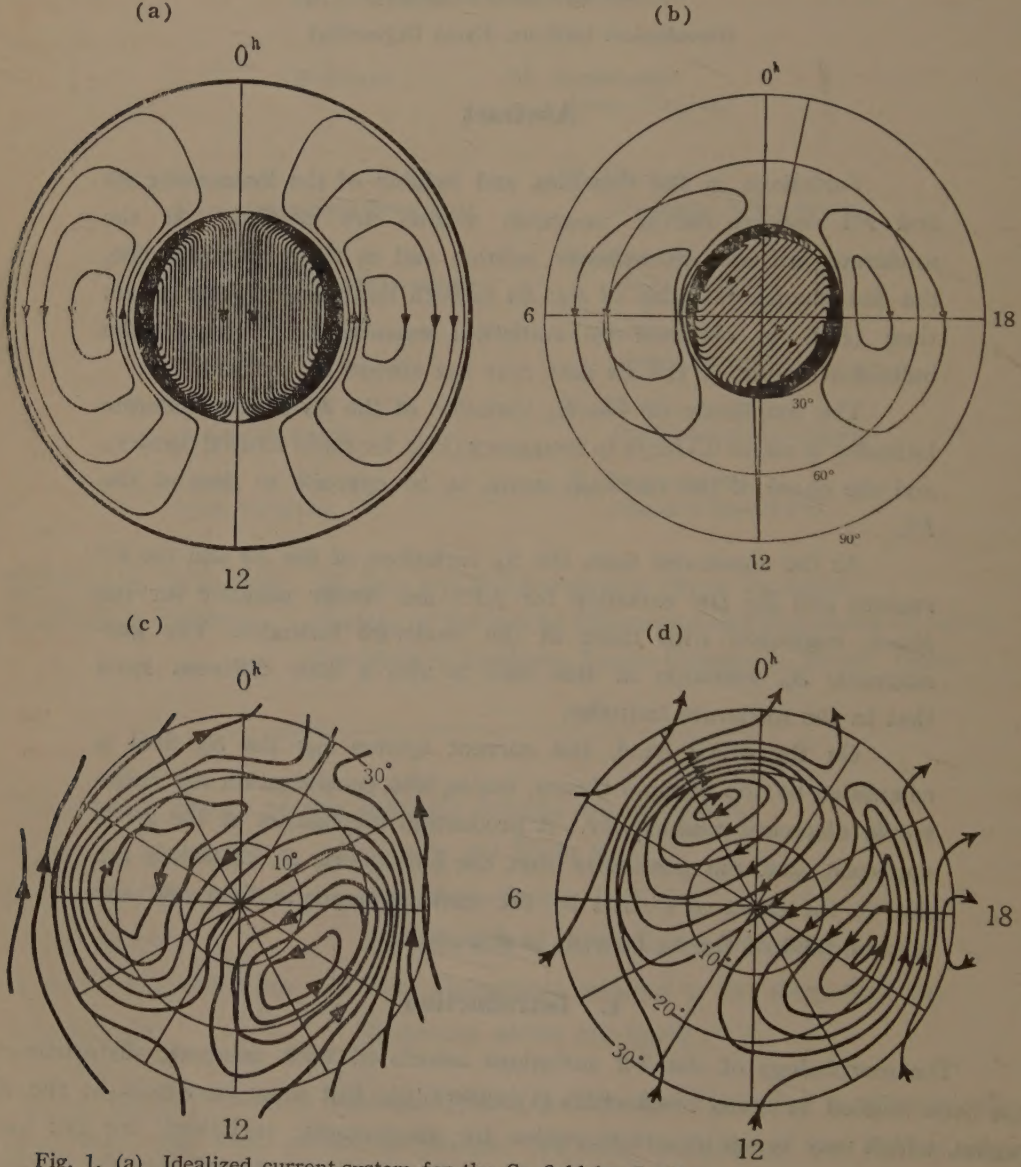

Fig. 1. (a) Idealized current-system for the S_D field by S. Chapman,
(b) S_D current-system for main phase of a storm according to E.H. Vestine,
(c) a mean current system for polar magnetic storms during the Second Polar Year obtained by M. Hasegawa, and
(d) by T. Nagata. (viewed from the north pole)

the S_D field was investigated from geomagnetic data by S. Chapman [10], and more detailed examinations were carried out by M. Hasegawa [11], E.H. Vestine [12], L. Harang [13], T. Nagata [14], and N. Fukushima [15]. The polar current of the S_D flows parallel with the meridian of local noon in Chapman's idealized current-system, but of about 09 h. in Hasegawa's and Vestine's systems, and of about 07.5 h. in Nagata's and Harang's, as will be seen in Fig. 1. In the current system of the geomagnetic bay, the polar current flows parallel with the meridian of about 07.5 h. according to H. Hatakeyama or H.C. Silsbee and E.H. Vestine, and of about 05 h. according to N. Fukushima. On the other hand, the current focuses closed at moderate latitudes may be situated on the meridian of 06 h. and 18 h. for the average S_D variation, though it is a little different for the bay disturbance.

As a theoretical approach to the S_D current-system, T. Rikitake [16] has tried to explain the current system by the dynamo theory making the assumption that the electrical conductivity at the auroral zone is higher than that in the other regions. A further investigation of the dynamo theory for the S_D current was carried out by N. Fukushima [17]. But both these cases were calculated postulating the isotropic electrical-conductivity, and cosequently the results of the calculation may not always be complete.

Theoretical studies of the ionospheric conductivity have been made by D.F. Martyn [18], T.G. Cowling [19], M. Hirono [20] and K. Maeda [21]. The dynamo theory, taking into consideration the anisotropic conductivity of the ionosphere investigated by them, seems to succeed in interpreting the S_q field. It has been reported by the present writer [9] that the S_D field is similarly calculated by the dynamo theory taking into consideration the anisotropic conductivity, under the assumption that the electrical conductivity at the auroral zone (and the polar cap) and at the equatorial zone is higher than that in the moderate region. A further investigation is carried out in this report.

It has recently been reported by D.F. Martyn [5] and K. Maeda [22] that the S_D variation of the $F2$ layer is due to the effect of a drift of the earth's magnetic field and the electric field of the S_D current-system. But both studies for the S_D current-system are not entirely adequate. In this report, a theoretical basis for my statistical results using Martyn and Maeda's principle is sought following a further examination of the S_D current-system.

2. The Disturbance Daily Variations (S_D)

2. 1. The S_D Variations of the Sporadic-E Region

In the case of studying the variation of the Es, the data may, unfortunately, not always be accurate, because the fEs value is influenced by incoming interference [23]. However, they are not without value. Accordingly, statistical examination must be conducted as far as it is possible.

The S_D variations of the Es have been studied statistically as follows: The

list of principal magnetic storms tabulated in the *Journal of Geophysical Research* and the report of magnetic storms issued from the Magnetic Observatory (Kakioka) have been prepared. Severe and moderately severe storms which were comparatively isolated, were selected from the lists and classified under three seasonal headings, Dec. solstice (Nov., Dec., Jan. and Feb.), equinox (Mar., April, Sept. and Oct.) and June solstice (May, June, July and Aug.). In order to derive the S_D variation from the data of hourly values, the *fEs* value for the hour nearest to that of the beginning of the selected magnetic storm was picked up, and the monthly median value subtracted from it (ΔfEs). The same process was followed for the succeeding 48 hrs. (i.e. 1st and 2nd 24 hrs.) and for the preceding 24 hrs. This process was repeated for each selected storm, and the result for each 24 hrs. was arranged and averaged in each local time. This method was applied to each season.

When the resulting ΔfEs for the selected storms with sudden commencement is arranged and averaged in the storm time, the storm-time variation can be obtained, as mentioned in Paragraph 3.

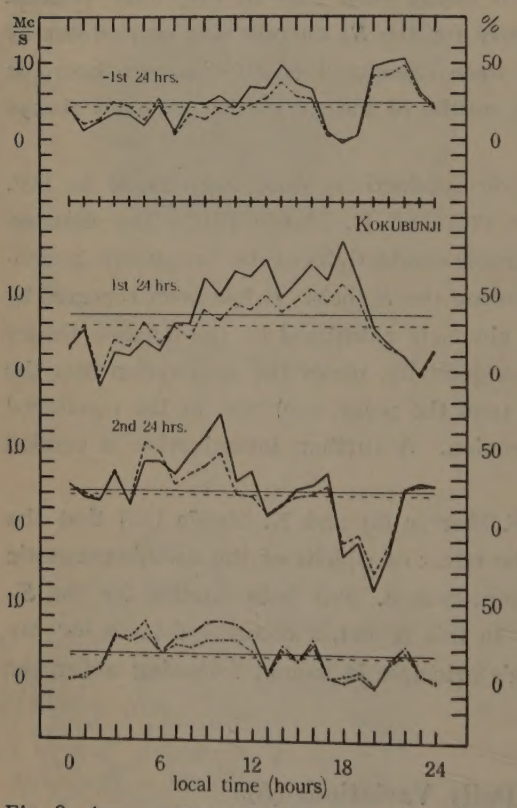

Fig. 2. Average disturbance variations of ΔfEs in local time at Kokubunji for 35 storms in the *summer* solstice of 1949–1952, for preceding 24 hrs. (top) and succeeding 48 hrs. (middle two) from the beginning of the magnetic storm. Bottom is ΔfEs average-variation during the ionospheric *F*2 storm at Kokubunji in the same period. The dotted line in percentage is for 200 ΔfEs/median *fEs*.

The average disturbance variations of ΔfEs in local time, from these treatments of data at Kokubunji (139°29.3′E, 35°42.4′N) for 35 storms in the *summer* solstice of 1949–1952, are shown in Fig. 2. In the same way, the variation for 200ΔfEs/median *fEs*, showing the density variation in percentage, is also plotted by the dotted line in the figure. It will be seen in the figure that the 1st and the 2nd 24 hrs. variations after the beginning of the magnetic storm have a greater diurnal variation than the preceding (–1st) 24 hrs. On the other hand, the ΔfEs variation in local time during the ionospheric *F*2 storm (i.e. the case in which the data are symbolized by the mark K) at Kokubunji in the same period is shown at the bottom of the figure. The amplitude is 0.3 Mc/s (10.7%) and the maximum occurs at 8.7 h. (7.9 h. for 200 ΔfEs/median *fEs*).

The S_D(*fEs*) variation at Brisbane (153.0°E, 27.5°S) for 17 storms in the

Dec. solstice of 1949–1952 was also examined in the same way (see Fig. 3). The phase and the amplitude for all these results are shown in Table 1, and these amplitudes during the storms are significant with a significance-level of less than 10%. It will be seen in the table that the amplitude of the variation is about 0.5 Mc/s (15% for mean ionized density), and the phase is *opposite* to the S_D variation of the $F2$ in summer.

Reliable $S_D(fEs)$ variation at the moderate latitudes for the winter months and equinoxes was difficult to obtain, because of few occurrences of the Es in these seasons.

As the $S_D(fEs)$ variation for the

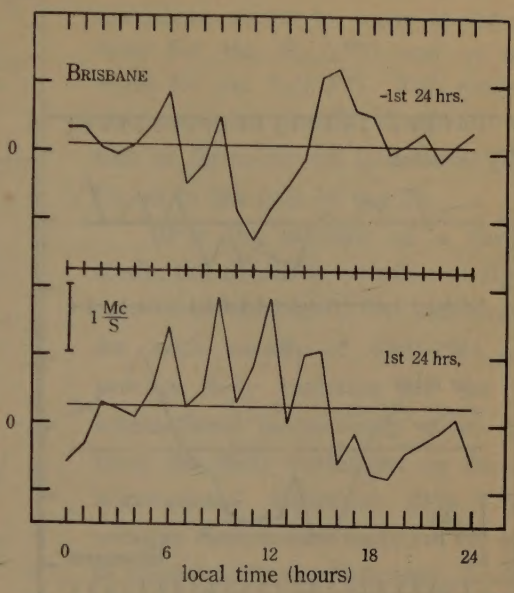

Fig. 3. Average disturbance variations of ΔfEs in local time at Brisbane for 17 storms in the summer solstice of 1949–1952.

Table 1.

Stations	Periods of data studied	Number of storms for the study	Data analized	24 hrs. before the beginning of the storms		1st 24 hrs. after the beginning of the storms		2nd 24 hrs. after the beginning of the storms	
				P_1	t_1	P_1	t_1	P_1	t_1
Kokubunji	June solstice, 1949–1952	35	ΔfEs	0.14 Mc/s	16.5 h.	0.65 Mc/s	14.0 h.	0.50 Mc/s	08.0 h.
,,	,,	,,	$\frac{200\,\Delta fEs}{\text{median } fEs}$	4.6 %	19.8 h.	19.0%	13.9 h.	19.6%	06.9 h.
Brisbane	Dec. solstice, 1949–1952	17	ΔfEs	0.32 Mc/s	21.0 h.	0.76 Mc/s	09.3 h.	0.42 Mc/s	13.3 h.
Huancayo	Jan. 1951–July 1952	28	ΔfEs	0.38 Mc/s	01.3 h.	1.00 Mc/s	23.3 h.	0.46 Mc/s	01.2 h.

equatorial zone, the variation at Huancayo (75.3°W, 12.0°S) for 28 storms through all seasons from Jan. 1951 to July 1952 is shown in Fig. 4, and the amplitude (it has a significance-level of less than 10% during the storm) and the phase will be seen in Table 1. The variation maximum in the equatorial zone seems to occur at earlier hour than that in the moderate latitudes.

Although the individual values of the $h'Es$ data may have less accuracy and the period examined was short, the $S_D(h'Es)$ variation at Brisbane was also studied in the same way, for 7 storms in the Dec. solstice, 1951–1953. The results are shown in Fig. 5, and the amplitude and the phase are compared in Table 2. The former during the storm have a significance-level of less than 15%, but the variation must be further examined for longer period data.

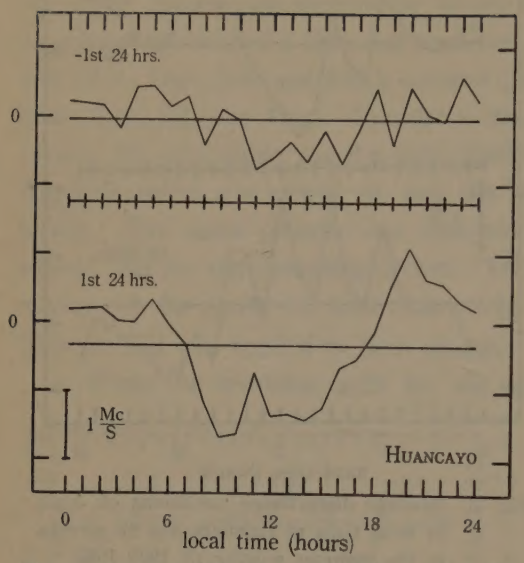

Fig. 4. Average disturbance variations of ΔfEs in local time at Huancayo for 28 storms in Jan. 1951–July 1952.

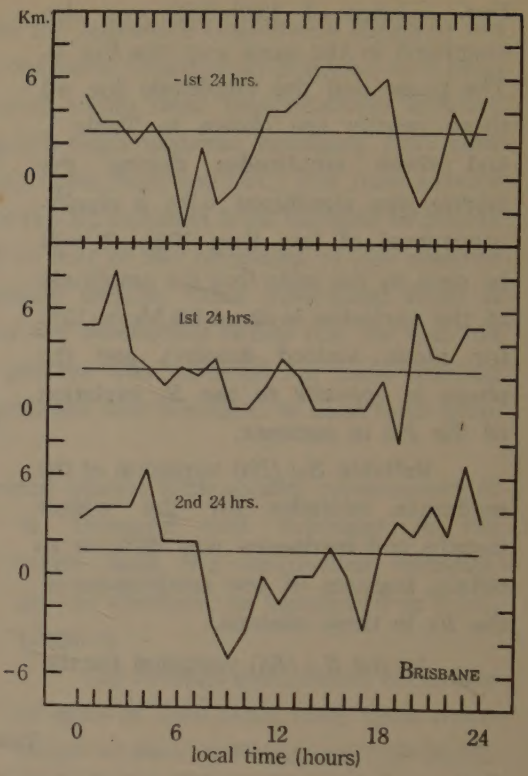

Fig. 5. Average disturbance variations of $\Delta h'Es$ in local time at Brisbane for 7 storms in the summer solstice 1951–1953.

Table 2. $S_D(h'Es)$ at Brisbane

24 hrs. before the beginning of the storms		1st 24 hrs. after the beginning of the storms		2nd 24 hrs. after the beginning of the storms	
P_1	t_1	P_1	t_1	P_1	t_1
1.9 Km.	16.5 h.	2.2 Km.	01.2 h.	3.3 Km.	23.9 h.

The $S_D(h'Es)$ variation for Huancayo was also investigated during the same period as the study of fEs. P_1 and t_1 for the 2nd 24 hrs. are 1.7 Km. and 5.6 h. respectively, although they seem to be less accurate, tested statistically.

2. 2. The S_D Variations of the $F2$ Layer at Huancayo

The S_D variations in the critical frequencies, $S_D(f_0F2)$, and in the minimum virtual heights, $S_D(h'F2)$, of the $F2$ layer at Huancayo are studied for the same period as the treatment of fEs, following the same method as in Paragraph 2.1. The $S_D(h'F2)$ variation is obvious, as will be seen in Fig. 6, though the $S_D(f_0F2)$ is not so clear. The amplitude and the phase of the variations are shown in Table 3, and the former for the $S_D(h'F2)$ has a significance-level of less than 10%. The variation

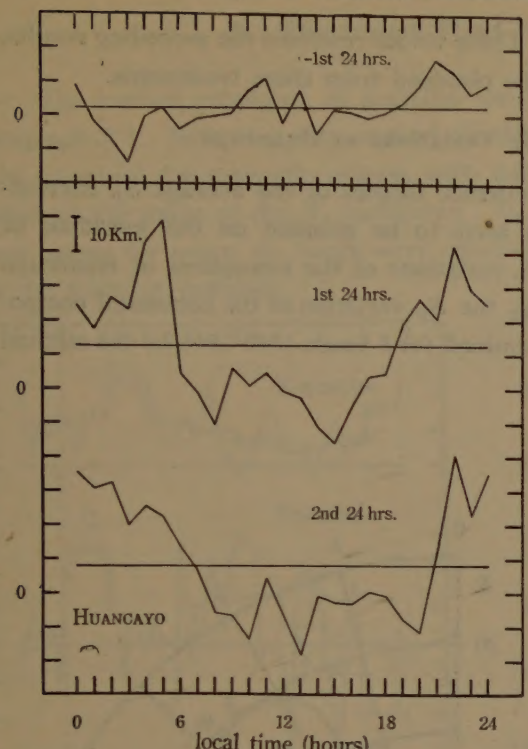

Fig. 6. Average disturbance variations of $\Delta h'F2$ in local time at Huancayo for 28 storms in Jan. 1951–July 1952.

maximum seems to occur in the day time for the $S_D(f_0F2)$ and at midnight for the $S_D(h'F2)$. This mode is also somewhat peculiar compared with that of the moderate latitudes [1][3][4][5], as in the case of the *Es*.

For the purpose of a further study, the $S_D(h'F2)$ variation at Huancayo was computed, by subtracting, for each month of 1940–1944, the average daily variation for the five international magnetically quiet days from the daily variations on the five international disturbed days. The average disturbance variation of $h'F2$ in local time during 1940–1944, obtained from this treatment, is shown in Fig. 7. a, and the harmonic results for each year and for each season are shown by the harmonic dial in Fig. 7.b. Taking the mean value of these harmonic results, the amplitude is 14.2 Km. and the

Table 3. $S_D(F2)$ at Huancayo

Data analized	24 hrs. before the beginning of the storms		1st 24 hrs. after the beginning of the storms		2nd 24 hrs. after the beginning of the storms	
	P_1	t_1	P_1	t_1	P_1	t_1
Δf_0F2	0.29 Mc/s	12.1 h.	0.35 Mc/s	14.2 h.	0.27 Mc/s	15.4 h.
$\Delta h'F2$	3.0 Km.	18.9 h.	20.0 Km.	00.8 h.	20.0 Km.	01.3 h.

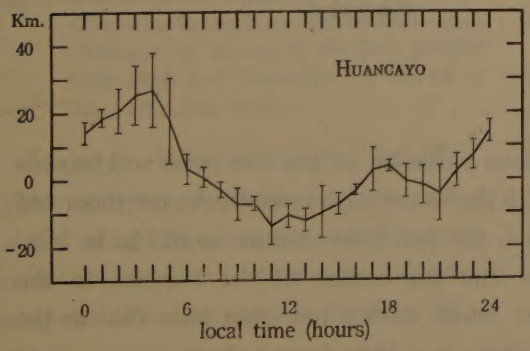

Fig. 7.a. Average disturbance variation of $\Delta h'F2$ in local time during 1940–1944 at Huancayo.

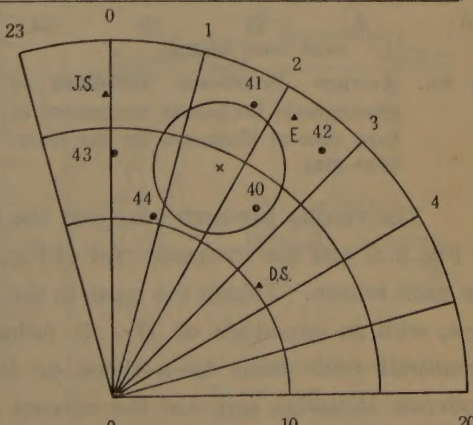

Fig. 7.b. Harmonic dial of the $S_D(h'F2)$ variation at Huancayo for each year of 1940–1944 and for each season (Dec. solstice, equinox and June solstice) during the period.

maximum occurs at 01.7 h. in local time. These values resemble the preceding results, but reliable $S_D(f_0F2)$ variation could not be obtained from these treatments.

2. 3. The Geomagnetic S_D Variations at Huancayo

As mentioned in Paragraph 1, the current focuses of the average S_D current-system enclosed in the moderate latitudes, seem to be situated on the meridian of 06 h. and 18 h. in local time. Since the S_D variations of the ionosphere at Huancayo differ from those in the moderate latitudes, the S_D variation of the horizontal component of geomagnetic variation was also examined for 5 years, 1940–1944, by the method mentioned in Paragraph 2. 2.

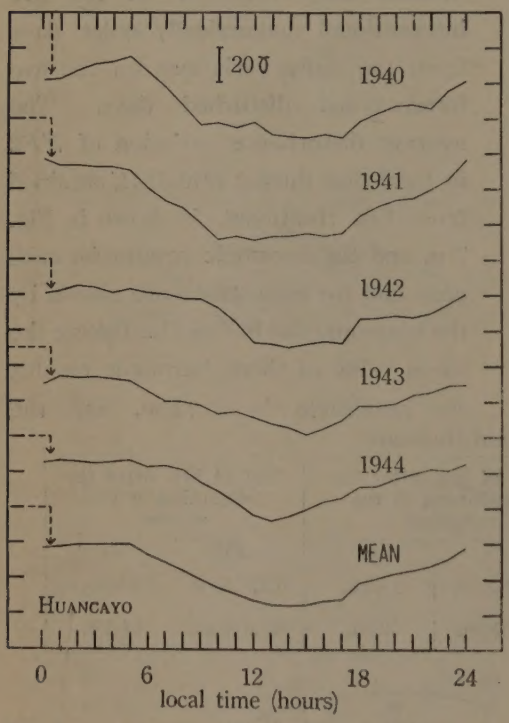

Fig. 8.a. Average disturbance variations of geomagnetic horizontal component in local time at Huancayo for five years, 1940–1944.

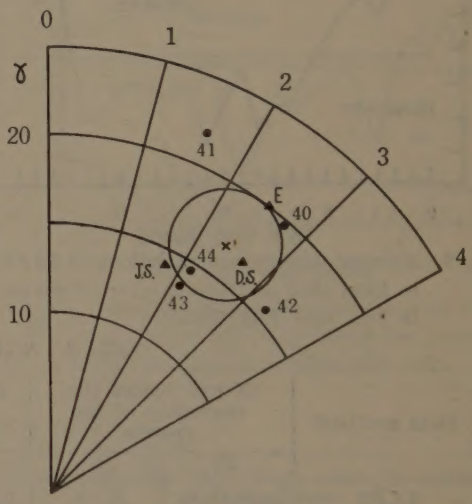

Fig. 8.b. Harmonic dial of the $S_D(H)$ variation at Huancayo for each year of 1940–1944 and for each season (Dec. solstice, equinox and June solstice) during the period.

The results for each year and the mean variation of the five years will be seen in Fig. 8. a, and the harmonic dial of Fig. 8. b shows the harmonic results for them and for each season. Taking the mean in the dial, the maximum occurs at 02.4 h. in local time, with an amplitude of 17γ. It follows that the center of the current in the equatorial zone shifts to a three or four hours earlier meridian than that in the moderate latitudes, and that the current density is a little larger there.

It may be concluded, accordingly, that the S_D variations at the equatorial zone, for the Es region, the $F2$ layer and geomagnetic variation, have some peculiarity compared with those in the moderate latitudes.

3. The Storm-Time Variations (*Dst*)

The method employed in deriving the *Dst* variations has been described in Paragraph 2.1. Following that method, the data at Kokubunji, Brisbane and Huancayo were examined for magnetic storms with sudden commencement during the same period as the study of the S_D variations. As the variation was somewhat irregular, mean values for every six hours were obtained (dividing a day into four periods) to see the mode of variation.

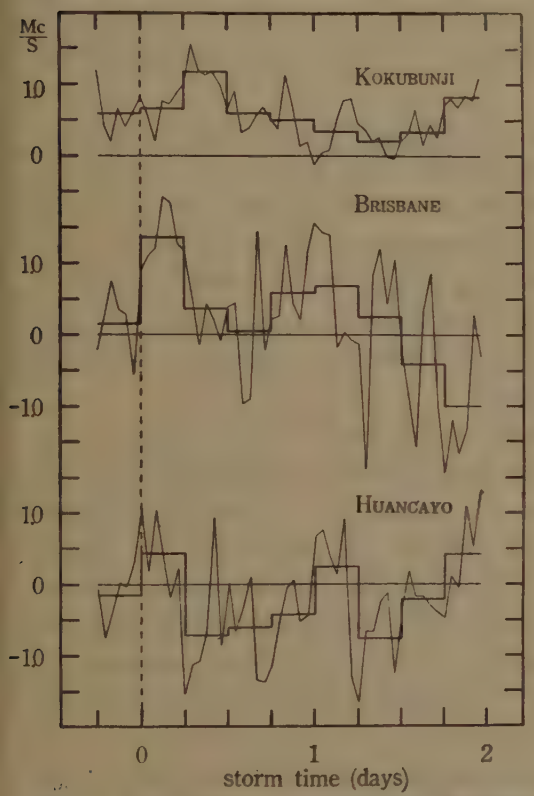

Fig. 9. The *Dst*(*fEs*) variations for Kokubunji (20 storms in the June solstice 1949–1952), Brisbane (9 storms in the Dec. solstice 1949–1952) and Huancayo (19 storms in Jan. 1951–July 1952).

From these studies for the *Dst* (*fEs*) variations at three stations, *fEs* seems to increase during several hours after the sudden commencement of magnetic storms, as will be seen in Fig. 9.

The *Dst*(*h'Es*) variations were also examined for Brisbane and Huancayo. A small increase of about 2 Km.

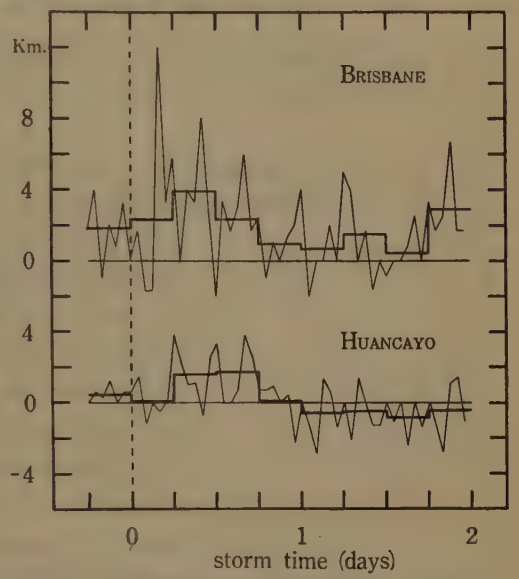

Fig. 10. The *Dst*(*h'Es*) variations for Brisbane (4 storms in the Dec. solstice of 1951–1953) and Huancayo (19 storms in Jan. 1951–July 1952).

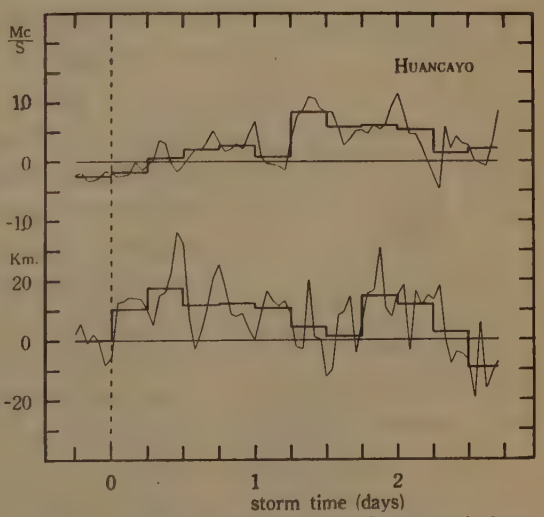

Fig. 11. The *Dst*(f^0F2) and *Dst*(*h'F2*) variations at Huancayo for 19 storms in Jan. 1951–July 1952.

on the 1st day seems to occur in both moderate and equatorial regions (see Fig. 10).

Fig. 11 shows the $Dst(f_0F2)$ and $Dst(h'F2)$ variations for Huancayo, and both f_0F2 and $h'F2$ seem to increase during magnetic storms. This result of the increase of f_0F2 is the reverse of that in the moderate latitudes in summer, and it coincides with the result obtained by Appleton [1], though the method used is not the same.

4. The Current System for the S_D-Field

4. 1. The Auroral Zone and the Equatorial Zone of the *Es* Region

For the purpose of calculating the current system for the S_D field, the position and breadth of the auroral and the equatorial zones must be decided at the outset.

It has been reported by the writer [24] that the world-wide distribution of the *fEs* may be divided into three groups: the auroral zone (intense at night), the equatorial zone (abnormally intense in the day time) and the intermediate zone (proportional to $\cos\chi$, where χ is the sun's zenith distance). From a further study for monthly median values of *fEs* (CRPL-F series report) at the auroral and the equatorial regions, the distributions in Fig. 12 and 13 were obtained.

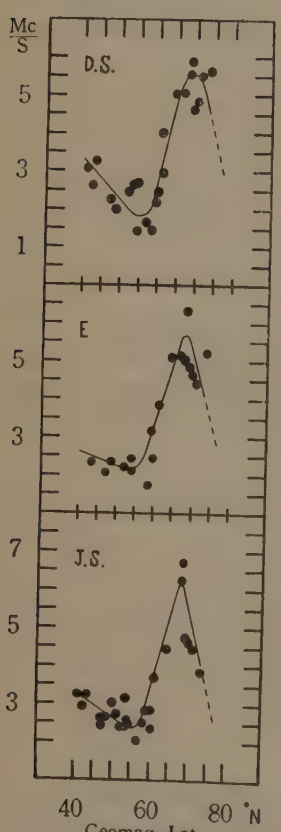

Fig. 12. *fEs* distributions for three seasons (Dec. solstice, equinox and June solstice, 1951) on geomagnetic latitudes at night. (They are vague in the day time.)

Fig. 12 shows *fEs* distributions for three seasons on geomagnetic latitudes at night (mean values from 22 h. to 02 h.). It increases at latitudes higher than about geomagnetic 60°N, and reaches the maximum at about 69°N. In still higher latitudes, the *fEs* decreases, and at Resolute Bay (geomagnetic 83°N) in Canada the *fEs* becomes very small. The auroral zone of the *Es* region, accordingly, may be considered as a region from 65°N to 75°N in the geomagnetic latitude.

As will be seen in Fig. 13, *fEs* in the day time (mean values from 09 h. to 15 h.) is abnormally large near the magnetic equator. This abnormality resembles the range distribution of daily variation of the horizontal magnetic force by J. Egedal [25] in the left part of the figure, and also resembles the range distribution observed at South America, India and Togoland by J. Egedal and A.A. Giesecke [26]. Accordingly, this intense *Es* zone may be due to the effect of the Hall drift [20] related to the intense eastward current flow that produces the large daily magnetic variation, as mentioned in Paragraph 5. As another peculiar character of the *Es* at this zone, *fEs* values at Huancayo may have some correlation with the sun-spot cycle (the correlation coefficient between them

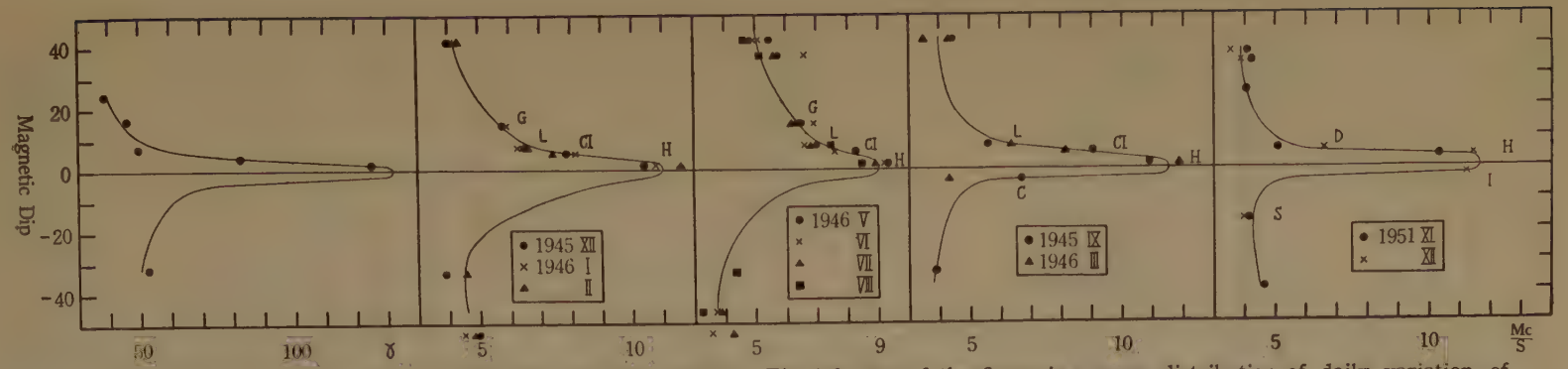

Fig. 13. *fEs* distributions in the day time near the magnetic equator. The left part of the figure is a range distribution of daily variation of the horizontal magnetic force (after J. Egedal). Names of stations are Guam, Leyte, Christmas Is., Djibouti, Huancayo, Ibadan Nigeria, Colombo and Singapore.

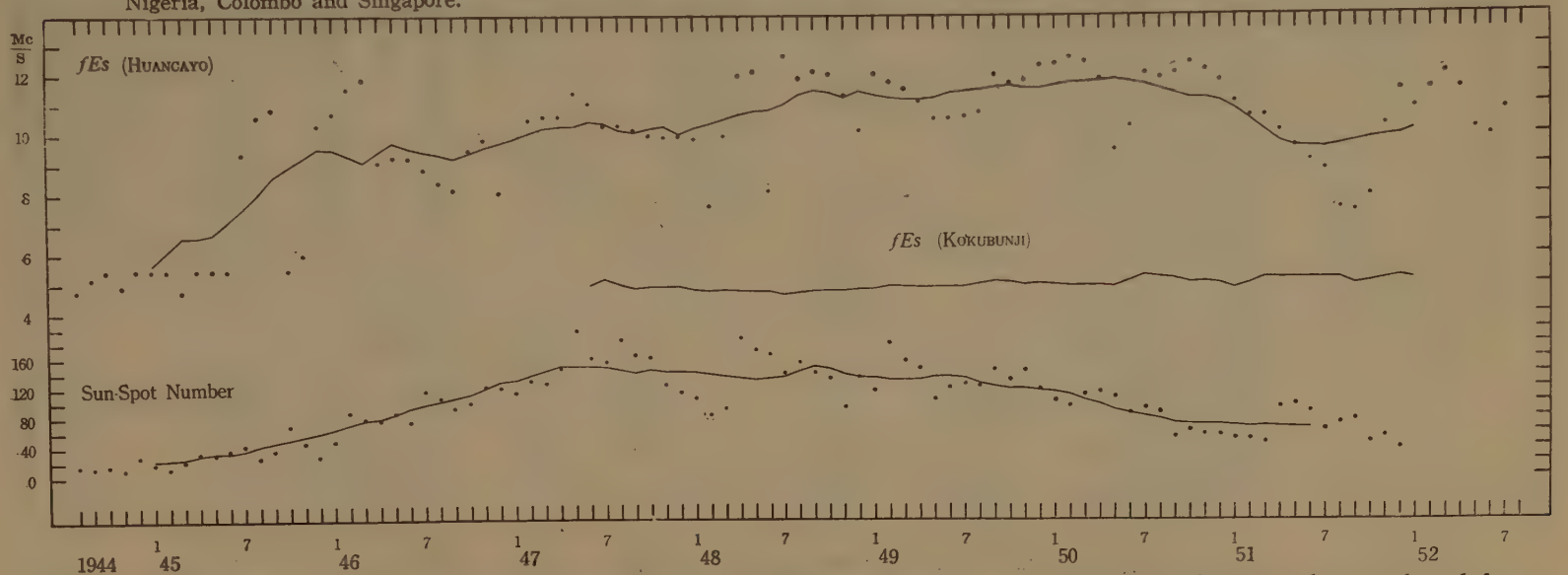

Fig. 14. Wolf's relative sun-spot number and *fEs* values in the day time for each month, Aug. 1944–July 1952. Average values overlapped for twelve months of the preceding five and the succeeding six months are shown by lines. The correlation coefficient between *fEs* at Huancayo and the sun-spot number is 0.66 for the overlapped means.

being 0.60 for monthly median values and 0.66 for overlapped means), as will be seen in Fig. 14, although such a relation can not be obtained in the moderate latitudes. Judging from these results, the equatorial zone may be considered as a region between 5° and −5° of the magnetic dip.

4. 2. The Dynamo Theory, Taking into Consideration the Anisotropic Electrical-Conductivity

The electrical conductivity of the ionosphere and—taking this into consideration—the dynamo theory have recently been studied by many researchers [18][19][20][21]. These results will be briefly introduced below.

Ions and electrons are distinguished respectively by the suffixes i and e. The mass, charge (in e.m.u.) and number density of r th molecules are denoted by m_r, e_r and n_r, respectively, and the charge of an electron is specially denoted by $-e$. Thus, the formulae for the ionospheric conductivities are expressed as follows:

the direct conductivity is $\sigma_0=e^2\sum_r(n_r/m_r\nu_r)$,

the Pedersen conductivity is $\sigma_1=e^2\sum_r(n_r/m_r)\{\nu_r/(\nu_r^2+\omega_r^2)\}$,

the Hall conductivity is $\sigma_2=(n_e e/H)\{\omega_e^2/(\nu_e^2+\omega_e^2)-\omega_i^2/(\nu_i^2+\omega_i^2)\}$,

and $\sigma_3\equiv\sigma_1+\sigma_2^2/\sigma_1$,

where, $\omega_r=e_rH/m_r$, H is the intensity of the geomagnetic field, and ν_r is the collisional frequency of the r th molecule with the neutral one.

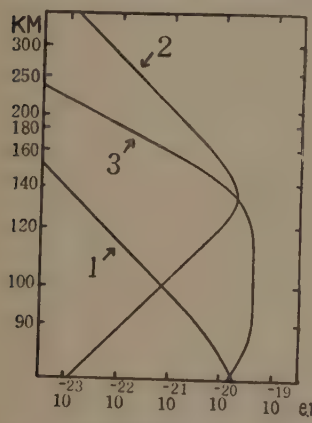

Fig. 15. Variations with height of σ_{1e}/n_e (1), σ_{1i}/n_i (2) and σ_2/n_e (3). (after M. Hirono)

It must be noticed that σ_2 is larger than σ_1 at 105±25 Km. (see Fig. 15) and that σ_3 has a pronounced sharp maximum at about 100 Km. level near the magnetic equator.

When x- and y-axes are taken respectively as southward and eastward directions, the effective direct conductivities are

$$\sigma_{xx}=\sigma_0\sigma_1/Q,$$
$$\sigma_{yy}=(\sigma_0\sigma_1\sin^2\phi+\sigma_1\sigma_3\cos^2\phi)/Q,$$

and the effective Hall conductivities are

$$\sigma_{xy}=-\sigma_{yx}=\sigma_0\sigma_2\sin\phi/Q,$$

where ϕ is the magnetic dip angle, and

$$Q=\sigma_0\sin^2\phi+\sigma_1\cos^2\phi.$$

If the permanent magnetism of the earth is assumed to be a dipole magnet with its axis coincident with the earth's rotation, then, the upward component of H, H_z, is

$$H_z=C\cos\theta,$$

where $C=-\frac{2}{3}$ (e.m.u.) and θ is co-latitude.

Now, we shall consider a case where the region between h_0, the bottom of the E region, and the upper height h_1, makes a uniform horizontal tidal oscillation with the velocity

potential

$$\psi = k_m^m P_m^m(\cos\theta)\sin(m\lambda + \alpha_m^m), \qquad (1)$$

where $P_m^m(\cos\theta)$ denotes associated Legendre function of Neumann, and λ is longitude reckoned from the midnight meridian, and k_m^m is taken to be positive. When $\boldsymbol{E}^i$ is the dynamo field ($=\boldsymbol{C}_0 \times \boldsymbol{H}$, and $\boldsymbol{C}_0$ is the mass velocity), and $\boldsymbol{E}^s$ is the electrostatic field having three components X (southward), Y (eastward) and Z (upward), then the electric field $\boldsymbol{E}$ is their sum.

First we shall consider all the regions except the zone near the equator. In the dynamotheoretical calculation, the effect of the region higher than h_1 must also be taken into consideration. This time we can use the same horizontal electrostatic field for both the lower ($h_0 \leq h \leq h_1$) and the upper ($h_1 \leq h \leq h_2$) region of the ionosphere, as a first approximation. The conductivity $\sum$ and current density $\boldsymbol{I}$ integrated with height for these upper and lower regions are

$$\sum_p{}^L = \int_{h_0}^{h_1} \sigma_p dz, \qquad \sum_p{}^U = \int_{h_1}^{h_2} \sigma_p dz, \qquad (p = xx, yy, xy, yx, 1, 2, 3)$$

$$\boldsymbol{I}^L = \int_{h_0}^{h_1} \boldsymbol{J} dz, \qquad \boldsymbol{I}^U = \int_{h_1}^{h_2} \boldsymbol{J} dz.$$

Then we get the following equations,

$$\left.\begin{aligned} I_x^L &= \sum_{xx}^L (vH_z + X) + \sum_{xy}^L (-uH_z + Y), \\ I_y^L &= \sum_{yx}^L (vH_z + X) + \sum_{yy}^L (-uH_z + Y), \end{aligned}\right\} \text{ for the lower region,}$$

$$\left.\begin{aligned} I_x^U &= \sum_{xx}^U \cdot X + \sum_{xy}^U \cdot Y, \\ I_y^U &= \sum_{yx}^U \cdot X + \sum_{yy}^U \cdot Y, \end{aligned}\right\} \text{ for the upper region,}$$

where R_0 is the radius of the conducting sphere, and $u = \partial\psi / R_0 \partial\theta$, $v = \partial\psi / R_0 \sin\theta \partial\lambda$. The components of $\boldsymbol{I} = \boldsymbol{I}^L + \boldsymbol{I}^U$ are accordingly,

$$\left.\begin{aligned} I_x &= \sum_{xx}^L \cdot vH_z + (\sum_{xx}^L + \sum_{xx}^U)X - \sum_{xy}^L \cdot uH_z + (\sum_{xy}^L + \sum_{xy}^U)Y, \\ I_y &= \sum_{yx}^L \cdot vH_z + (\sum_{yx}^L + \sum_{yx}^U)X - \sum_{yy}^L \cdot uH_z + (\sum_{yy}^L + \sum_{yy}^U)Y. \end{aligned}\right\} \qquad (2)$$

We adopt $h_1 = 180$ Km., $h_2 = 300$ Km. and take the gas density distribution assumed by M. Hirono [20] from rocket observations. Then, except near the equator,

$$\sum_{xx} = \sum_1 / \sin^2\phi, \qquad \sum_{yy} = \sum_1, \qquad \sum_{xy} = \sum_2 / \sin\phi, \qquad \text{for both regions,}$$

and

$$\sum_1{}^L = 6.86 \times 10^{-9}, \qquad \sum_2{}^L = 1.45 \times 10^{-8},$$
$$\sum_1{}^U = 1.59 \times 10^{-9} < \sum_1{}^L, \ \sum_2{}^L, \qquad \sum_2{}^U \simeq 0.$$

Therefore, we can neglect the terms containing $\sum_p{}^U$ in Eq. (2), and substitute 1 for the denominators $\sin\phi$ and $\sin^2\phi$, as the first approximation. Then we get from Eq. (2), for the northern hemisphere,

$$\left.\begin{aligned} I_x &= \Sigma_1(vH_z+X)+\Sigma_2(-uH_z+Y), \\ I_y &= -\Sigma_2(vH_z+X)+\Sigma_1(-uH_z+Y). \end{aligned}\right\} \qquad (3)$$

(Suffix L for Σ is neglected.)

When we introduce the current function R, $I_x=\partial R/R_0\sin\theta\cdot\partial\lambda$, $I_y=-\partial R/R_0\partial\theta$. From these equations and $\partial X/\partial\lambda-\partial(\sin\theta\cdot Y)/\partial\theta=0$ and also Eq. (3), X and Y are eliminated, giving

$$\frac{\partial^2 R}{\sin\theta\partial\lambda^2}+\frac{\partial}{\partial\theta}\left(\sin\theta\frac{\partial R}{\partial\theta}\right)=R_0K\left\{\frac{\partial(vH_z)}{\partial\lambda}+\frac{\partial(uH_z\sin\theta)}{\partial\theta}\right\},$$

where $K=\Sigma_1+(\Sigma_2)^2/\Sigma_1$. This equation is satisfied in the range $0\leq\theta\leq\theta_1$, and, from the statistical result mentioned in Paragraph 4. 1., $\theta_1=85°$ is adopted. The solution of this equation is

$$R=\frac{m}{(m+1)(2m+1)}Ck_m^mK\left[\left\{P_{m+1}^m+C_{m_1}\tan^m\frac{\theta}{2}\right\}\sin(m\lambda+\alpha_m^m)+C_{m_2}\tan^m\frac{\theta}{2}\cos(m\lambda+\alpha_m^m)\right],$$

where C_{m_1} and C_{m_2} are constants for each value of m. In the same way, we get the solution for the zone $85°\leq\theta\leq\pi$.

In the zone $85°<\theta<95°$, we can assume $H_z\simeq0$. Thus it follows that $\sigma_{xx}=\sigma_0$, $\sigma_{yy}\sim\sigma_3$, $\sigma_{xy}=0$. We take σ_{xx} as infinite because of $\sigma_0\gg\sigma_3$. Then $X=0$ or $\frac{\partial S}{\partial\theta}=0$, and we have

$$I_y=K_e\cdot Y, \qquad \text{where} \qquad K_e\sim\Sigma_3. \qquad (4)$$

Accordingly we get $\partial R/\partial\theta=K_e(\partial S/\sin\theta\partial\lambda)$. Electrostatic potential S is eliminated, giving $\frac{\partial}{\partial\theta}\left(\frac{\sin\theta}{K_e}\cdot\frac{\partial R}{\partial\theta}\right)=0$. On the assumption that K_e is independent of θ, the solution of this equation is

$$R=\frac{m}{(m+1)(2m+1)}Ck_m^mK\log\left(\tan\frac{\theta}{2}\right)\{C_{m_3}\sin(m\lambda+\alpha_m^m)+C_{m_4}\cos(m\lambda+\alpha_m^m)\},$$

where C_{m_3} and C_{m_4} are also constants.

The current function R_q for the S_q field is accordingly,

$$\left.\begin{aligned} &\text{in the zone } 0°\leq\theta\leq85°, \quad R_q=\frac{m}{(m+1)(2m+1)}Ck_m^mK\left[\left\{P_{m+1}^m+C_{m_1}\tan^m\frac{\theta}{2}\right\}\right. \\ &\qquad\left.\sin(m\lambda+\alpha_m^m)+C_{m_2}\tan^m\frac{\theta}{2}\cos(m\lambda+\alpha_m^m)\right], \\ &\text{in the zone } 85°<\theta<95°, \quad R_q=\frac{m}{(m+1)(2m+1)}Ck_m^mK\log\left(\tan\frac{\theta}{2}\right) \\ &\qquad\{C_{m_3}\sin(m\lambda+\alpha_m^m)+C_{m_4}\cos(m\lambda+\alpha_m^m)\}, \\ &\text{in the zone } 95°\leq\theta\leq180°, \quad R_q=\frac{m}{(m+1)(2m+1)}Ck_m^mK\left[\left\{P_{m+1}^m-C_{m_1}\tan^m\frac{\theta}{2}\right\}\right. \\ &\qquad\left.\sin(m\lambda+\alpha_m^m)-C_{m_2}\tan^m\frac{\theta}{2}\cos(m\lambda+\alpha_m^m)\right]. \end{aligned}\right\} \qquad (5)$$

Electrostatic components X and Y for each zone can be obtained from Eqs. (3), (4) and (5).

For $m=1$,

in the zone $0°\leqq\theta\leqq85°$,

$$X=\frac{Ck_1^1}{R_0}\left[\left\{-\frac{\cos\theta}{2}+\frac{1}{6}\frac{1}{1+\cos\theta}(C_1+\gamma C_2)\right\}\cos(\lambda+\alpha_1^1)+\left\{\frac{\gamma}{2}\cos2\theta+\frac{1}{6}\frac{1}{1+\cos\theta}(\gamma C_1-C_2)\right\}\sin(\lambda+\alpha_1^1)\right],$$

$$Y=\frac{Ck_1^1}{R_0}\left[\left\{\frac{1}{2}-\frac{1}{6}\frac{1}{1+\cos\theta}(C_1+\gamma C_2)\right\}\sin(\lambda+\alpha_1^1)+\left\{\frac{\gamma}{2}\cos\theta+\frac{1}{6}\frac{1}{1+\cos\theta}(\gamma C_1-C_2)\right\}\cos(\lambda+\alpha_1^1)\right],$$

in the zone $85°<\theta<95°$,

$$X=0,$$

$$Y=-\frac{1}{6}\frac{Ck_1^1}{R_0}\frac{K}{K_e}\operatorname{cosec}\theta\{C_3\sin(\lambda+\alpha_1^1)+C_4\cos(\lambda+\alpha_1^1)\},$$

in the zone $95°\leqq\theta\leqq180°$, they are obtained in the same way, where $\gamma=\Sigma_2/\Sigma_1$.

For $m=2$,

in the zone $0°\leqq\theta\leqq85°$,

$$X=\frac{Ck_2^2}{R_0}\left[\left\{-\sin2\theta+\frac{4}{15}\frac{\sin\theta}{(1+\cos\theta)^2}(C_1+\gamma C_2)\right\}\cos(2\lambda+\alpha_2^2)+\left\{2\gamma\sin\theta(3\cos^2\theta-1)+\frac{4}{15}\frac{\sin\theta}{(1+\cos\theta)^2}(\gamma C_1-C_2)\right\}\sin(2\lambda+\alpha_2^2)\right],$$

$$Y=\frac{Ck_2^2}{R_0}\left[\left\{2\sin\theta-\frac{4}{15}\frac{\sin\theta}{(1+\cos\theta)^2}(C_1+\gamma C_2)\right\}\sin(2\lambda+\alpha_2^2)+\left\{2\gamma\sin2\theta+\frac{4}{15}\frac{\sin\theta}{(1+\cos\theta)^2}(\gamma C_1-C_2)\right\}\cos(2\lambda+\alpha_2^2)\right],$$

in the zone $85°<\theta<95°$,

$$X=0,$$

$$Y=-\frac{2}{15}\frac{Ck_2^2}{R_0}\frac{K}{K_e}\operatorname{cosec}\theta\left\{C_3\sin(2\lambda+\alpha_2^2)+C_4\cos(2\lambda+\alpha_2^2)\right\}.$$

The constants C_1, C_2, C_3 and C_4, in the current functions and the electrostatic components, are determined from the continuity of the normal component of the current and the tangential component of the electric field along the boundary. They are as follows, assuming $K_e=2K$,

for $m=1$,

$$\left.\begin{aligned}&C_1=(0.0226-0.0006\gamma^2)/\Gamma_1, \quad C_2=0.0073\gamma/\Gamma_1,\\&C_3=-0.5134/\Gamma_1, \quad C_4=-0.0765\gamma/\Gamma_1,\end{aligned}\right\}\tag{6}$$

where $\Gamma_1=0.0929+0.0021\gamma^2$,

for $m=2$,

$$\left.\begin{aligned}&C_1=(1.0726-0.0967\gamma^2)/\Gamma_2, \quad C_2=0.6510\gamma/\Gamma_2,\\&C_3=-24.152/\Gamma_2, \quad C_4=-6.254\gamma/\Gamma_2,\end{aligned}\right\}\tag{7}$$

where $\Gamma_2=0.9321+0.0625\gamma^2$.

4. 3. The S_D Current-System by the Dynamo Theory, Taking into Consideration the Anisotropic Electrical-Conductivity

The S_D current-system may be calculated as follows by the dynamo theory, assuming that the electrical conductivity at the auroral zone (and the polar cap) is higher than that in the moderate latitudes.

As will be seen in Fig. 16, the electrically conductive layer of radius R_0 is divided into seven parts, which are founded on the statistical results obtained in Paragraph 4. 1. The height-integrated effective-conductivity in each region is assumed as follows:

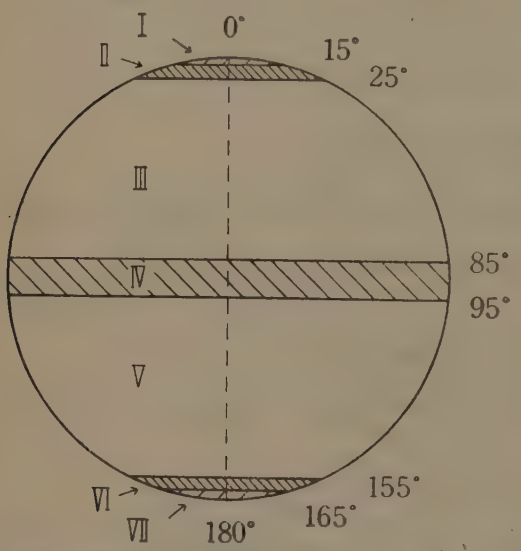

Fig. 16. Division of zones I, II, III, IV, V, VI and VII.

zone I, northern polar cap,
$0° \leq \theta < 15°$, conductivity AK,
zone II, northern auroral zone,
$15° \leq \theta \leq 25°$, conductivity BK,
zone III, northern middle zone,
$25° < \theta \leq 85°$, conductivity K,
zone IV, equatorial zone,
$85° < \theta < 95°$, conductivity $2K$,
zone V, southern middle zone,
$95° \leq \theta < 155°$, conductivity K,
zone VI, southern auroral zone,
$155° \leq \theta \leq 165°$, conductivity BK,
zone VII, southern polar cap,
$165° < \theta \leq 180°$, conductivity AK,

where θ is colatitude, A and B are constants larger than unity and $K=\sum_1+(\sum_2)^2/\sum_1$.

At about 100 Km. level, σ_2 is much larger than σ_1, as already mentioned in the preceding paragraph (see Fig. 15). Accordingly, in consideration of the increase of the conductivity at the auroral zone (and the polar cap), it may be assumed that only $\sum_2$ increases, and $\sum_1$ does not change. Then, the height-integrated Hall conductivity at the polar cap and the auroral zone may be $A'\sum_2$ and $B'\sum_2$ respectively, where A' and B' are constant. In the preceding paragraph, we put $\sum_2/\sum_1$ as γ, and now the ratio at the auroral zone becomes $B'\gamma$, and the ratio at the polar cap $A'\gamma$. It may be estimated, accordingly, that the height-integrated effective-conductivity at the auroral zone has the relation

$$BK=B\{\sum_1+(\sum_2)^2/\sum_1\}$$
$$=\sum_1\{1+(B'\gamma)^2\}. \qquad \text{(similarly for } A \text{ and } A')$$

Now, we can obtain the equations of the current functions and electrostatic fields at each zone, for the velocity potential ψ of Eq. (1), following the same principle as in Paragraph 4. 2. The current functions are

in zone I,

$$R=\frac{m}{(m+1)(2m+1)}Ck_m^mAK\left[\left\{P_{m+1}^m+C_{m_1}\tan^m\frac{\theta}{2}\right\}\sin(m\lambda+\alpha_m^m)\right.$$
$$\left.+C_{m_2}\tan^m\frac{\theta}{2}\cos(m\lambda+\alpha_m^m)\right],$$

in zone II,

$$R=\frac{m}{(m+1)(2m+1)}Ck_m^mBK\left[\left\{P_{m+1}^m+C_{m_3}\tan^m\frac{\theta}{2}+C_{m_4}\cot^m\frac{\theta}{2}\right\}\sin(m\lambda+\alpha_m^m)\right.$$
$$\left.+\left\{C_{m_5}\tan^m\frac{\theta}{2}+C_{m_6}\cot^m\frac{\theta}{2}\right\}\cos(m\lambda+\alpha_m^m)\right],$$

in zone III,

$$R=\frac{m}{(m+1)(2m+1)}Ck_m^mK\left[\left\{P_{m+1}^m+C_{m_7}\tan^m\frac{\theta}{2}+C_{m_8}\cot^m\frac{\theta}{2}\right\}\sin(m\lambda+\alpha_m^m)\right.$$
$$\left.+\left\{C_{m_9}\tan^m\frac{\theta}{2}+C_{m_{10}}\cot^m\frac{\theta}{2}\right\}\cos(m\lambda+\alpha_m^m)\right],$$

in zone IV,

$$R=\frac{m}{(m+1)(2m+1)}Ck_m^mK\log\left(\tan\frac{\theta}{2}\right)\{C_{m_{11}}\sin(m\lambda+\alpha_m^m)+C_{m_{12}}\cos(m\lambda+\alpha_m^m)\}.$$

In zones V, VI and VII, R is expressed in the same way as in zones III, II and I respectively. Twelve constants in these equations are determined by the conditions that the normal component of the current and the tangential component of the electric field are continuous along the boundaries.

As a first approximation, we consider that the current function is divided into two parts, namely $R=R_q+R_D$, where the current system derived from R_D corresponds to the S_D field, and that derived from R_q causes the S_q field. The equation for R_q is already discussed in the preceding paragraph. Accordingly, the remaining part R_D is,

in zone I,

$$R_D=\frac{1}{(m+1)(2m+1)}Ck_m^mK\left[\left\{(A-1)P_{m+1}^m+(AC_{m_1}-q_{m_1})\tan^m\frac{\theta}{2}\right\}\sin(m\lambda+\alpha_m^m)\right.$$
$$\left.+(AC_{m_2}-q_{m_2})\tan^m\frac{\theta}{2}\cos(m\lambda+\alpha_m^m)\right],$$

in zone II,

$$R_D=\frac{1}{(m+1)(2m+1)}Ck_m^mK\left[\left\{(B-1)P_{m+1}^m+(BC_{m_3}-q_{m_1})\tan^m\frac{\theta}{2}+BC_{m_4}\cot^m\frac{\theta}{2}\right\}\sin(m\lambda+\alpha_m^m)\right.$$
$$\left.+\left\{(BC_{m_5}-q_{m_2})\tan^m\frac{\theta}{2}+BC_{m_6}\cot^m\frac{\theta}{2}\right\}\cos(m\lambda+\alpha_m^m)\right],$$

in zone III,

$$R_D=\frac{1}{(m+1)(2m+1)}Ck_m^mK\left[\left\{(C_{m_7}-q_{m_1})\tan^m\frac{\theta}{2}+C_{m_8}\cot^m\frac{\theta}{2}\right\}\sin(m\lambda+\alpha_m^m)\right.$$
$$\left.+\left\{(C_{m_9}-q_{m_2})\tan^m\frac{\theta}{2}+C_{m_{10}}\cot^m\frac{\theta}{2}\right\}\cos(m\lambda+\alpha_m^m)\right],$$

in zone IV,

$$R_D=\frac{1}{(m+1)(2m+1)}Ck_m^mK\log\left(\tan\frac{\theta}{2}\right)\{(C_{m_{11}}-q_{m_3})\sin(m\lambda+\alpha_m^m)+(C_{m_{12}}-q_{m_4})\cos(m\lambda+\alpha_m^m)\},$$

where q_m is C_m in the equations of R_7. In zones V, VI and VII, R_D is expressed in the same way as in zones III, II and I respectively. The components of the electrostatic field X_D and Y_D for the S_D in each zone are also obtained in the same way, as shown in the succeeding paragraphs.

4. 4. Results of Numerical Calculations for the Diurnal Wind Variation ($m=1$)

As a simple case, m in Eq. (1) is assumed to be 1, namely

$$\psi = k_1{}^1 P_1{}^1(\cos\theta)\sin(\lambda+\alpha_1{}^1).$$

Then, the current function R_D and electrostatic components X_D and Y_D in each zone are,

in zone I,

$$R_D=\frac{1}{6}Ck_1{}^1K\left[\left\{(A-1)P_2{}^1+(AC_1-q_1)\tan\frac{\theta}{2}\right\}\sin(\lambda+\alpha_1{}^1)+(AC_2-q_2)\tan\frac{\theta}{2}\cos(\lambda+\alpha_1{}^1)\right],$$

$$X_D=\frac{Ck_1{}^1}{R_0}\left[\frac{1}{6}\frac{C_1+A'\gamma C_2-q_1-\gamma q_2}{1+\cos\theta}\cos(\lambda+\alpha_1{}^1)+\left\{\frac{\gamma}{2}(A'-1)\cos 2\theta+\frac{1}{6}\frac{A'\gamma C_1-C_2-\gamma q_1+q_2}{1+\cos\theta}\right\}\sin(\lambda+\alpha_1{}^1)\right],$$

$$Y_D=\frac{Ck_1{}^1}{R_0}\left[-\frac{1}{6}\frac{C_1+A'\gamma C_2-q_1-\gamma q_2}{1+\cos\theta}\sin(\lambda+\alpha_1{}^1)+\left\{\frac{\gamma}{2}(A'-1)\cos\theta+\frac{1}{6}\frac{A'\gamma C_1-C_2-\gamma q_1+q_2}{1+\cos\theta}\right\}\cos(\lambda+\alpha_1{}^1)\right],$$

in zone II,

$$R_D=\frac{1}{6}Ck_1{}^1K\left[\left\{(B-1)P_2{}^1+(BC_3-q_1)\tan\frac{\theta}{2}+BC_4\cot\frac{\theta}{2}\right\}\sin(\lambda+\alpha_1{}^1)+\left\{(BC_5-q_2)\tan\frac{\theta}{2}+BC_6\cot\frac{\theta}{2}\right\}\cos(\lambda+\alpha_1{}^1)\right],$$

$$X_D=\frac{Ck_1{}^1}{R_0}\left[\frac{1}{6}\left(\frac{C_3+B'\gamma C_5-q_1-\gamma q_2}{1+\cos\theta}-\frac{B'\gamma C_6-C_4}{1-\cos\theta}\right)\cos(\lambda+\alpha_1{}^1)+\left\{\frac{\gamma}{2}(B'-1)\cos 2\theta+\frac{1}{6}\left(\frac{B'\gamma C_3-C_5-\gamma q_1+q_2}{1+\cos\theta}-\frac{B'\gamma C_4+C_6}{1-\cos\theta}\right)\right\}\sin(\lambda+\alpha_1{}^1)\right],$$

$$Y_D=\frac{Ck_1{}^1}{R_0}\left[-\frac{1}{6}\left(\frac{C_3+B'\gamma C_5-q_1-\gamma q_2}{1+\cos\theta}+\frac{B'\gamma C_6-C_4}{1-\cos\theta}\right)\sin(\lambda+\alpha_1{}^1)+\left\{\frac{\gamma}{2}(B'-1)\cos\theta+\frac{1}{6}\left(\frac{B'\gamma C_3-C_5-\gamma q_1+q_2}{1+\cos\theta}+\frac{B'\gamma C_4+C_6}{1-\cos\theta}\right)\right\}\cos(\lambda+\alpha_1{}^1)\right],$$

in zone III,

$$R_D=\frac{1}{6}Ck_1{}^1K\left[\left\{(C_7-q_1)\tan\frac{\theta}{2}+C_8\cot\frac{\theta}{2}\right\}\sin(\lambda+\alpha_1{}^1)+\left\{(C_9-q_2)\tan\frac{\theta}{2}+C_{10}\cot\frac{\theta}{2}\right\}\cos(\lambda+\alpha_1{}^1)\right],$$

$$X_D=\frac{Ck_1{}^1}{R_0}\left[\frac{1}{6}\left(\frac{C_7+\gamma C_9-q_1-\gamma q_2}{1+\cos\theta}-\frac{\gamma C_{10}-C_8}{1-\cos\theta}\right)\cos(\lambda+\alpha_1{}^1)+\frac{1}{6}\left(\frac{\gamma C_7-C_9-\gamma q_1+q_2}{1+\cos\theta}-\frac{\gamma C_8+C_{10}}{1-\cos\theta}\right)\sin(\lambda+\alpha_1{}^1)\right],$$

$$Y_D=\frac{Ck_1^1}{R_0}\left[-\frac{1}{6}\left(\frac{C_7+\gamma C_9-q_1-\gamma q_2}{1+\cos\theta}+\frac{\gamma C_{10}-C_8}{1-\cos\theta}\right)\sin(\lambda+\alpha_1^1)\right.$$
$$\left.+\frac{1}{6}\left(\frac{\gamma C_7-C_9-\gamma q_1+q_2}{1+\cos\theta}+\frac{\gamma C_8+C_{10}}{1-\cos\theta}\right)\cos(\lambda+\alpha_1^1)\right],$$

in zone IV,

$$R_D=\frac{1}{6}Ck_1^1K\log\left(\tan\frac{\theta}{2}\right)\{(C_{11}-q_3)\sin(\lambda+\alpha_1^1)+(C_{12}-q_4)\cos(\lambda+\alpha_1^1)\},$$
$$X_D=0,$$
$$Y_D=-\frac{1}{6}\frac{Ck_1^1}{R_0}\frac{K}{K_e}\operatorname{cosec}\theta\{(C_{11}-q_3)\sin(\lambda+\alpha_1^1)+(C_{12}-q_4)\cos(\lambda+\alpha_1^1)\},$$

where q_1, q_2, q_3 and q_4 are given as C_m in Eq. (6). In zones V, VI and VII, they are obtained in the same way as in zones III, II and I.

Numerical calculations for many sorts of values of γ, A' and B' are carried out, and a typical example showing the mode of those results is given below.

When we adopt $\sum_1=6.86\times10^{-9}$, $\sum_2=1.45\times10^{-8}$, as mentioned in Paragraph 4.2., then $\gamma=2.114$. At that time, the calculated current-systems for the following four examples,

1, $A'=1$ hence $A=1$, $B'=2$ hence $B=3.45$,
2, $A'=1.5$ hence $A=2.02$, $B'=2$ hence $B=3.45$,
3, $A'=1$ hence $A=1$, $B'=6$ hence $B=29.60$,
4, $A'=3$ hence $A=7.54$, $B'=6$ hence $B=29.60$,

are given in Figs. 17. a, b, c and d, where α_1^1 is assumed to be 114°, and the density of stream lines in Figs. a and b is expressed as twice that in Figs. 17. c and d. From these examples, the following conclusions may be obtained:

1) When the height-integrated Hall conductivity $\sum_2$ at the auroral zone increases to only twice that of the other zones, as will be seen in Fig. 17. a, the focuses of the current circulating through the middle and the equatorial zones are situated on the meridian of about 04 h. 16 h., that is about 4 hours later compared with

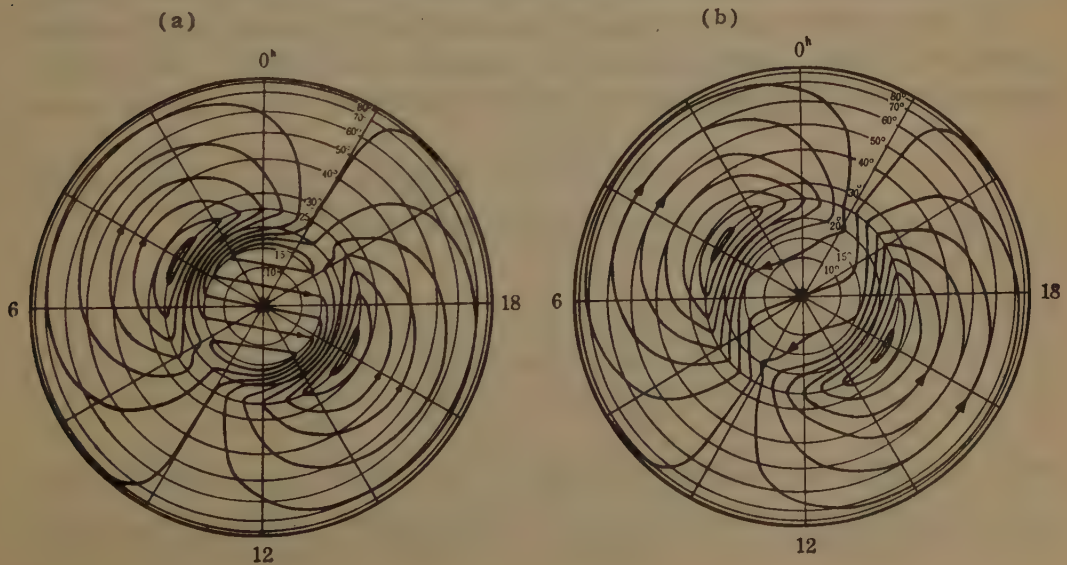

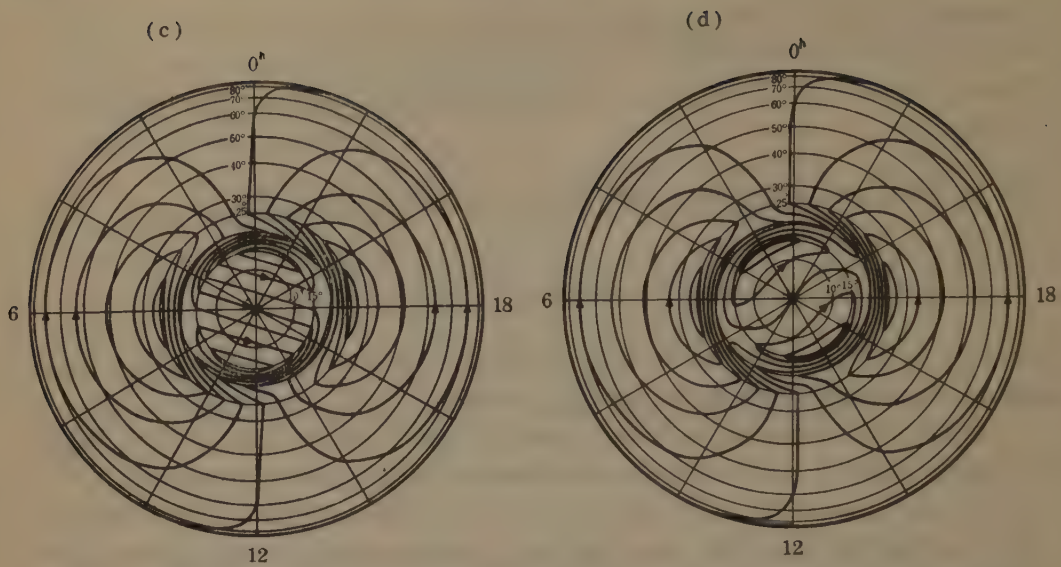

Fig. 17. Calculated S_D current-systems for $m=1$ and $\gamma=2.114$ (viewed from the north pole) a) $A'=1$ and $B'=2$, b) $A'=1.5$ and $B'=2$, c) $A'=1$ and $B'=6$, d) $A'=3$ and $B'=6$.

the calculated S_D current-system in the case of isotropic conductivity [17]. With further increase of $\sum_2$ at the auroral zone (or B'), the focuses shift more anticlockwise till about 06 h. 18 h. meridian. It may be found by comparing Fig. 17. a with Fig. 17. c.

2) The direction of the polar current hardly changes for any values of B', as shown in both cases of Figs. 17. a and c, but it turns anticlockwise with the increase of $\sum_2$ at the polar cap (or A'), in so far as B' is constant. Fig. 17. d is the case where the increase of $\sum_2$ at the polar cap is a half of that at the auroral zone ($A'/B'=0.5$). If A' increases almost to B', the polar current then finally flows as in Fig. 17. b,—it does not become the return current of the auroral current.

3) The electric current of 3.92×10^3 Amp. in Figs. 17. a and b, (and its double in Figs. 17. c and d) flows between the successive stream lines in the direction indicated by arrows, assuming that the current intensity for the S_q current-system

Table 4.

Case	1	2	3	4	Chapman's
Total amount of the auroral zone current	3.55	3.35	7.16	6.21	27.50
Amount of the polar closing current	1.11	0.53	2.89	1.95	22.50
Amount of the middle zone closing current	2.44	2.82	4.27	4.26	5.00

(unit in 10^4 Amp.)

agrees with Chapman's analysis. The amount of current is compared in Table 4, for the total auroral zone current, the polar closing current (the current circulating through the auroral zone and the polar cap) and the middle zone closing

current (the current circulating through the auroral, the middle and the equatorial zones). The current intensity of these results is rather small, compared with that of Chapman's S_D current-system. But excessive increase of B' for the purpose of producing a larger current may be impracticable.

4) The direction of these calculated currents does not coincide with the S_D current estimated from the geomagnetic variation as shown in Figs. 1. a, b, c, and d, for any values of γ, A' and B', but it seems to be in reverse phase. If α_1^1 can be assumed to be 294° instead of 114°, the difference in phase of both current systems dissapears, as may be supposed in Fig. 17. d. Accordingly, if the wind blows reverse direction to the wind producing the S_q current, the S_D may be explained by this principle, though the current intensity rather small compared with Chapman's. As an hypothesis, it may be reasonable, for our purpose, to consider double layers [27] [28] wherein the air motion is assumed to be reciprocally inverse and the conductivity differs, or to assume some coexistence of such a wind system during the storm with the wind producing the S_q current.

5) At the equatorial zone, the phase of the calculated S_D current is about two hours earlier than that in the middle zone for both the cases $\alpha_1^1=114°$ and $\alpha_1^1=294°$, as the 0-line in each figure shows. This result seems to coincide with the preceding statistical result for geomagnetic horizontal component at Huancayo.

4. 5. Results of Numerical Calculations for the Semi-Diurnal Wind Variation ($m=2$)

Assuming that $m=2$, then $\psi=k_2^2P_2^2(\cos\theta)\sin(2\lambda+\alpha_2^2)$. R_D, X_D and Y_D are also calculated in the same way. They are,

in zone I,

$$R_D=\frac{2}{15}Ck_2^2K\left[\left\{(A-1)P_3^2+(AC_1-q_1)\tan^2\frac{\theta}{2}\right\}\sin(2\lambda+\alpha_2^2)+(AC_2-q_2)\tan^2\frac{\theta}{2}\cos(2\lambda+\alpha_2^2)\right],$$

$$X_D=\frac{Ck_2^2}{R_0}\left[\frac{4}{15}\sin\theta\frac{C_1+A'\gamma C_2-q_1-\gamma q_2}{(1+\cos\theta)^2}\cos(2\lambda+\alpha_2^2)\right.$$
$$\left.+\left\{2(A'-1)\gamma\sin\theta(3\cos^2\theta-1)+\frac{4}{15}\sin\theta\frac{A'\gamma C_1-C_2-\gamma q_1+q_2}{(1+\cos\theta)^2}\right\}\sin(2\lambda+\alpha_2^2)\right],$$

$$Y_D=\frac{Ck_2^2}{R_0}\left[-\frac{4}{15}\sin\theta\frac{C_1+A'\gamma C_2-q_1-\gamma q_2}{(1+\cos\theta)^2}\sin(2\lambda+\alpha_2^2)\right.$$
$$\left.+\left\{2(A'-1)\gamma\sin2\theta+\frac{4}{15}\sin\theta\frac{A'\gamma C_1-C_2-\gamma q_1+q_2}{(1+\cos\theta)^2}\right\}\cos(2\lambda+\alpha_2^2)\right],$$

in zone II,

$$R_D=\frac{2}{15}Ck_2^2K\left[\left\{(B-1)P_3^2+(BC_3-q_1)\tan^2\frac{\theta}{2}+BC_4\cot^2\frac{\theta}{2}\right\}\sin(2\lambda+\alpha_2^2)\right.$$
$$\left.+\left\{(BC_5-q_2)\tan^2\frac{\theta}{2}+BC_6\cot^2\frac{\theta}{2}\right\}\cos(2\lambda+\alpha_2^2)\right],$$

$$X_D=\frac{Ck_2^2}{R_0}\left[\frac{4}{15}\sin\theta\left(\frac{C_3+B'\gamma C_5-q_1-\gamma q_2}{(1+\cos\theta)^2}-\frac{B'\gamma C_6-C_4}{(1-\cos\theta)^2}\right)\cos(2\lambda+\alpha_2^2)\right.$$
$$\left.+\left\{2(B'-1)\gamma\sin\theta(3\cos^2\theta-1)+\frac{4}{15}\sin\theta\left(\frac{B'\gamma C_3-C_5-\gamma q_1+q_2}{(1+\cos\theta)^2}-\frac{B'\gamma C_4+C_6}{(1-\cos\theta)^2}\right)\sin(2\lambda+\alpha_2^2)\right\}\right],$$

$$Y_D=\frac{Ck_2^2}{R_0}\left[-\frac{4}{15}\sin\theta\left(\frac{C_3+B'\gamma C_5-q_1-\gamma q_2}{(1+\cos\theta)^2}+\frac{B'\gamma C_6-C_4}{(1-\cos\theta)^2}\right)\sin(2\lambda+\alpha_2^2)\right.$$
$$\left.+\left\{2(B'-1)\gamma\sin 2\theta+\frac{4}{15}\sin\theta\left(\frac{B'\gamma C_3-C_5-\gamma q_1+q_2}{(1+\cos\theta)^2}+\frac{B'\gamma C_4+C_6}{(1-\cos\theta)^2}\right)\right\}\cos(2\lambda+\alpha_2^2)\right],$$

in zone III,

$$R_D=\frac{2}{15}Ck_2^2K\left[\left\{(C_7-q_1)\tan^2\frac{\theta}{2}+C_8\cot^2\frac{\theta}{2}\right\}\sin(2\lambda+\alpha_2^2)\right.$$
$$\left.+\left\{(C_9-q_2)\tan^2\frac{\theta}{2}+C_{10}\cot^2\frac{\theta}{2}\right\}\cos(2\lambda+\alpha_2^2)\right],$$

$$X_D=\frac{Ck_2^2}{R_0}\left[\frac{4}{15}\sin\theta\left(\frac{C_7+\gamma C_9-q_1-\gamma q_2}{(1+\cos\theta)^2}-\frac{\gamma C_{10}-C_8}{(1-\cos\theta)^2}\right)\cos(2\lambda+\alpha_2^2)\right.$$
$$\left.+\frac{4}{15}\sin\theta\left(\frac{\gamma C_7-C_9-\gamma q_1+q_2}{(1+\cos\theta)^2}-\frac{\gamma C_8+C_{10}}{(1-\cos\theta)^2}\right)\sin(2\lambda+\alpha_2^2)\right],$$

$$Y_D=\frac{Ck_2^2}{R_0}\left[-\frac{4}{15}\sin\theta\left(\frac{C_7+\gamma C_9-q_1-\gamma q_2}{(1+\cos\theta)^2}+\frac{\gamma C_{10}-C_8}{(1-\cos\theta)^2}\right)\sin(2\lambda+\alpha_2^2)\right.$$
$$\left.+\frac{4}{15}\sin\theta\left(\frac{\gamma C_7-C_9-\gamma q_1+q_2}{(1+\cos\theta)^2}+\frac{\gamma C_8+C_{10}}{(1-\cos\theta)^2}\right)\cos(2\lambda+\alpha_2^2)\right],$$

in zone IV,

$$R_D=\frac{2}{15}Ck_2^2K\log\left(\tan\frac{\theta}{2}\right)\{(C_{11}-q_3)\sin(2\lambda+\alpha_2^2)+(C_{12}-q_4)\cos(2\lambda+\alpha_2^2)\},$$

$$X_D=0,$$

$$Y_D=-\frac{2}{15}\frac{Ck_2^2}{R_0}\frac{K}{K_e}\operatorname{cosec}\theta\{(C_{11}-q_3)\sin(2\lambda+\alpha_2^2)+(C_{12}-q_4)\cos(2\lambda+\alpha_2^2)\},$$

where q_1, q_2, q_3 and q_4 are given as C_m in Eq. (7). In zones V, VI and VII, they are expressed in the same way.

If we assume in this case that $\sum_1=4.8\times10^{-9}$, $\sum_2=1.44\times10^{-8}$, then $\gamma=3$. At that time, the calculated current-system for the following two examples,

1, $A'=1$ hence $A=1$, $B'=6$ hence $B=32.50$,

2, $A'=3$ hence $A=8.20$, $B'=6$ hence $B=32.50$,

are given in Figs. 18. a and b, where α_2^2 is assumed to be 292°.

The density of stream lines for the polar closing current in Fig. 18. a is

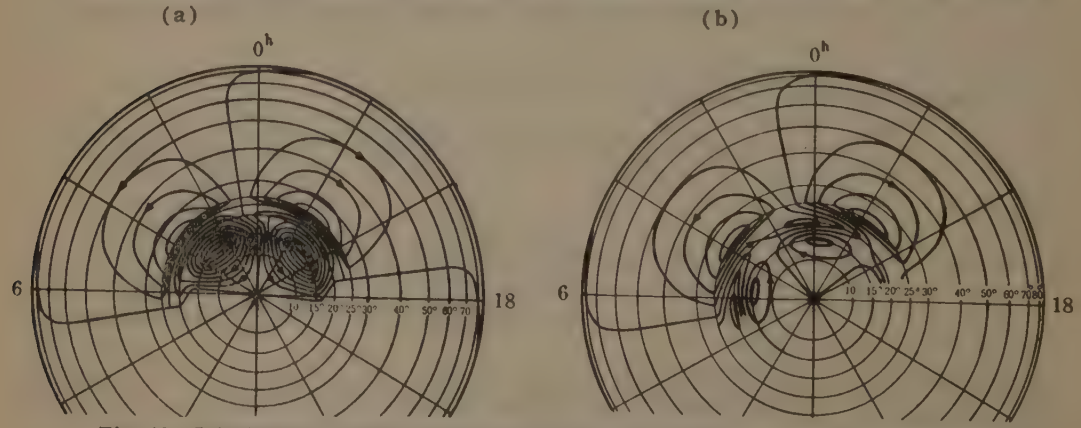

Fig. 18. Calculated S_D current-system for $m=2$ and $\gamma=3$ (viewed from the north pole)
a) $A'=1$ and $B'=6$, b) $A'=3$ and $B'=6$.

expressed as half of that for the middle zone closing current of the figure and for Fig. 18. b. If the current density for the S_q current in this case is assumed to be 62,000 Amp., it may be estimated that the electric current of 5.46×10^3 Amp. (and double that amount, for the polar closing current in Fig. 18. a) flows between the successive stream lines in the direction indicated by arrows. The amounts of the polar closing current and the middle zone closing current for Fig. 18. a are 9.83×10^4 Amp. and 2.50×10^4 Amp. respectively.

The second example seems to be too complicated at the polar cap, but in the first example of Fig. 18. a, it may be noticed that the amount of the polar closing current is about four times that of the middle zone closing current, and the ratio in Chapman's S_D current is 4.5.

The direction of the current in Fig. 18. a is also worthy of notice. As mentioned in Paragraph 4. 4, if the wind blows in the opposing direction to the wind producing the S_q current, the S_D may be explained to a certain degree. But when the wind is the same for both the S_q and the S_D currents, this case of semi-diurnal wind variation may possibly explain the S_D current, from the point of view of the direction of the current. In such a case, the daily variation of electrical conductivity must be taken into consideration.

Dynamo theoretical calculation for these conditions can be treated by means of a perturbation method [29]. It may be possible to assume that the height-integrated effective conductivity in each region is

in zone I and VII,	$K=AK_0$,	(The conductivity does not change.)
in zone II and VI,	$K=BK_0(1+\zeta\cos\lambda)$,	(The conductivity at midnight is $(1+\zeta)/(1-\zeta)$ times that at noon.)
in zone III and V,	$K=K_0(1-\zeta'\sin\theta\cos\lambda)$,	(The conductivity is proportional to $\cos\chi$, in the case when the sun's north declination is 0, where χ is zenith distance of the sun.)
in zone IV,	$K=2K_0(1-\zeta'\sin\theta\cos\lambda)$,	

where ζ and ζ' are smaller than 1. The current function R is assumed to be

$$R=R_q+R_D,$$

in the same way as in the preceding paragraph.

Then,

$$R_q=R_{q0}+\zeta' R'_{q\zeta'} ,$$

$$R_D=R_{D0}+\zeta' R'_{D\zeta'}+\zeta R'_{D\zeta} ,$$

where $\zeta R'_{D\zeta}$ is a perturbation term corresponding to $BK_0\zeta\cos\lambda$, and both $\zeta' R'_{q\zeta'}$ and $\zeta' R'_{D\zeta'}$ are perturbation terms for $-K_0\zeta'\sin\theta\cos\lambda$. R_{q0} and R_{D0} are the expressions for R_q and R_D when $\zeta=\zeta'=0$. Thus, we can calculate the S_D current for the semi-diurnal wind variation with a daily variation of electrical conductivity. Though these results will be discussed in the second report, it will be easily seen that the current at night in Fig. 18. a predominates, and accordingly it becomes similar to the S_D current obtained from the geomagnetic variation.

5. Ionospheric Variations due to the Drift

Ionospheric variations due to the effect of a drift by the electric field and the earth's magnetic field were discussed by many researchers, and it has been suggested recently by D.F. Martyn [5] and K. Maeda [22] that the $S_D(F2)$ variation is also due to a drift effect. Following their principles, some theoretical approach to explain the statistical results is carried out below.

For positive ions in the E layer, the equation

$$\partial n_+/\partial t = Q - \alpha n_+ n_e - \partial(n_+ W_+)/\partial z,$$

will hold, where Q is ion production per c.c. per sec., α is the effective recombination coefficient, and W is vertical upward velocity. The terms for horizontal velocity are neglected, since they are estimated to be small. When $\Delta\left(=\frac{n_+}{n_e}-1\right)$ is assumed to be independent of height, we have

$$\partial n_e/\partial t = q - \alpha n_e^2 - \partial(n_e W_+)/\partial z, \qquad (8)$$

where $q=Q/(\Delta+1)$.

According to M. Hirono [30], W_+ is expressed as

$$W_+ = \frac{1}{e n_e}(K_a \cdot \cos\phi \cdot \sin\phi \cdot J_x + K_t \cdot \cos\phi \cdot J_y),$$

where

$$K_a = -D\{-M^2 - L_1 L_2 + M(L_1 + L_2)\}, \quad K_t = D\{L_1 + L_2 + M(L_1 L_2 - 1)\},$$
$$D = L_1/\{(L_2 + \kappa L_1)(1+M^2)\}, \quad M = L_1(L_1 + \kappa L_2)/(L_2 + \kappa L_1),$$
$$L_1 = |\omega_i/\nu_i|, \quad L_2 = |\omega_e/\nu_e|,$$
$$\kappa = 2\Delta + 1.$$

Although the second term of the right hand side of the equation is smaller than the first in all zones except the equatorial, J_y is very large near the E level in the equatorial zone when $\Delta \ll 1$ [31], corresponding to the intense geomagnetic daily variation at this zone. It follows that W_+ is much larger there than in any other zone. Accordingly, in consideration of Eq. (8), some abnormality in the electron density or the height of the ionosphere at about the E level in the equatorial zone may be supposed. In the E layer, it seems to be difficult to obtain statistically such an abnormality. In the Es region, however, fEs is abnormally large in the equatorial zone as shown in Paragraph 4. 1., and the breadth of the zone coincides with that of intense J_y zone, statistically and theoretically.

Another expression of W by Hirono is

$$W_r = e_r\left(S_r - P_r \cdot \frac{S}{P}\right)(E_x^i + X) + \left(q_r + e_r \cdot P_r \cdot \frac{T}{P}\right)(E_y^i + Y), \qquad (9)$$

where

$$P_r = (1/m_r\nu_r)\{\cos^2\phi \cdot \nu_r^2/(\nu_r^2+\omega_r^2) + \sin^2\phi\}, \quad S_r = (1/m_r\nu_r)\sin\phi\cdot\cos\phi\cdot\omega_r^2/(\nu_r^2+\omega_r^2),$$
$$q_r = (1/H)\cos\phi\cdot\omega_r^2/(\nu_r^2+\omega_r^2), \quad P = e^2\sum_r n_r P_r = \sigma_1\cos^2\phi + \sigma_0\sin^2\phi,$$
$$T = n_e e(q_e - q_i) = \sigma_2\cos\phi, \quad S = e^2\sum_r n_r S_r = (\sigma_0 - \sigma_1)\sin\phi\cdot\cos\phi.$$

The variations of the E layer due to a vertical drift associated with the S_q and the L fields can be discussed by Eqs. (8) and (9). The $S_D(E)$ variation may be discussed in the same way for the S_D field, taking X_D and Y_D instead of $E_x^i + X$ and $E_y^i + Y$ in Eq. (9). At lower altitudes than 120 Km., the first term of the right hand side of

Eq. (9) is much larger than the second term in latitudes higher than about 5°, but it is very small near the magnetic equator. For the phase of the $S_D(E)$ variation, therefore, Y_D is effective in the equatorial zone and X_D is important in other zones.

In the E layer, however, it seems to be very difficult to obtain statistically the S_D variation and lunar tide, as in the case of the lack of abnormality at the equatorial zone. This is because α is about 10^{-8} cm^3/sec., so that the second term in Eq. (8) decreases the drift effect. In the Es region, on the other hand, intense lunar tidal variations were obtained by the writer [32], and the S_D variation is also obtained as already mentioned. Moreover, fEs is abnormally large in the equatorial zone. Therefore, these results suggest that the Es is much affected by the vertical drift, and in other words, they suggest a formation mechanism of the Es. That is to say, it may be supposed that the Es is a comparatively thin layer formed of ionic clouds, having the electron density of a few or several times that of the normal E, and that the intense ionic clouds are due to a drift effect on patches or blobs [33] of ionization, of different density from their surroundings, caused by meteors or other things. At the auroral zone, however, the Es may be formed mainly by the charged particles emitted from the sun.

Thus, it may be estimated that the $S_D(Es)$ variation may be due to a drift effect associated with the S_D field, and that Y_D may be effective for the drift in the equatorial zone and X_D may be important in other zones, for the purpose of considering the phase of the $S_D(fEs)$ variation. In the case of $\gamma=2.114$, $A'=3$, $B'=6$ and $\alpha_1{}^1=294°$, the minimum of X_D in the middle zone occurs at 07–08 h. in local time, and maximum of Y_D in the equatorial zone occurs at 05 h. Accordingly, already mentioned statistical results that the $S_D(fEs)$ has a maximum in the forenoon at the moderate latitudes, and that there is a phase difference between the middle zone and the equatorial, can be explained by these considerations.

In the $F2$ layer, ionospheric variations due to the effect of the vertical drift may be obvious, as α is small. For this layer, W can be expressed by the second term of the right hand side of Eq. (9). In the case of the $S_D(F2)$ variations, therefore, Y_D may be important in considering the phase of the variation, and Y_D has a phase difference between the middle and the equatorial zones. The increase at about 05 h. in the $S_D(h'F2)$ variation for Huancayo (see Fig. 6 and 7. a) may be explained, when Y_D at this zone is considered, as mentioned above. A.A. Weiss [34] has pointed out that the greater the vertical velocity the smaller the electron density of the $F2$ layer in the day time, and K. Maeda [21] has also obtained the same conclusion. Accordingly, it may be supposed that the $S_D(f_0F2)$ is at a minimum in the forenoon at the middle zone and that there is some phase difference between the equatorial and the middle zones, as obtained statistically.

It may be concluded, therefore, that the vertical drift associated with the S_D current differs in the middle and the equatorial zones, and its effect is opposite for the $F2$ layer and the Es region,—that is to say, the density decreases in the former and increases in the latter. These matters will be examined further in the second report.

6. Concluding Remarks

1) The S_D and *Dst* variations in the densities and heights of the *Es* and *F*2 regions are studied. The amplitude of the S_D variation of the *Es* in summer solstice at the moderate latitudes is about 0.5Mc/s in frequency (15% for mean ionized density) and the phase is opposite to that of the *F*2.

2) At the equatorial zone, the ionospheric S_D and *Dst* variations are a little peculiar compared with those at the moderate latitudes. The geomagnetic S_D variation at this zone is also a little different,—that is to say, the amplitude seems to be larger and the maximum occurs about three hours earlier than that in the moderate region.

3) The current system for the S_D field is calculated by the dynamo theory, taking into consideration the anisotropic electrical-conductivity, on the assumption that the conductivity at the auroral zone is higher than that in the other zones. In the case of the diurnal wind variation, it may be possible to consider double layers wherein the air motion in one layer is assumed to be the inverse of the wind producing the S_q current in the other and the conductivity differs between the two, or to assume the coexistence of such a reverse wind system during the storm with the wind producing the S_q current. In the case of the semi-diurnal wind variation, the daily variation of the electrical conductivity must be taken into consideration. The latter case seems to give rather better results, judging by the current density for the S_D current-system estimated from the geomagnetic variation. In both cases, the peculiarity of the geomagnetic S_D variation at the equatorial zone can be explained by these calculated current-systems.

4) The ionospheric S_D variations may be due to the effect of a vertical drift by the earth's magnetic field and the electric field of the S_D current. From the equations of vertical velocity and an estimation that the production of the *Es* is due to a drift effect, the statistical results that the phase of the S_D variation is opposite between the *F*2 and the *Es*, and that there is a phase difference between the equatorial and the middle zones in both ionospheric regions, may be explained.

Acknowledgements

The writer wishes to express his sincere thanks to Profs. M. Hasegawa, T. Nagata and K. Maeda for their valuable discussions and to Dr. J. Egedal for his kind encouragement and also to Dr. D.F. Martyn and Prof. H.S.W. Massey for their useful advice and various suggestions on their visit to Japan. He is pleased to acknowledge that the data used have been furnished by Radio Wave Laboratories. The writer's thanks are also due to Dr. M. Hirono for referring to his theoretical study, and to Miss. H. Yatake for her assistance.

(Read May 16 and Nov. 1, 1953)

References

[1] E.V. Appleton and W.R. Piggott, Nature, **165**, 130 (1950); Journ. Atmos. Terr. Phys., **2**, 236 (1952); *ibid.*, **3**, 121 (1953).

[2] H. Uyeda and Y. Arima, Rep. Ionosphere Res. Japan, **6**, 1 (1952).

[3] T. Obayashi, Rep. Ionosphere Res. Japan, **6**, 79 (1952).

[4] K. Sinno, Rep. Ionosphere Res. Japan, **7**, 7 (1953).

[5] D.F. Martyn, Proc. Roy. Soc. A, **218**, 1 (1953); Nature, **171**, 14 (1953).

[6] L.V. Berkner and H.W. Wells, Terr. Mag. Atmos. Elect., **42**, 73 (1937).

[7] E.V. Appleton, R. Naismith and L.J. Ingram, Phil. Trans. Roy. Soc. A, **236**, 191 (1937).

[8] W.R. Piggott, Nature, **171**, 124 (1953).

[9] S. Matsushita, Rep. Ionosphere Res. Japan, **7**, 161 (1953).

[10] S. Chapman, Terr. Mag. Atmos. Elect., **40**, 349 (1935).

[11] M. Hasegawa, Trans. Washington Meeting, A.T.M.E., I.U.G.G., 311 (1940).

[12] E.H. Vestine, Terr. Mag. Atmos. Elect., **43**, 261 (1938); Trans. Washington Meeting, A.T.M.E., I.U.G.G., 360 (1940).

[13] L. Harang, Terr. Mag. Atmos. Elect., **51**, 353 (1946).

[14] T. Nagata, Geophys. Notes, Tokyo Univ., **2**, No. 18 (1949); Journ. Geophys. Res., **55**, 127 (1950).

[15] N. Fukushima, Rep. Ionosphere Res. Japan, **5**, 85 & 191 (1951); T. Nagata and N. Fukushima, *ibid.*, **6**, 85 (1952).

[16] T. Rikitake, Rep. Ionosphere Res. Japan, **2**, 57 (1948).

[17] N. Fukushima, Journ. Faculty Science, Tokyo Univ., Section 2, Vol. 8, Part 5, 293 (1953).

[18] D.F. Martyn, Nature, **162**, 142 (1948); W.G. Baker and D.F. Martyn, Nature, **170**, 1090 (1952).

[19] T.G. Cowling, Proc. Roy. Soc. A, **183**, 453 (1945).

[20] M. Hirono, Journ. Geomag. Geoelect., **2**, 1 & 113 (1950); *ibid.*, **4**, 7 (1952).

[21] K. Maeda, Journ. Geomag. Geoelect., **4**, 63 & 83 (1952).

[22] K. Maeda, Rep. Ionosphere Res. Japan, **7**, 81 (1953).

[23] H. Uyeda, K. Miya and T. Kobayashi, Rep. Ionosphere Res. Japan, **6**, 179 (1952).

[24] S. Matsushita, Journ. Geomag. Geoelect., **3**, 44 (1951); Rep. Ionosphere Res. Japan, **6**, 118 & 123 (1952).

[25] J. Egedal, Nature, **161**, 443 (1948).

[26] J. Egedal, Trans. Brussels Meeting, A.T.M.E., I.U.G.G., (1951).

[27] N. Fukushima, Geophys. Notes, Tokyo Univ., **2**, No. 21 (1949).

[28] S. Matsushita, Journ. Geomag. Geoelect., **1**, 41 (1949).

[29] N. Fukushima, Journ. Geomag. Geoelect., **2**, 113 (1950).

[30] M. Hirono, Journ. Geomag. Geoelect., **5**, 22 (1953).

[31] D.R. Bates and H.S.W. Massey, Proc. Roy. Soc. A, **187**, 261 (1946).

[32] S. Matsushita, Rep. Ionosphere Res. Japan, **7**, 45 (1953).

[33] D.F. Martyn, (in the Press).

[34] A.A. Weiss, Journ. Atmos. Terr. Phys., **3**, 30 (1952).

Latitude Effect of the Intensity Decrease in the Cosmic-Ray Storm*

By Sekiko YOSHIDA and Yoshiko KAMIYA
(Physical Institute, Nagoya University)

Abstract

The latitude effect of the cosmic-ray decrease associated with the magnetic storm was determined from the data obtained in 13 periods of observation at various stations over the world. The result was in accordance with Nagashima's electric field theory.

Nagashima[1][2] proposed an explanation of the world-wide decrease (ΔI) of the cosmic-ray intensity associated with the magnetic storm, assuming an electric field, and calculated the latitude effect of ΔI according to his theory. The latitude effect was found by Forbush[3] and by Wada[4] through the analysis of observations. But, neither the number of stations nor the procedure in their analysis is satisfactory to compare with the theoretical result. We have made this analysis, taking the following points into account.

1) In order to decrease the error due to the variations except the cosmic-ray storm, only the storms with large decrease are subjected to the analysis. The criterion adopted by us is $\Delta I_0 \geqq 2\%$, where ΔI_0 is the difference between the averaged intensity during the three days just before the storm and the daily mean intensity on the day of intensity minimum, calculated from the data observed at Cheltenham. Among the materials ready to our hands, 13 storms were available by this criterion, as shown in Table I and II.

Table I Cosmic-ray storms

No.	Period (U.T.) used in the analysis	Date of S.C. (U.T.) of magnetic storm	ΔI_0 %
1	Apr. 16—May. 10, 1937	Apr. 24, 25, 26	3.3
2	Jan. 10—Jan. 31, 1938	Jan. 16, 17,* 22, 25	5.8
3	Apr. 20—Apr. 28, 1939	Apr. 23, 24	2.9
4	May. 3—May. 11, 1939	May. 5	3.0
5	Aug. 9—Aug. 20, 1939	Aug. 11, 12	2.4
6	Mar. 27—Apr. 5, 1940	Mar. 29	2.0
7	Feb. 26—Mar. 9, 1941	Mar. 1	2.6
8	Feb. 26—Mar. 6, 1942	Mar. 1	6.0
9	Feb. 1—Feb. 14, 1946	Feb. 7	6.1
10	May. 1—May. 20, 1946	May. 6	2.0
11	Jul. 26—Jul. 30, 1946	Jul. 26	6.3
12	Jan. 24—Jan. 29, 1949	Jan. 24	3.0
13	Apr. 12—Apr. 15, 1949	Apr. 12	3.0

* Gradual commencement

* Contribution of Geophysical Papers dedicated to Prof. M. Hasegawa on his sixtieth birthday.

Table II Cosmic-ray stations

Abbreviation	Station	Longitude	Geomagnetic Latitude	Altitude	Equipment	Reference
H	Huancayo	75.3°W	0.6° S	3350m	I.C. model C meter	(5) (7)
Ec	East China Sea	124 E	22 N	sea level	I.C. Neher type	(6)
T_1	Tokyo	139.8 E	25.4 N	sea level	I.C. Neher type	(7)
T_2					I.C. Steinke type	(7)
T_3					I.C. Nishina type	(6) (7)
T_4					C.T. ±85°	(7)
Te	Teoloyucan	99.2 W	29.7 N	2285	I.C. model C meter	(8) (9)
Ca	Canberra	141 E	45 S	800	I.C. volume 17.6^l	(10)
Ha_1	Hafelekar	11.3 E	48.4 N	2300	I.C. Steinke type	(11)
Ha_2					C.T.	(11)
Ch	Christchurch	172.6 E	48.6 S	sea level	I.C. model C meter	(5) (8) (13)
F	Friedrichshafen	9.3 E	49.0 N	sea level	C.T.	(7)
C	Cheltenham	76.8 W	50.1 N	sea level	I.C. model C meter	(5) (7) (8)
B	Boston	71 W	54 N		I.C. model C meter	(14)
M	Manchester	0	56.5 N	sea level	C.T. ±60°	(7) (15)
Be	Bergen	5 E	61 N	sea level	C.T.	(16)
G	Godhavn	53.5 W	79.9 N	sea level	I.C. model C meter	(5) (8)

C.T.: Counter telescope I.C.: Ionization chamber

2) In order to decrease the error due to the local slow variation, such as the atmospheric effect, especially the temperature effect, only a short period including each storm was subjected to the analysis (see Table I).

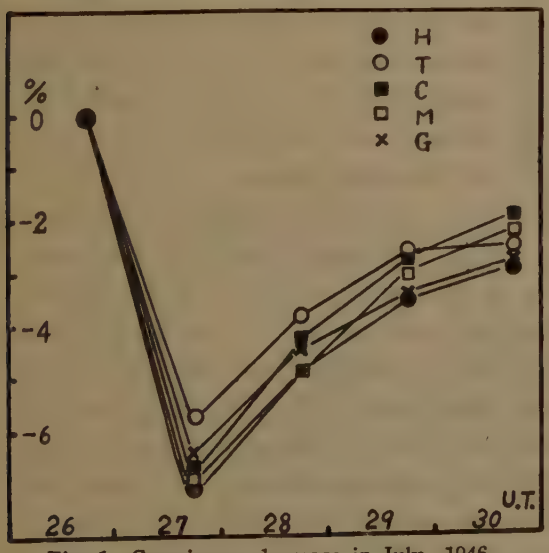

Fig. 1 Cosmic-ray decrease in July, 1946. observed at various stations.

3) In order to decrease the error due to the variation in cosmic-ray anisotropy during the storm,[7] observations at various stations were arranged in the universal time (U.T.), and the simultaneous 24-hour averaged intensities were treated as a set of data.

As an example of the procedure, the day-to-day plot of a cosmic-ray storm is shown in Fig. 1. The correlation diagrams between the decrease at a certain station and that at Cheltenham are shown in Fig. 2. From each of diagrams, the correlation coefficient r, the constant factor k, and the probable error of k (small sample) were calculated, and shown in Table III together with the results from the other storms. The factor k may be considered as the ratio of the decrease (ΔI) at a certain station

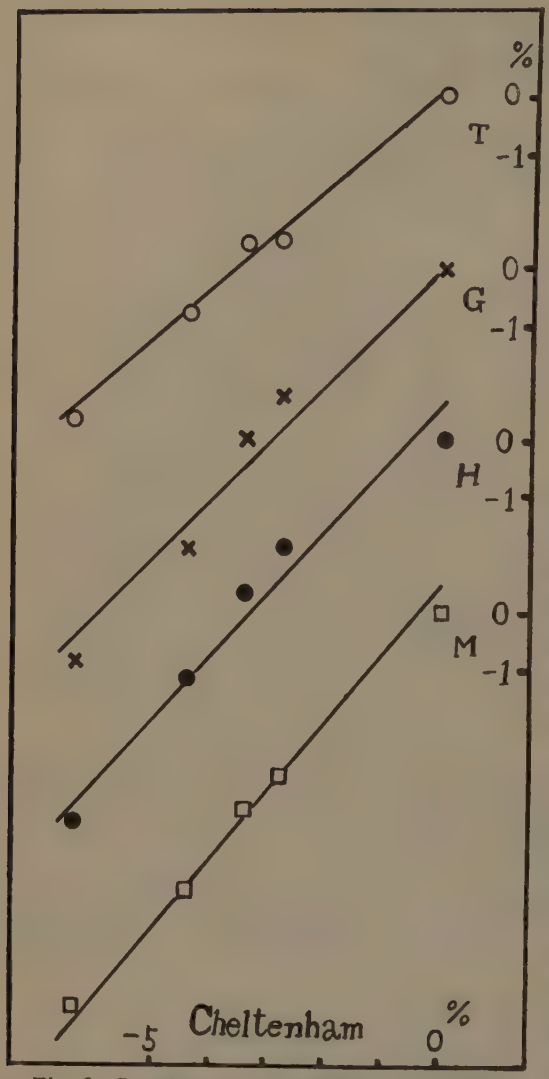

Fig. 2 Correlation of cosmic-ray decreases observed at pairs of stations, in July, 1946.

Table III (uncorrected for altitude effect)

No.	H		Ec			T		
	r	k	r	k		r	k	r
1	.96	0.99±.04						.97
2	.90	0.78±.07	.86	0.87±.10	2	.94	0.73±.06	
3	.94	0.84±.09						
4	.97	0.73±.06						
5	.93	0.81±.08						
6	.83	0.88±.15			3	.72	0.80±.10	
7	.76	0.89±.17						
8	.97	0.93±.02			3	.89	0.91±.08	.97
9	.99	0.80±.03						
10	.83	1.08±.10						
11	.98	1.08±.07			1	.99	0.88±.05	
12	.96	1.00±.07			4	.97	0.95±.06	
13	.98	0.79±.08			4	.99	0.82±.06	
mean		0.89±.07					0.85±.05	

to that at Cheltenham. k-values or their average obtained at each geomagnetic latitude are shown in Fig. 3. The averaged point is the weighted mean of k-values obtained at the same latitude on individual storms, were the weight is the accuracy of individual k-value. The sign of error attached to the averaged point is the unbiased dispersion among the individual k-values, the weight being taken into account. The curves are the result of Nagashima's theory,[2] corresponding to his two extreme assumptions.

From this figure, it can be seen that the latitude effect is in accordance with Nagashima's electric field theory, even if the result of high altitude stations (Huancayo, Teoloyucan, Canberra and Hafelekar) are omitted. There are sea level stations at about the same geomagnetic latitudes as those of high altitude stations respectively, except Huancayo. The altitude effect obtained from the comparison of these pairs of stations are listed in Table IV, together with the values expected from Nagashima's theory. The observed effect is not appreciably different from the theoretical result. For the four high altitude stations, the correction for the altitude effect were done according to Nagashima's theory, using the average of the two values obtained from his extreme assumptions respectively, and both of the corrected and uncorrected values are shown in Fig. 3. The corrected values and the sea level observations make a nearly smooth curve of the latitude effect. Thus, Nagashima's

Cheltenham : $k=1$

Te	Ca		Ha		Ch		F		B		M		Be		G	
k	*r*	*k*	*r*	*k*	*r*	*k*	*r*	*k*	*r*	*k*	*r*	*k*	*r*	*k*	*r*	*k*
1.35±.07	.87	1.13±.08	1 .98	1.30±.05	.91	1.19±.09										
			2 .91	1.29±.05												
	.95	0.91±.04	1 .91	1.41±.09	.99	0.57±.02			.94	0.97±.06						
	.98	0.76±.05			.94	0.96±.09									.97	0.94±.09
	.97	0.76±.06			.93	0.41±.09									.84	1.15±.16
	.85	0.91±.13			.29	0.99±.67									.96	0.95±.06
	.92	1.48±.12			.90	1.11±.11									.93	1.28±.09
															.90	0.97±.10
1.10±.02					.90	0.67±.08	.97	1.13±.03							.99	1.05±.04
															.97	1.08±.04
															.89	1.67±.08
											.92	1.15±.15			.99	1.06±.06
					.85	0.83±.15					.78	1.02±.19	.94	1.02±.21		
											.94	0.96±.15				
1.18±.03		0.94±.15		1.33±.03		0.92±.21						1.06±.07				1.12±.13

No. : see Table I

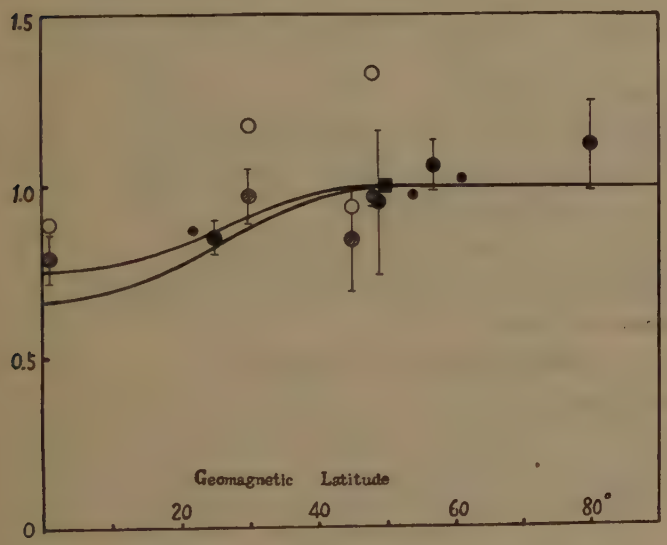

Fig. 3 Latitude effect of the cosmic-ray decrease.
●◕○ Average of *k*-values obtained at the same latitude
• *k*-value obtained for a single storm
○ High altitude station, uncorrected
◕ Corrected for the altitude effect
■ Normalization point (Cheltenham)

Table IV Altitude effect

Stations			Altitude effect		
Geomagnetic latitude	high altitude (h)	sea level (s)	observed k_h/k_s	theoretical assumption I.	assumption II.
30°–25°	Teoloyucan (2285)m	Tokyo	1.39±.06	1.30	1.15
48 –50	Hafelekar (2300)	Cheltenham	1.33±.03	1.45	1.30
45 –50	Canberra (800)	Cheltenham	0.94±.15	1.15	1.09

electric field theory may be considered to be able to explain the latitude effect and also the altitude effect of the intensity decrease in the cosmic-ray storm.

This work suported by the scientic research found of Ministry of Education. The authors wish to express their sincere thanks to Dr. J.W. Beagley of the Christ-

church observatory and Mr. Y. Miyazaki of the Scientific Research Institute for his prompt supply of available data, and to Professor Y. Sekido, Mr. K. Nagashima and the members of the working association of primary cosmic-ray research for their valuable discussions.

(Read Oct. 29, 1953)

Refercences

(1) K. Nagashima: J. Geomag. Geoel. Japan. **3**, 100 (1951)
(2) K. Nagashima: J. Geomag. Geoel. Japan. this issue (1953)
(3) S.E. Forbush: Phys. Rev., **54**, 975 (1938)
(4) M. Wada: Report of the Cosmic-ray Laboratory, Scientific Research Institute (Japan), **1**, 81 (1952)
(5) I. Lange, S.E. Forbush: "Cosmic-Ray Results from Huancayo Observatory" (1948)
(6) Y. Miyazaki: Private communication from the Scientic Research Institute.
(7) Y. Sekido, S. Yoshida, Y. Kamiya: Report of Ionosphere Research in Japan **6**, 195 (1952)
(8) S.E. Forbush: Terr. Mag. **43**, 203 (1938)
(9) S.E. Forbush, T.B. Stinchdomb, M. Schein: Phys. Rev. **79**, 501 (1950)
(10) A.R. Hogg: "Measurements of the Intensity of Cosmic Ray" (1949)
(11) V.F. Hess, A. Demmelmair: Nature **140**, 316 (1937)
(12) V.F. Hess, R. Steinmaurer, A. Dimmelmair: Nature **141**, 689 (1938)
(13) J.W. Beagley: Private communication from the Christchurch Observatory
(14) S.E. Forbush: Terr. Mag. **43**, 207 (1938)
(15) H. Elliot, D.W.N. Dolbear: J. Atmos. Terr. Phys., **1**, 205 (1951)
(16) B. Trumpy: Phsica **19**, 654 (1953)

The World-Wide Variation of Cosmic Ray Intensity by the Electro-Magnetic Field*

By Kazuo NAGASHIMA
Earth Science, Kyoto University

Abstract

The variation of cosmic ray intensity by the static electric field surrounding the earth was calculated in a previous paper.[1] In it a greater advantage was indicated in explaining the cosmic ray intensity decrease at the time of the magnetic storm by the electric field hypothesis than by the magnetic field hypothesis suggested by S. Chapman.[2] In the present paper, the intensity variations of the ionizing and neutron components produced by the variation of the static electric field are calculated in detail extending over various altitudes and latitudes. By comparing these calculations with observations, it can be concluded that this electric field hypothesis is possible in explaining the phenomenon of the world-wide variations in intensity pointed out recently by various authors.[3],[4]

It may be possible that the diurnal variation of cosmic ray intensity can be produced by an electric field not derived from potential.

Introduction

Up to date, various types of cosmic ray intensity variation have been reported. Among these, the present paper is concerned with the following:

[A] The world-wide variation of cosmic ray intensity (not dependent on local time). This involves the following phenomena:

(a) The world-wide decrease of cosmic ray intensity at the time of the cosmic ray storm.[5]

(b) The world-wide fluctuations of cosmic ray intensity.[3],[4]

[B] The diurnal variation of cosmic ray intensity.

In order to explain phenomenon [A], any theory or hypothesis must correspond the following conditions:

[I] The variation is world-wide.

[II] The latitude dependence of the variation.

Based on his experiments,[3] H.V. Neher pointed out that:

(1) The changes in the ionizing component at sea level are nearly independent of latitude.

---

* Contributed to Geophysical Papers dedicated to Prof. M. Hasegawa on his sixtieth birthday.

(2) The changes in the ionizing component increase with the increase of latitude.

[III] The altitude dependence of the variation.

(1) The fluctuations in the ionizing component at high altitudes are larger than at intermediate altitudes or at ground level.[3]

(2) The changes in the neutron component are several times those of the ionizing component.[3),(6),(23)]

It was pointed out in a previous paper[1] that the variation of electric potential on the earth causes such world-wide variations in cosmic ray intensity, and suggested that the comparison between the variations at different stations would be a key towards determining the true cause of the production of such a world-wide variation. Recently, according to this electric field hypothesis, W.H. Fonger explained the phenomenon (2) in [III].[6] But, to explain all the above mentioned phenomena by this electric field hypothesis, it is necessary to calculate the cosmic ray intensity variations, produced by the electric field, over various altitudes and latitudes, more precisely.

In § 1, the general formula of the cosmic ray intensity variation which is produced by the static electric and magnetic field is discussed. Generally, in such a static electric and magnetic field, the cosmic ray intensity variation is due not only to the variation of the primary differential intensity spectrum caused by the variation of the static electric field but also to the variation of the cut-off energy (see § 1) caused by the variation of the static electric and magnetic field. In § 2, neglecting the influence of the variation of cut-off energy, there is calculated the intensity variation which is produced by the variation of the static electric field. The variation of cut-off energy cannot be determined unless the state of the static electric and magnetic field surrounding the earth is known. In case of a simple model of the field, the variation can be obtained analytically and is discussed in App. I. But the altitude curve of the intensity variation caused by the variation of cut-off energy can be obtained without such a model of the field and is discussed in § 3. In § 4, comparisons of the intensity variations calculated theoretically in § 2 and § 3 are made with those obtained by observation.

The diurnal variation of cosmic ray intensity is a world-wide phenomenon which is dependent on local time. The solar magnetic field theory was advocated by M.S. Vallarta[7] to explain this phenomenon, but at low latitudes this theory seems to be inadequate. In § 5, the possibility of explaining this phenomenon by the electric field hypothesis is discussed, although the origin of the electric field cannot be pointed out.

§ 1. The General Formula of Cosmic Ray Intensity Variation by the Static Electric and Magnetic Field

Let $N(\lambda, x)$ denote the directional cosmic ray intensity, observed at geomagnetic latitude λ° and atmospheric depth $x\,\mathrm{g\,cm^{-2}}$, and the following relation holds at the normal state;

$$N(\lambda, x)=\sum_{A}\int_{E_{\lambda, A, Z}}^{\infty} m_{A, Z}(E, x)\cdot i_{A, Z}(E)dE, \cdots\cdots \quad (1)$$

where $i_{A,Z}(E)$ is the primary differential intensity spectrum of the nucleus, its atomic number A and its charge number Z, and E is the kinetic energy per nucleon. $m_{A,Z}(E, x)$ is the number of secondary particles at $x\,\mathrm{g\,cm^{-2}}$ produced by one of the primary cosmic rays whose kinetic energy is E per nucleon and called the over-all multiplicity.[8] $E_{\lambda, A, Z}$ denotes the minimum kinetic energy per nucleon of primary particle which can be injected upon the earth at λ° from a given direction and is called the cut-off energy.

Strictly speaking, the formula of Eq. (1) is not correct because it may happen that the primary spectrum might in some way be interrupted in some energy region, and consequently $N(\lambda, x)$ cannot be expressed by only the upper and lower limits of integral in Eq. (1). For example, such a situation occurs when we intend to explain the diurnal variation of cosmic ray intensity by the solar magnetic field.[7],[9] In such a case, however, Eq. (1) can be easily expanded. The case chiefly discussed here is one where Eq. (1) holds.

If the state of the static electric and magnetic field surrounding the earth varies from the normal state, then, by the influence of this variation, the primary cosmic ray, reaching the earth, loses its energy to an amount of ΔE per nucleon, where

$$\Delta E=\frac{Z}{A}e\Delta\phi. \quad \cdots\cdots\cdots \quad (2)$$

$\Delta\phi$ is the variation of the earth's electric potential relative to the normal state. In this case, Eq. (1) changes as follows,

$$N(\lambda, x, \Delta E, \delta E_{\lambda})=\sum_{A}\int_{E_{\lambda, A, Z}+\delta E_{\lambda, A, Z}}^{\infty} m_{A, Z}(E, x)[1-L(E+\Delta E, \Delta E)]\cdot i_{A, Z}(E+\Delta E)dE, \cdots (3)$$

where $L(E, \Delta E)$ is Liouville's effect[1],[10] and given by Eq. (4).

$$L(E, \Delta E)=\frac{2(E+m_0c^2)\Delta E-(\Delta E)^2}{(E+m_0c^2)^2-(m_0c^2)^2}, \quad \cdots\cdots\cdots \quad (4)$$

where m_0c^2 is the rest energy per nucleon. In Eq. (3), $\delta E_{\lambda, A, Z}$ is the variation of cut-off energy, which is caused not only by the variation of the magnetic field but also by the variation of the electric field and cannot be uniquely determined unless the state of the electro-magnetic field is determined. δE_{λ} in the parenthesis on the left hand side of Eq. (3) denotes the occurrence of the variation of cut-off energy. On the contrary, the variation of the primary spectrum in Eq. (3) is determined if only the electric field is derived from potential[12] and is independent of the form of the static electric and magnetic field. More generally, the static magnetic field which is not symmetrical to the earth's magnetic dipole axis could change the primary spectrum in the low energy region. For example, we see that the solar magnetic field produces such a situation if we consider that, as pointed out above, the solar magnetic field[7],[9] has an agency to interrupt the primary spectrum in some energy region, and

moreover that the primary particles exist in some degree in such an interrupted energy region of the primary spectrum because, as pointed out by H. Alfven[13] and and J.A. Wheeler et al.,[14] there exist the primary particles in the forbidden region of the solar magnetic field. The intensity variation produced by such a static magnetic field depends on local time, so we will discuss this in § 5, and not consider it here.

The intensity variation relative to the normal state is defined by

$$y(\lambda, x, \Delta E, \delta E)=\frac{N(\lambda, x)-N(\lambda, x, \Delta E, \delta E_\lambda)}{N(\lambda, x)}. \quad \cdots\cdots\cdots \quad (5)$$

As seen from Eqs. (5) and (3), y is not proportional to ΔE.[11]

As mentioned above, the causes which produce the variation y, are divided into two classes as follows: (1) the variation of primary spectrum which is produced by the variation of electric potential and (2) the variation of cut-off energy which is produced by the variation of static electric and magnetic field. Hereafter, an examination is to be made of the variation y by these two causes individually.

§ 2. The Cosmic Ray Intensity Variation by the Static Electric Field (not considering the Variation of Cut-Off Energy)

Recently, the existence of heavy particles in the primary cosmic rays has been pointed out.[16] But, as their intensity spectrums in the high energy region are not yet well known, we assume that all the primary particles consist of protons only and adopt as its intensity spectrum that produced by H.V. Neher.[3),(16]

$$\left.\begin{aligned} i(E)dE&=\frac{0.048}{E^{2/3}(1+0.09E^{-1/3})^{3/2}}\,dE, \quad (E\geq E_g=0.8Bev.)\\ &=0, \qquad\qquad\qquad\qquad (E<E_g)\end{aligned}\right\} \quad \cdots\cdots\cdots \quad (6)$$

where E_g is the energy, in the lower energy region than which the primary particles do not exist, and is called hereafter the general cut-off energy to avoid being confused with the cut-off energy E_λ. This spectrum leads to a smaller absolute value of intensity compared to that observed by others.[17] But, it only is necessary that the distribution of the primary spectrum is correct and it is not necessary that the absolute value of intensity is correct, because the variation y in Eq. (5) depends only upon the distribution, but not upon the absolute value. In this point, it is reasonable to adopt the above spectrum.

Neglecting the variation of cut-off energy, and considering only the vertical cosmic ray intensity, Eqs. (1) and (3) becomes as follows,

$$N(\lambda, x)=\int_{E_\lambda}^{\infty} m(E, x)\cdot i(E)dE, \quad \cdots\cdots\cdots \quad (7)$$

$$N(\lambda, x, \Delta E, 0)=\int_{E_\lambda}^{\infty} m(E, x)[1-L(E+\Delta E, \Delta E)]\cdot i(E+\Delta E)\,dE, \quad \cdots\cdots\cdots \quad (8)$$

where E_λ denotes the cut-off energy of cosmic rays which are incident upon the earth at λ° from the vertical direction. To calculate y in Eq. (5), it is necessary to know the over-all multiplicity $m(E, x)$. By making an assumption that $m(E, x)$ is proportional to E^a, where a is constant, it is possible to obtain $m(E, x)$ of the ionizing and

neutron components by using the observations made by H.V. Neher and J.A. Simpson et al., respectively (see App. II). The results obtained are shown in Figs. 1 and 2, and in Table I. Two different $m(E, 1030)$ of the ionizing component are tabulated in Table I. These over-all multiplicities are those of the two extreme cases estimated on the basis of assumption (see App. II). The full lines in Figs. 1 and 2 denote the over-all multiplicities obtained directly from the observations without any assumption and E_c in Table I is the critical energy at which the distribution of $m(E, x)$ changes.

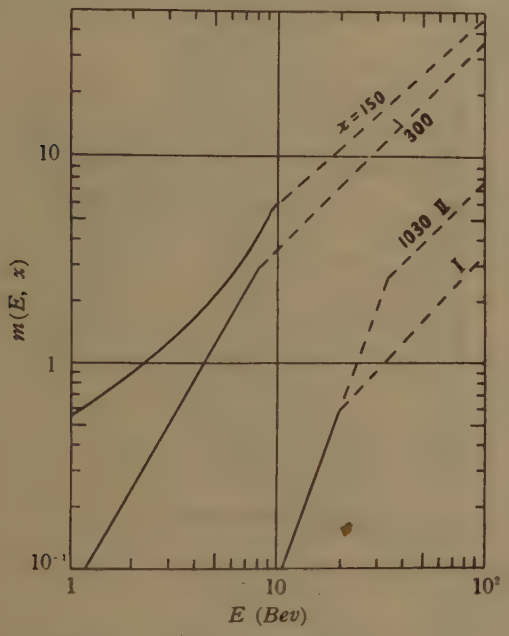

Fig. 1 Over-all multiplicity of the ionizing component.

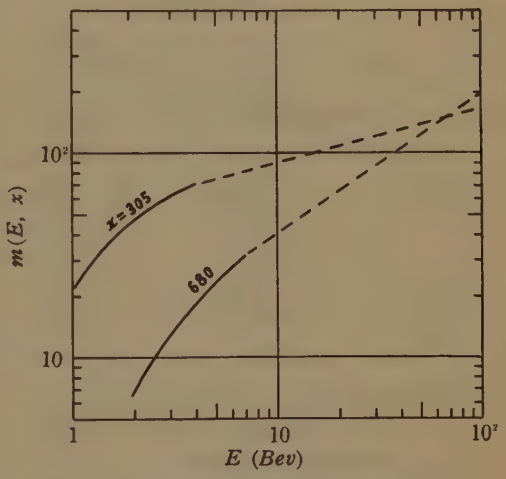

Fig. 2 Over-all multiplicity of the neutron component.

Table I $m(E, x)$

	x (g cm^{-2})		$m(E, x)$ $(E<E_c)$	E_c (Bev.)	$m(E, x)$ $(E\geqq E_c)$
ionizing component	0		1		1
	150		See Fig. 1.	10	$6.1\cdot\left(\frac{E}{E_c}\right)^{0.9}$
	300		$7.4\cdot10^{-2}\cdot E^{1.8}$	8.2	$3.0\cdot\left(\frac{E}{E_c}\right)^{1.0}$
	1030	I	$1.3\cdot10^{-1}\cdot E^{2.8}$	15	$2.8\cdot10^{-1}\cdot\left(\frac{E}{E_c}\right)^{1.3}$
		II	$1.3\cdot10^{-1}\cdot E^{2.8}$	23.1	$9.5\cdot10^{-1}\cdot\left(\frac{E}{E_c}\right)^{1.0}$
neutron component	305		See Fig. 2.	4	$50\cdot E^{0.26}$
	680	*	See Fig. 2.	7	$8.6\cdot E^{0.68}$

* (This over-all multiplicity was oftained from the latitude curve of intensity normalized to unity at the equator.)

In Figs. 3 and 4, the functions of $n(E, x)=m(E, x)\,i(E)$ of the ionizing and neutron components are shown respectively and normalized to unity at $E=10\,Bev.$ to facilitate their mutual comparison.

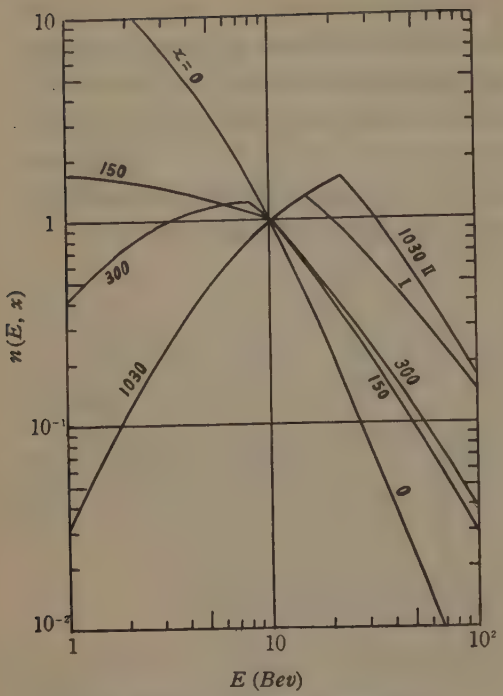

Fig. 3 Relative intensity spectrum, $n(E, x)=m(E, x)\cdot i(E)$, of the ionizing component.

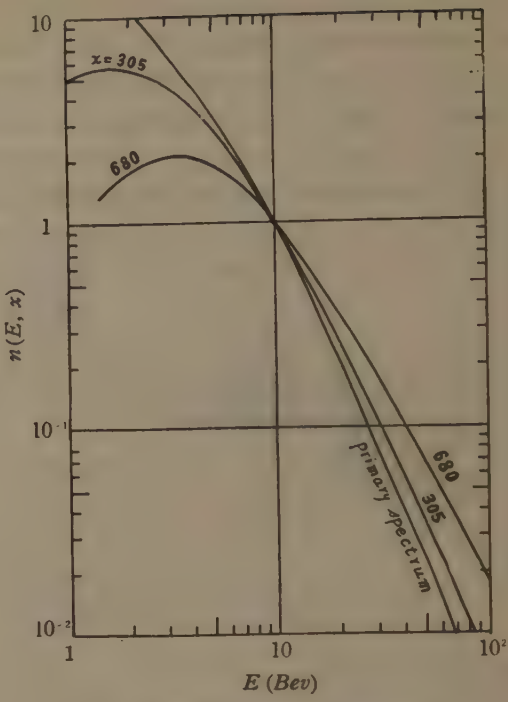

Fig. 4 Relative intensity spectrum, $n(E, x)=m(E, x)\cdot i(E)$, of the neutron component.

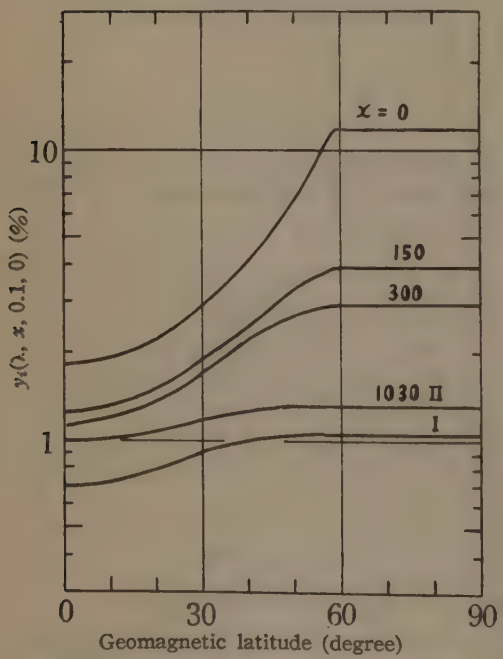

Fig. 5 Latitude dependence of y of the ionizing component by the variation of the static electric field.

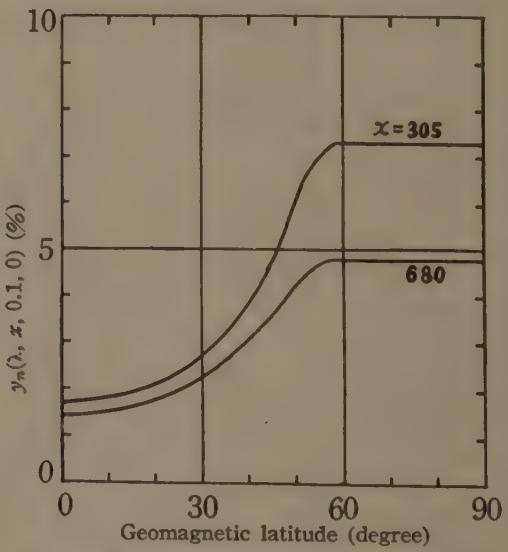

Fig. 6 Latitude depeddence of y of the neutron component by the variation of static electric field.

By using these over-all multiplicities and the primary spectrum given by Eq. (6), it is possible to calculate $y(\lambda, x, \Delta E, 0)$. Figs. 5 and 6 show the latitude curves of y of the ionizing and neutron components at various altitudes in case $\Delta E = 0.1\,Bev$. In these figures, the subscripts i and n of y represent the ionizing and neutron components respectively.

The altitude curves of y at various latitudes are obtained by drawing the smoothed curves through the calculated points and shown in Figs. 7 and 8. In Fig. 7, the curves of the ionizing component are normalized to unity at $x=0$.

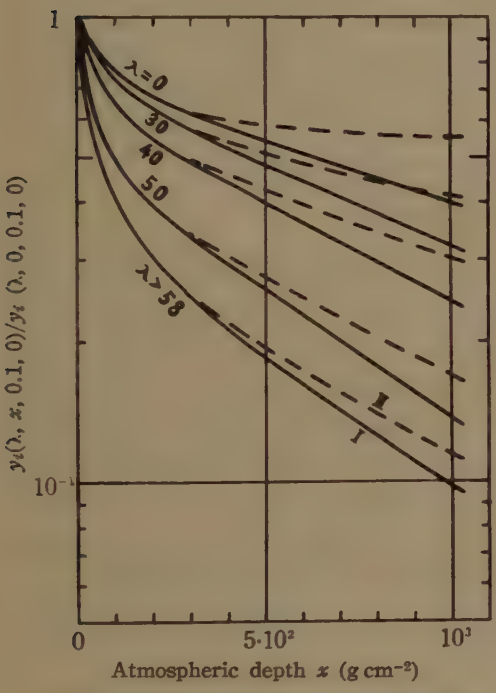

Fig. 7 Altitude dependence of y of the ionizing component by the variation of the static electric field.

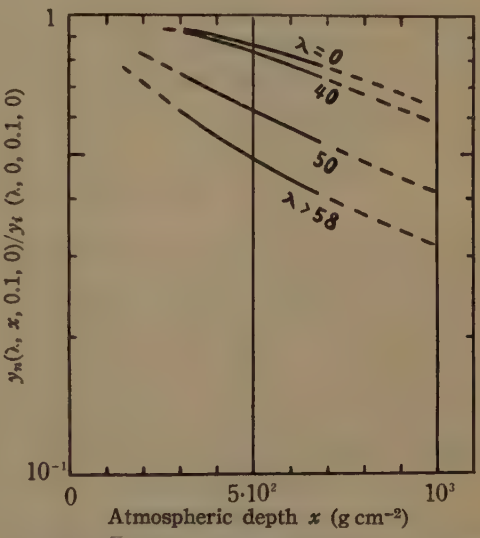

Fig. 8 Altitude dependence or y of the neutron component by the variation of the static electric field.

The variation of the neutron component is produced by the variation of the primary ionizing particles which is caused by the variation of the electric field, so that the curves of the neutron component are normalized so as to satisfy the condition that the variation of the primary particles becomes just to unity. J.A. Simpson et al.[18] reported that, in the atmospheric depth greater than 600 g cm^{-2}, there were no differences in the latitude dependence of the neutron intensity. If so, the variation y of the neutron component must be independent on altitude in such a region. On the contrary, Fig. 8 obtained by drawing the smoothed curves through the calculated points shows that y decreases slowly with the increase of x in such a region. This discrepancy between the theoretical and experimentally expected curves might be due to a lack of the calculated points.

§ 3. The Cosmic Ray Intensity Variation by the Variation of Cut-Off Energy

As discussed in § 1, the variation of cut-off energy is another cause which produces the cosmic ray intensity variation, and cannot be uniquely determined unless the state of the static electric and magnetic field surrounding the earth is determined. Even if the state is determined, it is still difficult to obtain the variation of cut-off energy. In App. I, this problem is treated in a simple case when the static electric and magnetic field is symmetrical to the earth's magnetic dipole axis.

The latitude curve of y cannot be obtained when the variation of cut-off energy is not known as a function of latitude, but it is possible to obtain the altitude curve of y if only $N(\lambda, x)$ can be known from the observations. If the cut-off energy E_λ changes to $E_\lambda+\delta E_\lambda$ by the influence of the static electric and magnetic field, y in Eq. (5) becomes as follows,

$$y(\lambda, x, 0, \delta E_\lambda) = \frac{\int_{E_\lambda}^{E_\lambda+\delta E_\lambda} m(E, x)\, i(E)\, dE}{N(\lambda, x)}. \quad \cdots\cdots \qquad (9)$$

Figs. 9 and 10 represent the variation y at various altitudes and latitudes in case $\delta E_\lambda = 0.1$ *Bev*. Care must be taken that, as mentioned above, these curves do not represent those of the latitude effect of y, different from those in Figs. 5 and 6. At high latitudes, $y=0$ as shown in Figs. 9 and 10. This phenomenon is partly due to the fact that there are no primary cosmic rays in the lower energy region other than the general cut-off energy E_g and partly to the fact that at the low atmosphere there is the knee of the latitude effect of cosmic ray intensity produced by atmospheric absorption. But if δE_λ becomes very large under the influence of some mechanism even in such high latitudes, the variation y occurs as well as at low latitudes.

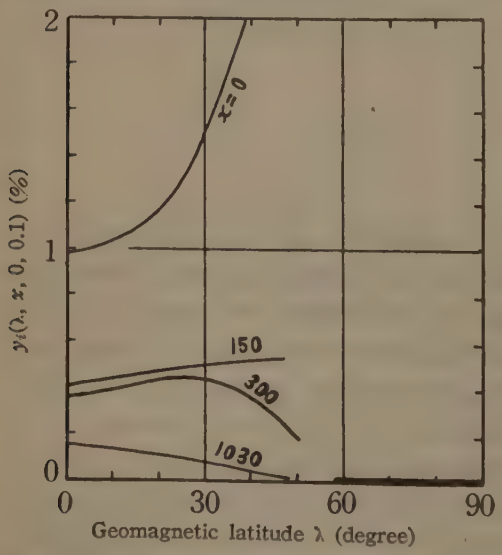

Fig. 9 Variation, y, of the ionizing component by the variation of the cut-off energy.

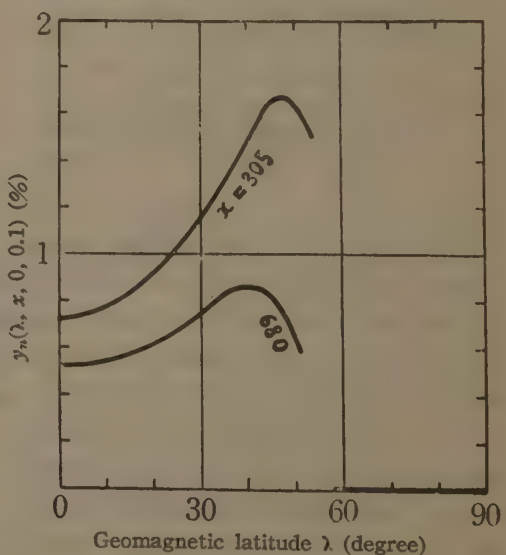

Fig. 10 Variation, y, of the neutron component by the variation of the cut-off energy.

Figs. 11 and 12 show the altitude curves of y produced by the variation of cut-off energy. The normalization is quite similar to that adopted in case of Figs. 7 and 8. As seen from Figs. 7, 8, 11 and 12, the altitude curves, in case of the variation of cut-off energy, decrease more rapidly with the increase of x, compared with those in case of the variation of electric field. Such a difference is caused by the fact that, in the former case, only the low energy particles are excluded; in the latter case, on the contrary, all the particles are influenced by the electric field.

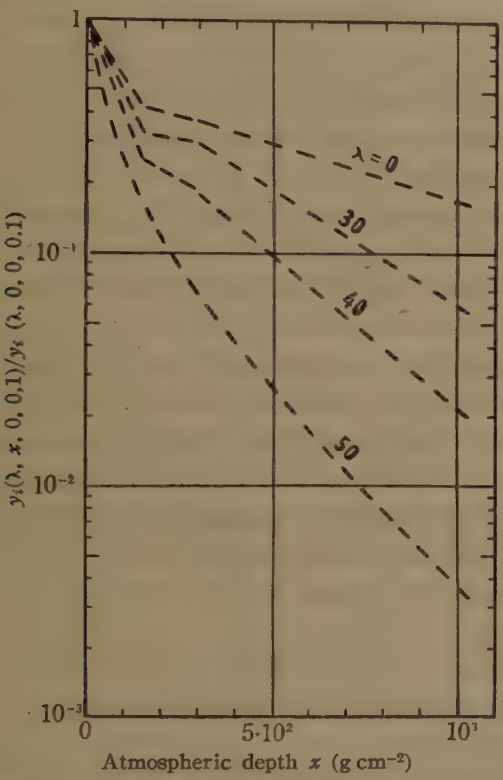

Fig. 11 Altitude dependence of y of the ionizing component by the variation of the cut-off energy.

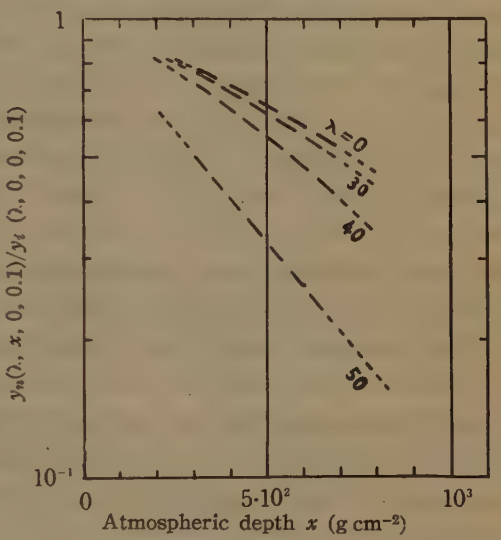

Fig. 12 Altitude dependence of y of the neutron component by the variation of the cut-off energy.

§ 4. Comparison with Observations and Discussion

Based on the calculations in § 2 and § 3, we consider which variation of either the electric field or the cut-off energy is best suited to explain the world-wide variation of cosmic ray intensity (not dependent on local time) which has three characteristics as cited in the Introduction.

[I] The variation is world-wide.

In case of the electric field:—This can be explained if only the potential on the earth varies. Moreover, as pointed out by H.V. Neher,[3] the fluctuation in intensity must be the same all over the knee of the latitude curve of intensity. This phenomenon can be also explained, independent of the formation of the knee, as shown in Figs. 5 and 6.

In case of the cut-off energy:—At low latitudes, the changes occur without any condition if the state of the static electric and magnetic field varies, but some difficulty arises in high latitudes. As pointed out by various authors,[1),6),19)] the change cannot be produced over the knee by the variation of the cut-off energy. They are right if the static electric and magnetic field is symmetrical to the earth's magnetic dipole axis,[3)] since such a field, however large, does not produce any variation of cut-off energy near the magnetic poles and then does not satisfy the condition that the variation must be the same all over the knee. On the contrary, if we consider the field not to be symmetrical to the earth's magnetic dipole axis, such a field has the possiblity of satisfying the above mentioned condition. The reason is that this field, a simple example of which is the solar magnetic field, has an agency to cut off the low energy region of the primary spectrum,[20)] so that, if such a field is produced or changed by some mechanism, the general cut-off energy E_g is changed and then the intensity variation is produced and is the same all over the knee. But a difficulty arises even in such a case; at the normal state, the knee at low altitude is caused by the atmospheric absorption and not by the general cut-off energy E_g, so that, in expectation of the intensity decrease over the knee at such a low altitude, the general cut-off energy must become greater than the cut-off energy E_λ at the latitude where the knee at low altitude begins. If such a variation of E_g is produced, the latitudes, at which the knees at various altitudes begin, must become constant. Such a phenomenon has not yet been reported. Moreover, we cannot expected any intensity increase from the normal state over the knee at low altitude by such a field, since the decrease of E_g gives no influence upon the intensity over the knee at low altitude.

As discussed above, it seems to be difficult to explain the phenomenon [I] by the variation of cut-off energy, although there is some slight possibility of doing so.

[II] The latitude dependence of the variation

Up to date, not much has yet been done about the latitude effect of the world-wide variation at sea level. This is due to the following difficulties: (1) The observation stations are not located at the same altitude, (2) each station is located at different longitude and (3) the type of the cosmic ray meter is different at each station. As we know nothing about these corrections for the variation, the true latitude dependence of y at sea level cannot be obtained. In these corrections, (1) gives the most important influence upon the latitude dependence of y.

In case of the electric field:—Keeping the above in mind, we discuss the latitude dependence of y, based on the observed results obtained by several authors.[4),6),21),22)] The relative values of y_t at each station, normalized to that at Cheltenham, are shown in Table II. As seen from this table, at some stations, there are some differences between the values obtained by these authors. For example, the value at Teoloyucan obtained by S.E. Forbush is exceedingly larger than that obtained by S. Yoshida and Y. Kamiya, and another example is that the value at Freiburg is extremely small compared to the values at other stations which are located at the

same altitude and nearly the same latitude as Freiburg. On the other hand, it is a remarkable point that at Huancayo there is quite a good agreement between them. To compare these data with the theoretical latitude curve of y_i in Fig. 5, it is necessary to make the altitude correction to the values at several stations (i.e. Huancayo, Teoloyucan, Canberra and Hafelekar).

Table II Relative value of y_i at each station normalized to that at Cheltenham and not correted the altitude effect.

No. Station	Geomagn. Latitude	Height above sea level (m)	Relative value of y_i obtained by			
			S. Yoshida[21]* Y. Kamiya	M. Wada[22]*	S.E. Forbush[4]	W.H. Fonger[6] §
1 Godhavn	80°N		1.12±.13	0.97		
2 Bergen	61 N		1.02			
3 Manchester	57 N		1.06±.07			
4 Boston	54 N		0.97			
5 Cheltenham	50 N		1.00	1.00	1.00	1.00
6 Christchurch	49 S		0.95±.21		0.95	
7 Friedrichshafen	49 N					
8 Freiburg	49 N					0.77
9 Hafelekar	48 N	2300	1.33±.03		1.43	
10 Canberra	45 S	800	0.94±.15			
11 Teoloyucan	30 N	2285	1.18±.08		1.42	
12 Tokyo	25 N		0.85±.05	0.93		
13 East China Sea	22 N		0.87			
14 Huancayo	1 S	3350	0.89±.07	0.92	0.90	0.91

* The values in this column were obtained from the data of cosmic ray storms.
§ The values in this column were obtained from the data of 27-day variations.

Let $c_j(\lambda, x'-x, \Delta E, 0)$ denote the altitude correction factor to alter y_j at x to that at x', and the following relation holds

$$y_i(\lambda, 1030, \Delta E, 0)=c_j(\lambda, 1030-x, \Delta E, 0)\, y_j(\lambda, x, \Delta E, 0). \quad (j=i \text{ or } n) \quad \cdots\cdot(10)$$

c_j is obtained theoretically by using the altitude curve of y_j as shown in Figs. 7 and 8, and is listed in the 4th and 5th columns of Table III for each station in case $j=i$ and $\Delta E=0.1$ *Bev*.

Using the altitude correction factor c_i^I, we can obtain the experimental relative value of y_i at sea level. The results are shown in Fig. 13 together with the latitude curve of y_i^I $(\lambda, 1030, 0.1, 0)$ obtained theoretically. As seen from this figure, there is a fairly good agreement between the observations and the theoretical curve, although the

Table III Altitude correction factor $c_i(\lambda, 1030-x, 0.1, 0)$

Station	Geomagn. Latitude	Height above sea level (m)	c_i^I *	c_i^{II} *	Observed value of c_i [21]
Boulder	49°N	1600	0.77	0.83	
Climax	48 N	3500	0.60	0.70	
Hafelekar	48 N	2300	0.69	0.77	0.71 (Cheltenham/Hafelekar)
Bagnéres	46 N	550	0.94	0.95	
Canberra	45 S	800	0.87	0.92	1.06 (Cheltenham/Canberra)
Teoloyucan	30 N	2285	0.77	0.87	0.725 (Tokyo/Teoloyucan)
Huancayo	1 S	3350	0.80	0.96	

* I and II denote the correction factors obtained by using the value y_i^I $(\lambda, 1030, 0.1, 0)$ and y_i^{II} $(\lambda, 1030, 0.1, 0)$ respectively, as shown in Figs. 5 and 7.

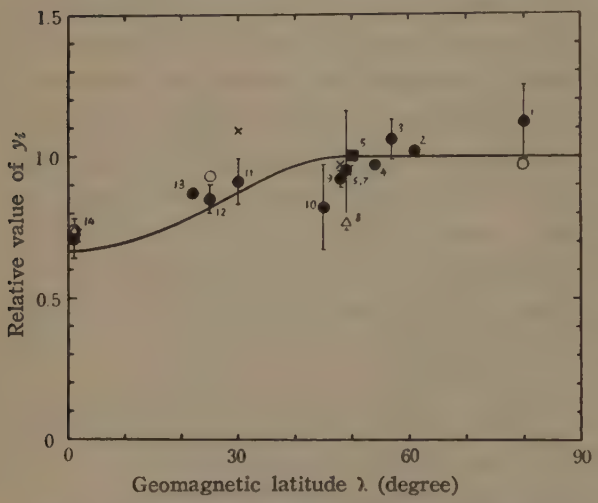

Fig. 13 Latitude dependence of y_i at sea level, normalized to that at Cheltenham. Numbers denote Stations in Table III.
● S. Yoshida and Y. Kamiya
○ M. Wada
× S.E. Forbush
△ W.H. Fonger
■ Normalization point (Cheltenham)

differences between them are large at some stations (for example, Freiburg and Canberra). The experimental latitude dependence of y_i at sea level, corrected by c_i^{II}, also has a fairly good agreement with the theoretical one, but is not shown here. As pointed out previously, there is quite a good agreement between the experimental values of y_i at Huancayo, obtained by various authors. The value without the altitude correction is equal to 0.89 ± 0.07 which was obtained by S. Yoshida and Y. Kamiya. On the other hand, the theoretical value is obtained from Figs. 5 and 7 and equal to 0.82 in case y_i^I is adopted and 0.78 in case y_i^{II} is adopted. The theoretical value in the former case is better than that in the latter, and is in accordance with the observed value within the experimental error. From Figs. 5 and 6, we see that the latitude dependence of y at high altitude satisfies qualitatively the condition that the changes must increase with the increase of latitude.

S. Yoshida and Y. Kamiya[21] obtained the altitude correction factors at several stations from the observation by comparing the values of y_i at two stations which were located at different altitudes respectively and nearly the same latitude each other. The results are tabulated in the last column of Table III. We see that there

are fairly good agreements between the theoretical and experimental altitude correction factors except that at Canberra. Although it is difficult to interpret that the experimental value at Canberra becomes larger than unity, this might be due to the scarcity of observations or the difference of cosmic ray meter compared with that at other stations.

As seen from the above comparisons of the theoretical values with the observations, the latitude dependence of the world-wide variation is explained by the variation of the static electric field.

In case of the cut-off energy:—As pointed out in § 3, the latitude dependence of the variation cannot be obtained unless the state of the electro-magnetic field is determined, so that the comparison of the theoretical curve with the observation cannot be done.

[III] The altitude dependence of the variation

Recently, the world-wide variations of the ionizing and neutron components at various altitudes have been observed by various authors.[3),(23),(24)] H.V. Neher pointed out that the ratio of the variation at high altitude to the variation at sea level is always constant. Such ratios obtained experimentally are reproduced in the 3rd column of Table IV. The theoretical ratios expected from the variation of the static electric field are in the 4th column where I and II represent the values obtained by using $y_i^I(\lambda, 1030, 0.1, 0)$ and $y_i^{II}(\lambda, 1030, 0.1, 0)$, respectively. In case of the variation of cut-off energy, it is possible to obtain the ratio of the variation at the same

Table IV Altitude dependence of y

No.	$y_j(\lambda, x) : y_k(\lambda, x)$	Observed value	Value expected from electric field		Value expected from cut-off energy	Remarks
			I	II		
1	$y_i(56, 50) : y_i(56, 1030)$ Bismarck	7 : 1	7 : 1	5.6 : 1		(3)
2	$y_i(45, 50) : y_i(1, 700)$ Chicago Huancayo	6 : 1	4.6 : 1	3.6 : 1	50 : 1	(3)
3	$y_i(43, 50) : y_i(41, 880)$ Ft. Worth Texas Mt. Wilson	4 : 1	2.6 : 1	2.3 : 1	12 : 1	(3) This ratio was obtained at the time of the magnetic storm
4	$y_n(48, 680) : y_i(50, 1030)$ Climax Cheltenham	4.0 : 1	3.9 : 1	3.1 : 1	50 : 1	(6)
5	$y_n(48, 680) : y_i(49, 1000)$ Climax Freiburg	5.5 : 1				(6)
6	$y_n(48, 680) : y_i(1, 700)$ Climax Huancayo	4.5 : 1	4.8 : 1	4.0 : 1	50 : 1	(6)

Numbers in the remarks column denote those of References quoted.

latitude, but not possible to obtain the ratio if stations are located at different latitudes, because, as stated in § 3, the latitude curve of y cannot be obtained unless the state of the electro-magnetic field is determined. But, if it is assumed that the intensity variation caused by the variation of cut-off energy shows no latitude effect

at ground level as the world-wide variation actually observed at the ground shows no remarkable latitude effect, it is possible to obtain the ratio between two stations which are located at different latitudes. The results are shown in the 5th column of Table IV. As stated above in [I], the variation of cut-off energy could possibly produce the intensity variation at high latitude, but here no such ratio is obtained.

As seen from this Table, the observed ratios show better agreements with the theoretical ones expected from the variation of electric field than that expected from the variation of cut-off energy. Moreover, in case of the electric field, the values in case I are better than those in case II. But, in point of detail, there are some discrepancies observable between the theoretical and experimental values as shown in the 2nd and 3rd rows of Table IV. These discrepancies seem to increase with the decrease of latitude.

In the 4th, 5th and 6th rows, the ratios between the neutron variation at Climax and the ionizing variations at several stations are shown. The observed ratio adopted by W.H. Fonger in order to compare with his theoretical calculation is that cited in the 5th row. But, as pointed out previously and seen from Table II and Fig. 13, the variation of the ionizing component at Freiburg is very small, compared with the variations at other stations which are located at the same latitude as Freiburg, so that the ratio in the 5th row is much larger than that obtained by using the variation at the other stations. Then, in order to compare with the theoretical value, it is more reasonable to adopt the values given in the 4th and 6th rows, than to adopt the value given in the 5th row. As for the ratio of the neutron component at Climax to the ionizing component at Cheltenham or Huancayo, there is quite a good agreement between the experimental and theoretical values in case I.

As stated in § 2, the variation of the neutron component must be independent on altitude in the atmospheric depth greater than 600 g cm^{-2}, if the observation of the neutron intensity made by J.A. Simpson et al.[18] is correct. Therefore, to confirm this fact, it is most desirable to make the comparisons between the variation of the neutron component at Climax and those at the other stations.

As seen from the above various considerations and discussions, it is possible to explain all the phenomena of the world-wide variation by the variation of the earth's potential, although in point of detail there are some discrepancies observable between the experimental and theoretical values. On the contrary, the variation of cut-off energy cannot explain the altitude dependence even though it may possibly satisfy the phenomenon [I].

[IV] The large variation of cosmic ray intensity

The large decrease of 6% or more in cosmic ray intensity at sea level are often observable at the time of the cosmic ray storm.[25] In such cases, the altitude and latitude dependences of the variation calculated in § 2 do not hold, because, as pointed out in § 1, they depend on the magnitude of the variation of earth's potential.[11] We must therefore calculate them when the variation of earth's potential is large. Figs. 14 and 15 represent the latitude dependences of y and Figs. 16 and 17, the altitude

dependences of y, in case $\Delta E = 1\,Bev$. The method of the normalization of the curves in Figs. 16 and 17 is the same as that adopted in Figs. 7 and 8. From these figures, we see that the altitude and latitude dependences become smaller if ΔE becomes larger. Moreover, to make this feature more clear, Figs. 18 and 19 are shown, representing the variations of the ionizing and neutron components at various altitudes

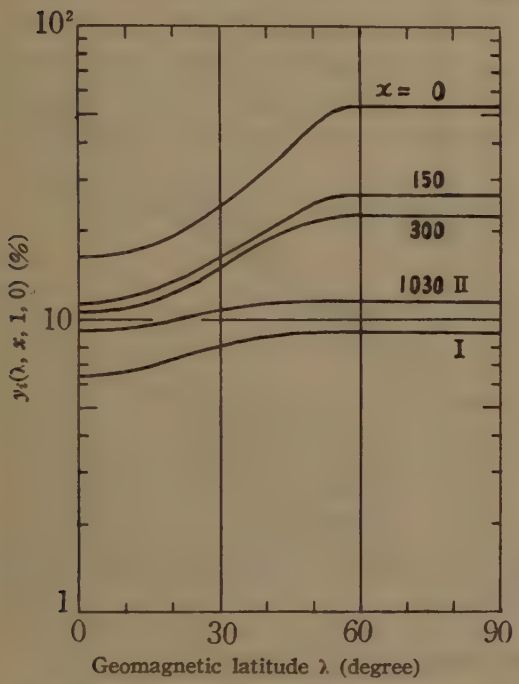

Fig. 14 Latitude dependence of y of the ionizing component.

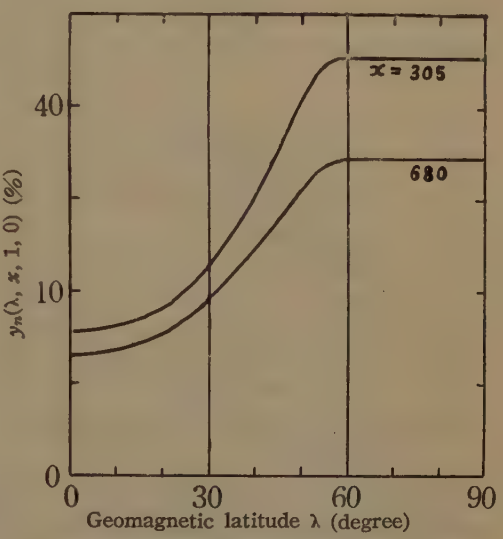

Fig. 15 Latitude dependence of y of the neutron component.

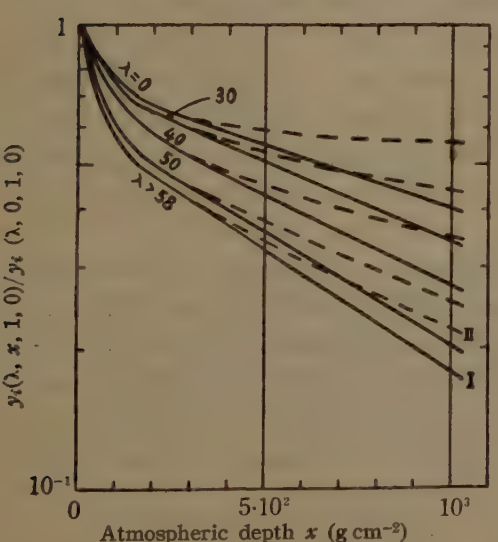

Fig. 16 Altitude dependence of y of the ionizing component.

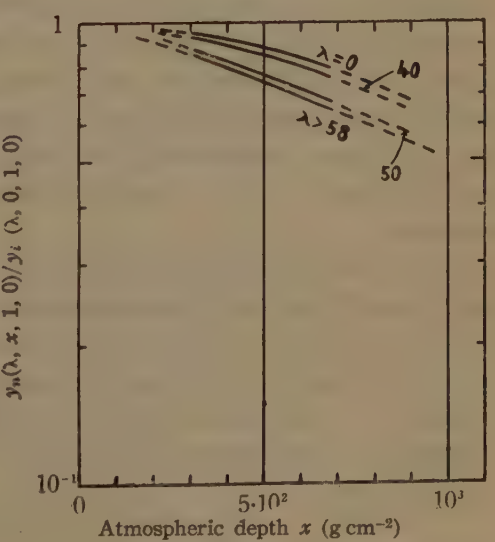

Fig. 17 Altitude dependence of y of the neutron component.

as a function of ΔE, in case $\lambda \geq 58°$. As seen from these figures, the dependence of y on ΔE becomes smaller with the increase of x, and it can be concluded that y is approximately proportional to ΔE at low altitudes and latitudes. But, at high altitudes and latitudes, it depends exceedingly on the magnitude of ΔE. Then it is necessary

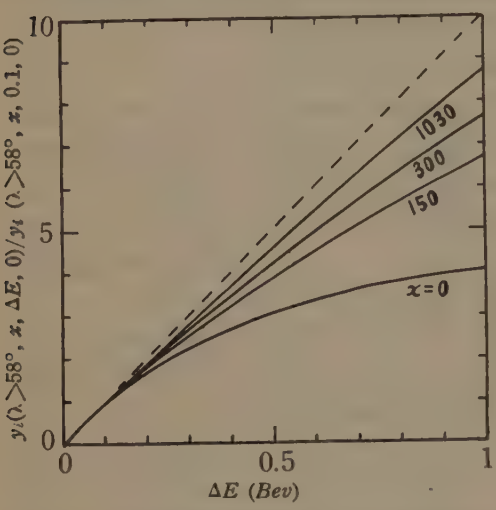

Fig. 18 ΔE dependence of y of the ionizing component.

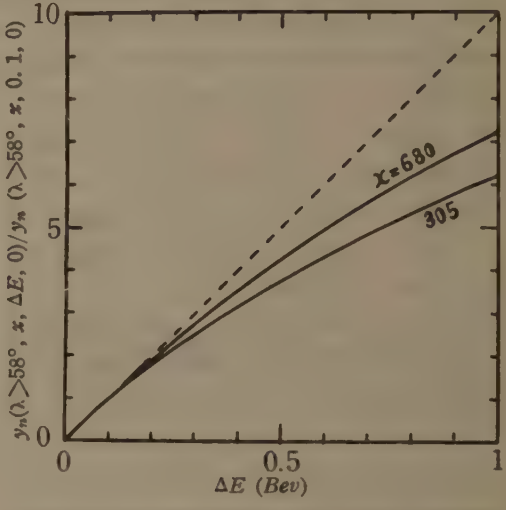

Fig. 19 ΔE dependence of y of the neutron component.

to consider such an influence upon the variation in order to compare the experimental altitude dependence of y with the theoretical one.

§ 5. The Diurnal Variation of Cosmic Ray Intensity

The diurnal variation of cosmic ray intensity is also a world-wide phenomenon at sea level, whose difference from the world-wide variation discussed in the previous sections is that the former depends on local time. Here, an examination is to be made of the possibility that the diurnal variation can be explained by an electric field[26] although the origin of such an electric field cannot be pointed out at present; and a qualitative comparison of the diurnal variation expected from such an electric field hypothesis is to be made with that expected from the static magnetic field hypothesis.[7]

The electric field derived from a potential can no longer explain the variation which depends on local time, because the variation is produced simultaneously all over the world as long as the electric field is derived from a potential.[27] Then, to explain such a variation, it is necessary to consider an electric field not derived from a potential. In such a general electro-magnetic field as well as the static electric and magnetic field, the intensity of cosmic rays, whose momentum are P at any point, is also expressed by

$$i = P^2 D, \quad \cdots\cdots\cdots\cdots \quad (11)$$

where

$$D = \frac{\delta N}{\delta \upsilon}, \quad \text{with} \quad \delta \upsilon = \delta x \delta y \delta z \delta P_x \delta P_y \delta P_z, \quad \cdots\cdots\cdots\cdots \quad (12)$$

and δN is the number of particles in the volume δv. Even in such a general field, the extended Liouville's theorem[28],[29] holds and then D in Eq. (11) is constant as well as in the static electric and magnetic field.[30] But, the difference in both cases is that, in the latter case, P is determined if only the electric potential at any point is known; in the former case, on the contrary, P cannot be determined unless the trajectory of charged particle can be obtained in the general electro-magnetic field. Keeping this point in mind and assuming that the primary particles consist of protons only, we are able to obtain also the vertical cosmic ray intensity at geomagnetic latitude $\lambda°$ and atmospheric depth $x\,\mathrm{g\,cm^{-2}}$ in the general field, using the method similar to that adopted in the static field.[1]

$$N\{\lambda, x, \Delta E(E,\lambda,t), \delta E_\lambda\} = \int_{E_\lambda+\delta E_\lambda}^{\infty} m(E,x)[1-L\{E+\Delta E(E,\lambda,t), \Delta E(E,\lambda,t)\}] \times i\{E+\Delta E(E,\lambda,t)\}\,dE, \quad \cdots\cdots(13)$$

where $N, \delta E_\lambda, m, L$ and i are the same notations as those in Eq. (3), and $\Delta E(E,\lambda,t)$ is the energy loss which the primary particle, having its kinetic energy E at $\lambda°$ on the earth, undergoes during its passage through the electro-magnetic field, and is a function of E, λ and local time t, since ΔE depends upon the particle's trajectory which can be determined by parameters E, λ and t. Although it is meaningless to try to determine whether such a variation is caused by the electric field or the magnetic field, we designate such a variation for the variation caused by the general electric field in distinction from the variation caused by the static electric field or by the static magnetic field, since the agency of the electro-magnetic field upon the intensity variation is similar to that of the static electric field as seen from Eqs. (8) and (13).

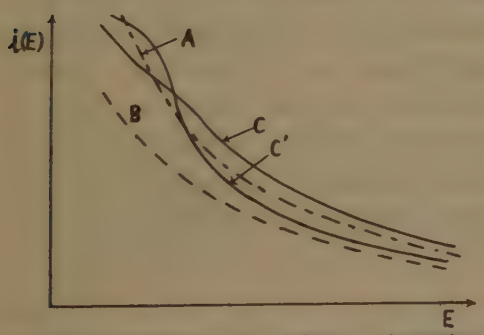

Fig. 20 Variation of primary intensity spectrum produced by the electric field.
1. Curve A represents the spectrum at the normal state.
2. Curve B represents the variation of the spectrum from the normal state produced by the static electric field.
3. Curve C and C′ represent the variations of the spectrum produced by the general electric field at the times t and t′ respectively.

Fig. 20 is a schematic representation of deformations of the primary spectrum which will be caused by the general electric field. The distinction between the intensity variation caused by the static electric field and that caused by the general electric field is as follows: In the former case, the relative contribution of the primary particles, each having a different energy, to the intensity variation is uniquely determined (see Eq. (8) and Curve B in Fig. 20). In the latter case, on the contrary, the relative contribution varies with local time (see Eq. (13) and Curves C and C′ in Fig. 20). Then, the altitude dependence of diurnal variation is different from that of the world-wide variation expected from the static electric field and cannot be obtained theoretically unless

the state of the electo-magnetic field is determined.

Comparing the diurnal variation of neutron component at Climax with that of ionizing component at Freiburg, W.H. Fonger[6] showed that the ratio between the amplitudes of variation at the two stations is nearly equal to the ratio of the world-wide variation (not dependent on local time) expected from the static electric field hypothesis (here-after referred to as Phenomenon b). If we substitute the altitude dependence curve obtained from the static electric field for the true altitude dependence curve of diurnal variation as a rough approximation because of the existence of Phenomenon b, the amplitude of diurnal variation of the ionizing component at high latitude will be expected to be about 10 times that of sea level at the top of the atmosphere and about 7 times at $x=50\,\mathrm{g\,cm^{-2}}$.

The static electric and magnetic field also has the possibiblity of producing the diurnal variation, if the field is not symmetrical to the earth's magnetic dipole axis. There is the solar magnetic field theory adovocated by M.S. Vallarta,[7] as the representative example. The altitude dependence of diurnal variation expected from this theory is smaller than that expected from the variation of cut-off energy, because, as pointed out in § 1, the diurnal variation is caused by the variation of primary spectrum at intermediate energy region and not by the variation of cut-off energy. The distinction between the general electric field hypothesis and the solar magnetic field theory is as follows: The altitude dependence of diurnal variation expected from the former is smaller than that expected from the latter,[31] since, in the latter case, only the primary particles in the low energy region are influenced; in the former case, on the contrary, all the particles in all of the energy region are influenced.

As above, the diurnal variation could possibly be explained by the electric field not derived from potential, even though it cannot indicate the mechanism producing such an electric field. Recently, the diurnal variation at high altitude was observed by various authors[32] in order to confirm the existence of solar magnetic field. But, none of them has reported the ratio between the amplitude of diurnal variation at high altitude and that at sea level. It is most important to examine the altitude dependence from the experimental and theoretical points of view in order to determine the cause of the diurnal variation.

Concluding Remarks

It is concluded that the world-wide variation of cosmic ray intensity not dependent on local time can be explained by the variation in the distribution of the primary cosmic ray intensity spectrum which is caused by the variation of the static electric field, but not explained by the variation of cut-off energy which is caused by the variation of the electro-magnetic field.

The diurnal variation of cosmic ray intensity could possibly be explained by an electric field not derived from potential. The existence of Phenomenon b seems to be favourable to the general electric field hypothesis.

Acknowledgements

In conclusion, the writer wishes to express his hearty thanks to Prof. M. Hasegawa, for his constant interest in and encouragement of the present research, and to Profs. Y. Sekido and T. Nagata as well as Mr. S. Hayakawa for their many valuable criticisms and discussions in relation to this work. Many thanks are due to Profs. M.S. Vallarta and J.A. Wheeler for their valuable discussions relative to this work on their visit to Japan.

Appendix I The Variation of Cut-Off Energy by the Static Electric and Magnetic Field

The relativisitic equation of the charged particle's motion in the electro-magnetic field is

$$\frac{d}{dt}(m\boldsymbol{v})=e\boldsymbol{E}+\frac{e}{c}[\boldsymbol{v}\boldsymbol{H}]. \quad \cdots\cdots\cdots\cdots \quad (A,1)$$

General solution of Eq. (A, 1) cannot be obtained analytically even in case of the motion in the earth's dipole magnetic field. Then it is extremely difficult to solve Eq. (A, 1) in case the static electric and magnetic field surrounding the earth exists in addition to the earth's magnetic field. But, in one special case, it is possible to obtain the Störmer cone[33] and then to obtain the variation of cut-off energy caused by the static electric and magnetic field. As the coordinate system, here are the spherical coordinates (R, λ, φ) adopted, as shown in Fig. 21, and the z-axis coinciding with the earth's magnetic dipole axis and directed towards the North Pole.

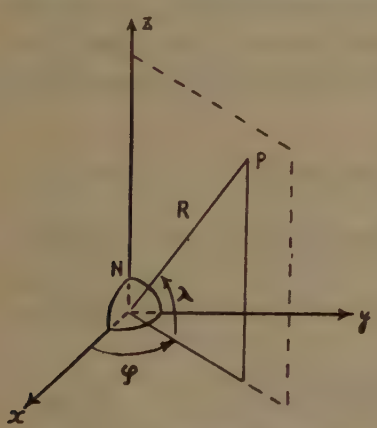

Fig. 21 Coordinate system

If the static electric and magnetic field surrounding the earth is symmetrical to z-axis, the following conditions hold;

$$\boldsymbol{E}_\varphi=0 \quad \text{and} \quad \boldsymbol{H}_\varphi=0. \quad \cdots\cdots(A,2)$$

Then, in such a case, the φ-component of Eq. (A, 1) becomes

$$\frac{d}{dt}(m\boldsymbol{v})_\varphi=\frac{e}{c}[\boldsymbol{v}\boldsymbol{H}]_\varphi. \quad \cdots\cdots\cdots \quad (A,3)$$

In Eqs. (A, 1) and (A, 3), the mass m is not constant because of the existence of the electric field. But, quite similar to the case that only the static magnetic field exists, Eq. (A, 3) can be integrated, and the solution is

$$m(R\cos\lambda)^2\frac{d\varphi}{dt}=\frac{e}{c}\left\{-(R\cos\lambda)\boldsymbol{A}_\varphi+\Gamma\right\} \quad \cdots\cdots\cdots\cdots \quad (A,4)$$

where Γ is an integral constant, and A_φ is the φ-component of vector potential and in this case is given by

$$A_\varphi = -\frac{M\cos\lambda}{R^2} - A^0_\varphi. \quad \cdots\cdots\cdots\cdots \quad (A,5)$$

The 1st term on the right hand side of Eq. (A, 5) is due to the earth's dipole magnetic field, M denoting the magnetic dipole moment, and $-A^0_\varphi$ to the outer field. Let θ denote the angle between the particle's orbit and the meridian plane, and the next relation is obtained by using Eq. (A, 4).

$$\sin\theta = \frac{R\cos\lambda}{v}\cdot\frac{d\varphi}{dt} = \frac{e}{mvc}\left\{\frac{M\cos\lambda}{R^2} + A^0_\varphi(R,\lambda) + \frac{\Gamma}{R\cos\lambda}\right\}. \quad \cdots\cdots (A,6)$$

Then, the motion must satisfy the following condition:

$$\left|\frac{e}{mvc}\left\{\frac{M\cos\lambda}{R^2} + A^0_\varphi(R,\lambda) + \frac{\Gamma}{R\cos\lambda}\right\}\right| \leqq 1. \quad \cdots\cdots\cdots\cdots \quad (A,7)$$

Next, we consider the extended Störmer transformation[33],[34] as follows,

$$l = \sqrt{\frac{|e|M}{(mvc)_0}} \quad \text{and} \quad R = lr, \quad \text{etc.}, \quad \cdots\cdots\cdots\cdots \quad (A,8)$$

and

$$(mvc) = (mvc)_0[1 - L\{E_0, e\delta\phi(R,\lambda)\}]^{\frac{1}{2}}, \quad \cdots\cdots\cdots\cdots \quad (A,9)$$

where L is Liouville's effect and given by Eq. (4), E is the kinetic energy corresponding to the value of mvc, and subscript $_0$ denotes the value on the earth. $\delta\phi(R,\lambda)$ is the difference in electric potential relative to the earth's potential at any point (R,λ). Appling these transformations to Eqs. (A, 6) and (A, 7), the following relations can be obtained;

$$\sin\theta = \frac{1}{(1-L)^{1/2}}\left\{\frac{\cos\lambda}{r^2} - \frac{2\gamma_1}{r\cos\lambda} + \frac{l^2}{M}A^0{}_\varphi(lr,\lambda)\right\}. \quad \cdots\cdots\cdots (A,6)'$$

$$\left|\frac{1}{(1-L)^{1/2}}\left\{\frac{\cos\lambda}{r^2} - \frac{2\gamma_1}{r\cos\lambda} + \frac{l^2}{M}A^0_\varphi(lr,\lambda)\right\}\right| \leqq 1, \quad \cdots\cdots\cdots (A,7)'$$

where $2\gamma_1$ is the integral constant. From Eq. (A, 7)′, we can obtain the following relation;

$$r\cos\lambda\left(\frac{\cos\lambda}{r^2} + 1 + \alpha - \beta\right) \geqq 2\gamma_1 \geqq r\cos\lambda\left(\frac{\cos\lambda}{r^2} - 1 + \alpha + \beta\right), \quad \cdots\cdots (A,10)$$

where

$$\left.\begin{aligned} \alpha(r,\lambda,r_0) &= \frac{l^2}{M}A^0_\varphi(lr,\lambda), \\ \beta(r,\lambda,r_0) &= 1 - [1 - L\{E_0, e\delta\phi(lr,\lambda)\}]^{\frac{1}{2}}. \end{aligned}\right\} \quad \cdots\cdots\cdots (A,11)$$

α and β are the terms due to the outer magnetic and electric fields respectively, and are functions of r, λ, and r_0 (which is the particle's energy in Störmer unit[33] corresponding to E_0 or $(mvc)_0$). Eq. (A, 10) depends upon the particle's energy, different from the case where only the earth's magnetic field exists. Hence, the Störmer transformation loses its usefulness in this case.

As the influence of the outer magnetic field upon the cut-off energy has been examined by various authors,[35] here that of the electric field only is considered. In this case, Eq. (A, 10) becomes as follows,

$$r\cos\lambda\left(\frac{\cos\lambda}{r^2}+1-\beta\right)\geq 2\gamma_1\geq r\cos\lambda\left(\frac{\cos\lambda}{r^2}-1+\beta\right). \quad \cdots\cdots\cdots (A, 12)$$

Fig. 22 is a schematic representation of Eq. (A, 12) in case $\lambda=0$. The full lines represent the curves $\gamma_1=\frac{r}{2}\left(\frac{1}{r^2}+1\right)$ and $\gamma_1=\frac{r}{2}\left(\frac{1}{r^2}-1\right)$, which equations denote the non-existence of the electric field and are tenable independent of the particle's energy under consideration. When the electric field exists, these curves cease to be independent of the particle's energy. The dotted lines in Fig. 22 represent an example of the deviations from the normal state produced under the influence of the electric field, in case of the particle's energy becoming r_0 Störmer ($r_0<1$) on the earth. To examine the variation of cut-off energy in such a case, it is necessary to obtain the minimum value of the following curve;

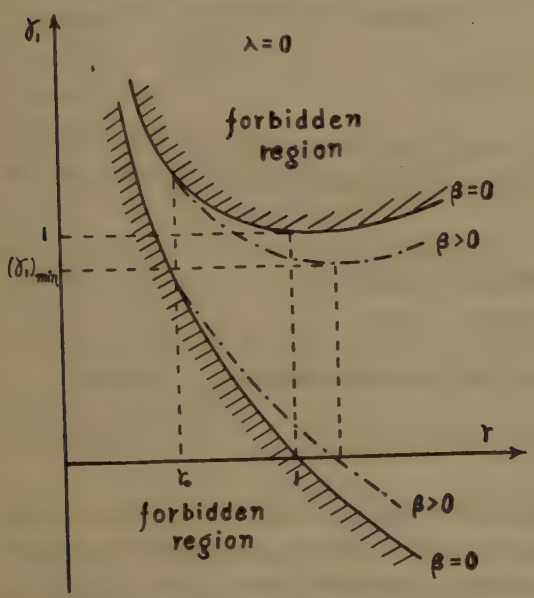

Fig. 22 γ_1-r diagram

$$2\gamma_1=r\left\{\frac{1}{r^2}+1-\beta(r, 0, r_0)\right\}. \quad \cdots\cdots\cdots\cdots (A, 13)$$

Generally, this problem cannot be solved unless the form of β is determined. But an analysis can proceed when the disturbance by the electric is small. Under such a condition, β in Eq. (A, 11) is approximately given by

$$\beta(r, 0, r_0)\approx\beta_{ap.}(r, 0, r_0)=\frac{1}{2}L\{E_0, e\delta\phi(r, 0, r_0)\}$$
$$\approx\frac{(E_0+m_0c^2)\cdot e\delta\phi(r, 0, r_0)}{(E_0+m_0c^2)^2-(m_0c^2)^2}\ll 1, \quad \cdots\cdots\cdots\cdots (A, 14)$$

where E_0 is the particle's energy in *Bev.*, corresponding to r_0 Störmer. The above equation holds if only $E_0\gg e\delta\phi(r, 0, r_0)$. As the minimum value of γ_1 in Eq. (A, 13) is 1 at $r=1$ in case $\beta=0$, it can be assumed that the minimum value of γ_1 will be given by

at
$$\left.\begin{aligned}(\gamma_1)_{min}&=1+\Delta\gamma_1(r_0, \beta), \quad (\Delta\gamma_1\ll 1)\\ r\quad&=1+\Delta r(r_0, \beta). \quad (\Delta r\ll 1)\end{aligned}\right\} \quad \cdots\cdots\cdots\cdots (A, 15)$$

Let β be further developed in the power series at $r=1$:

$$\beta(r, 0, r_0)=\beta(1, 0, r_0)+\frac{\beta'(1, 0, r_0)}{1!}(r-1)+\frac{\beta''(1, 0, r_0)}{2!}(r-1)^2+\cdots, \quad \cdots\cdots \text{(A, 16)}$$

where $\beta(1, 0, r_0)$ is the value at $r=1$ and $\beta'(1, 0, r_0)$ is that of the 1st derivative of β with respect to r. Using Eqs. (A, 13), (A, 15) and (A, 16), and neglecting the higher order of Δr as small, we can obtain the following relations:

$$\left.\begin{aligned}\Delta\gamma_1(r_0, \beta)&=-\frac{1}{2}\left[\beta(1, 0, r_0)+\frac{\{\beta(1, 0, r_0)+\beta'(1, 0, r_0)\}^2}{2-2\beta'(1, 0, r_0)-\beta''(1, 0, r_0)}\right].\\ \Delta r(r_0, \beta)&=\frac{\beta(1, 0, r_0)+\beta'(1, 0, r_0)}{2-2\beta'(1, 0, r_0)-\beta''(1, 0, r_0)}.\end{aligned}\right\} \quad \cdots\cdots \text{(A, 17)}$$

Next, we examine the variation of cut-off energy produced by such a variation of the minimum value of γ_1. In case only the electric field exists, Eq. (A, 6)′ becomes as follows,

$$\sin\theta=\frac{1}{(1-L)^{1/2}}\left(\frac{\cos\lambda}{r^2}-\frac{2\gamma_1}{r\cos\lambda}\right). \quad \cdots\cdots\cdots\cdots \text{(A, 18)}$$

Introducing, into the above, the values $\theta=\theta$, $r=r_0$, $\gamma_1=(\gamma_1)_{min.}$, and $L=0$ (as the potential difference $\delta\phi$ is zero on the earth), the following relation is obtained,

$$\cos\lambda_1=\frac{1}{2}[r_0^2\sin\theta+\sqrt{(r_0^2\sin\theta)^2+8r_0(\gamma_1)_{min.}}]. \quad \cdots\cdots\cdots \text{(A, 19)}$$

λ_1, satisfying Eq. (A, 19), denotes the latitude at which r_0 Störmer, being the particle's energy on the earth, the particle entering into the earth from the given direction θ, exactly becomes the cut-off energy. In case the electric field does not exist, let λ_0 be the latitude at which r_0 Störmer becomes the cut-off energy, and λ_0 is given by

$$\cos\lambda_0=\frac{1}{2}[r_0^2\sin\theta+\sqrt{(r_0^2\sin\theta)^2+8r_0}]. \quad \cdots\cdots\cdots\cdots \text{(A, 20)}$$

From Eqs. (A, 19) and (A, 20), we get

where

$$\left.\begin{aligned}&\cos\lambda_1\approx\cos\lambda_0+\eta,\\ &\eta=\frac{2r_0\cdot\Delta\gamma_1}{\sqrt{(r_0^2\sin\theta)^2+8r_0}},\end{aligned}\right\} \quad \cdots\cdots\cdots\cdots \text{(A, 21)}$$

in which $\Delta\gamma_1$ is given by Eq. (A, 17). Moreover, in case the electric field does not exist, let r_1 Störmer be the cut-off energy at the latitude λ_1, we get the following relation,[36]

$$r_1=\cos^2\lambda_1[1+\sqrt{\cos^3\lambda_1\sin\theta}]^{-1}. \quad \cdots\cdots\cdots\cdots \text{(A, 22)}$$

Introducing Eq. (A, 21) into the above, the following relation holds between r_1 and r_0,

where

$$\left.\begin{aligned}&r_1\approx r_0(1+\delta),\\ &\delta=\left(\frac{2}{\cos\lambda_0}-\frac{3}{2}\cdot\frac{r_0\sin\theta}{r_0\cos\lambda_0\sin\theta+1}\right)\eta.\end{aligned}\right\} \quad \cdots\cdots\cdots\cdots \text{(A, 23)}$$

If the energies r_1 and r_0 Störmers in Eq. (A, 23) are converted into the energies E_1 and E_0 in *Bev.* respectively, Eq. (A, 23) becomes

$$\left.\begin{aligned} &E_1=E_0+\zeta,\\ \text{where}\quad &\zeta=\frac{(E_0+m_0c^2)^2-(m_0c^2)^2}{E_0+m_0c^2}\cdot(2\delta),\\ \text{and}\quad &r_0=\left(\frac{R_e}{e^2M^2}\right)^{\frac{1}{4}}[(E_0+m_0c^2)^2-(m_0c^2)^2]^{\frac{1}{4}}, \end{aligned}\right\}\quad\cdots\cdots\quad(\text{A},24)$$

in which R_e is the earth's radius. From Eqs. (A, 21) and (A, 24), we see that the particle's energy E_0, which is the cut-off energy at $\lambda=\lambda_0$ and $\theta=\theta$ in case of the non-existence of the electric field, becomes the cut-off energy at $\lambda=\lambda_1$ and $\theta=\theta$ in case of the existence of the electric field, and that the relation between E_0 and E_1 (which is the cut-off energy at $\lambda=\lambda_1$ and $\theta=\theta$ in case of the non-existence of the electric field) is given by Eq. (A, 24).

To make the physical meaning of these equations more clear, the simplification of these equations is carried out. In Eq. (A, 17), $\Delta\gamma_1$ is a function of β, β' and β'', and then cannot be determined unless the space distribution of the electric potential is known. But, if we assume that the potential does not vary rapidly near the point where $r=1$ and $\lambda=0$ so as to satisfy the following relations,

$$\beta'\leqq\beta\ll1 \qquad \text{and} \qquad \beta''\leqq\beta\ll1,$$

and then, neglecting the higher order of β, β' and β'', Eq. (A, 17) becomes as follows,

$$\Delta\gamma_1\approx-\frac{1}{2}\beta(1,0,r_0)\approx-\frac{1}{2}\frac{(E_0+m_0c^2)}{(E_0+m_0c^2)^2-(m_0c^2)^2}\cdot e\delta\phi(1,0,r_0). \quad\cdots\cdot(\text{A},25)$$

Using the above equation, in case of the vertical incidence ($\theta=0$), Eq. (A, 24) becomes as follows,

$$E_1=E_0-e\delta\phi(1,0,r_0). \quad Bev. \qquad\cdots\cdots\cdots\cdots \quad(\text{A},26)$$

As seen from the above, the variation of the cut-off energy produced by the static electric field is approximately determined only by the earth's potential, and is $-e\delta\phi(1,0,r_0)$ in case of the vertical incidence. When the potential at the point where $r=1$ and $\lambda=0$ is higher than that of the earth ($\delta\phi>0$), the cut-off energy becomes larger than that of the normal state and then, as discussed in § 3, the cosmic ray intensity is decreased by such a variation. But, as seen from Fig. 9, such a decrease is exceedingly small even in the high atmosphere if $e\delta\phi\leqq10^{-2}$ *Bev.* As pointed out by H.V. Neher,[3] there exists the general cut-off energy $E_g(=0.8$ *Bev.* for proton) which corresponds to about 0.16 Störmer. The distance from the earth's center to the point where $r=1$ becomes nearly 6 times the earth's radius even if we consider the lowest energy 0.16 Störmer. Therefore, if the following relation is satisfied over the region less than 6 times the earth's radius,

$$e\delta\phi\leqq10^{-2}\ Bev.,$$

the cosmic ray intensity variation is not produced over all the latitude by the variation of cut-off energy.

In conclusion, the variation of cut-off energy can be solved analytically in case the static electric and magnetic field is symmetrical to the earth's magnetic dipole

axis. The variation of cut-off energy caused by the static electric field can be determined approximately by the potential difference at the point where $r=1$ and $\lambda=0$, relative to the earth's potential, as long as the disturbance by the electric field is small.

Appendix II Determination of Over-all Multiplicity

(1) In case of the ionizing component

From Eq. (7), we can obtain the following relation

$$m(E, x)=-\frac{1}{i(E)}\cdot\frac{dN(\lambda, x)}{d\lambda}\cdot\frac{d\lambda}{dE}. \quad \cdots\cdots\cdots\cdots \quad (A, 27)$$

H.V. Neher[8] obtained $m(E, x)$ at low energy region, using the primary spectrum in Eq. (6) and the vertical intensity of the ionizing component at various altitudes. The results are reproduced in Fig. 1 as the full lines. In the high energy region, although $m(E, x)$ cannot be obtained directly from observation, it is possible to obtain it approximately under the following considerations: As shown in Fig. 1, in case x is small, the full line has a critical energy $E_c(x)$, in the energy region larger than which $m(E, x)$ changes more slowly compared with that in the low energy region. In such a high energy region where $E\geq E_c(x)$, we assume that $m(E, x)$ is expressed by the following formula,

$$m(E, x)=m_c(x)\left[\frac{E}{E_c(x)}\right]^{a(x)}, \quad \cdots\cdots\cdots\cdots \quad (A, 28)$$

where $m_c(x)$ is the value of $m(E, x)$ in case $E=E_c(x)$. Introducing Eq. (A, 28) into Eq. (7), we obtain the following relation,

$$N(\lambda_c, x)=\int_{E_c(x)}^{\infty} m_c(x)\left[\frac{E}{E_c(x)}\right]^{a(x)}\cdot i(E)\,dE, \quad \cdots\cdots\cdots \quad (A, 29)$$

where λ_c is the latitude at which $E_c(x)$ becomes the cut-off energy. As $N(\lambda_c, x)$, $m_c(x)$, $E_c(x)$ and $i(E)$ are known, $a(x)$ can be determined so as to satisfy Eq. (A, 29). The results obtained by such a procedure are shown in Fig. 1 and Table I, in case $x=150$ and 300.

In case $x=1030$, although E_c cannot be known directly from the observation, it seems to be reasonable to assume that the over-all multiplicity is similar to that in the case where x is small, and that there also exists the critical energy E_c. If we adopt as E_c the largest value of E for which $m(E, 1030)$ can be obtained from the observation and assume that $m(E, 1030)$ is also given by Eq. (A, 28) in the energy region where $E\geq E_c$, $a'(1030)$ can be determined so as to satisfy Eq. (A, 29) and gives the upper limit of $a(1030)$. The over-all multiplicity $m'(E, 1030)$ obtained by such a procedure is shown in Fig. 1 and Table I. On the other hand, there is another way to determine $m(E, 1030)$ as follows; $a(x)$ in Eq. (A, 28) increases with the increase of x, so that if $a(300)$ is adopted as $a(1030)$, this gives the lower limit of $a(1030)$. In such a case, $E_c(1030)$ and $m_c(1030)$ can be determined so as to satisfy the following equation,

$$N(\lambda, 1030)=\int_{E_\lambda}^{E_c(1030)} m(E, 1030)\, i(E)\, dE+\int_{E_c(1030)}^{\infty} m_c(1030)\left[\frac{E}{E_c(1030)}\right]^{\gamma(300)}\cdot i(E)\, dE, \quad \text{(A, 30)}$$

where the over-all multiplicity obtained from the observation and its prolongation are used as $m(E, 1030)$ in the 1st term on the right hand side. The over-all multiplicity thus obtained is shown in Fig. 1 and Table I with the notation $m^{II}(E, 1030)$. The variations $y^I(\lambda, 1030, \Delta E, 0)$ and $y^{II}(\lambda, 1030, \Delta E, 0)$ obtained by using $m^I(E, 1030)$ and $m^{II}(E, 1030)$ give the lower and upper limits of y, respectively.

(2) In case of the neutron component

The latitude dependence curves of the neutron intensity used to obtain the over-all multiplicity are those of the Simpson observation[37],[38] made at the atmospheric depthes $x=305$ and $x=680$. As these intensities are omnidirectional, the vertical intensities at $x=305$ can be obtained after the Gross transformation[38] by using the absorption mean free path obtained by J.A. Simpson.[37] But, in case $x=680$, it is not necessary to make the Gross transformation[18] and here the latitude dependence curve normalized to unity at equator is adopted. Assuming that the over-all multiplicity is also expressed by Eq. (A, 28) in the high energy region, we can determine $a(x)$ in the same way, and the results are shown in Fig. 2 and Table I. The over-all multiplicities obtained here are different in form with those obtained by S.B. Treiman.[39] This difference will be caused by the following facts that (1) the primary spectrums used are different from each other and (2) it is unreliable to determine m at the energy region in the neighbourhood of 10 *Bev.* by observations only. But the variation y at high latitude is almost not influenced by the adoptation of different over-all multiplicities, because the contribution of the high energy primary particles to the neutron intensity at high latitude is negligibly small as the latitude effect of the neutron component is very large.

(Read Oct. 30, 1953)

References

(1) K. Nagashima, Jour. Geomag. Geoelect., **3**, 100 (1951).
(2) S. Chapman, Nature, **140**, 425 (1937).
(3) H.V. Neher, V.Z. Peterson and E.A. Stern, Phys. Rev., **90**, 655 (1953).
(4) S.E. Forbush, Rev. Mod. Phys., **11**, 168 (1939).
(5) Y. Sekido, International Conference on Theoretical Physics, Symposium on Cosmic Rays, Tokyo, Japan (1953).
(6) W.H. Fonger, Phys. Rev., **91**, 351 (1953).
(7) M.S. Vallarta and O. Godart, Rev. Mod. Phys., **11**, 180 (1939).
(8) H.V. Neher, "Progress in Cosmic Ray Physics," North-Holland Publishing Co. Amsterdam, pp. 241–314 (1950).
(9) K. Dwight, Phys. Rev., **78**, 40 (1950).
(10) Thanks are due to Mr. W.H. Fonger for pointing out author's inadquacy. In this paper, the expression of the Liouville's effect is corrected and used in a more accurate form than that which was adopted by W.H. Fonger. But the

original expression in the previous paper[1] holds good in the high energy region because $pc \approx E$.

(11) If we neglect the higher order of ΔE in Eq. (5), y becomes to be proportional to ΔE. But such an approximate formula of y leads to the error which is nearly equal to that pointed out in Ref. (10), even if ΔE is small. Moreover, if ΔE becomes larger, this approximate formula is not correct and leads to a large error.

(12) The variation of the primary spectrum which is caused by the electric field not derived from potential will be discussed in § 5.

(13) H. Alfvén, Phys. Rev., **72**, 88 (1947).

(14) E.O. Kane, T.J.B. Shanely and J.A. Wheeler, Rev. Mod. Phys., **21**, 51 (1949).

(15) B. Peters, "Progress in Cosmic Ray Physics," North-Holland Publishing Co. Amsterdam, p. 191 (1950).

(16) H.V. Neher, Phys. Rev., **83**, 649 (1951).

(17) J.A. Van Allen and S.F. Singer, Phys. Rev., **78**, 819 (1950).
J.R. Winckler, T. Stix, K. Dwight and R. Sabin, Phys. Rev., **79**, 656 (1950).

(18) J.A. Simpson and W.C. Fagot, Phys. Rev., **90**, 1068 (1953).

(19) D.H. Loughridge and P.F. Gast, Phys. Rev., **57**, 937 (1940).
J.A. Simpson, Phys. Rev., **81**, 639 (1951).

(20) L. Jànossy, Zeit. f. Phys., **104**, 430 (1937).

(21) S. Yoshida and Y. Kamiya, Jour. Geomag. Geoelect., **5**, 136 (1953).

(22) M. Wada, Report of Cosmic-Ray Laboratory, Scientific Research Institute (Japan) **1**, 81 (1952).

(23) J.A. Simpson, W. Fonger and L. Wilcox, Phys. Rev., **85**, 366 (1952).

(24) H.V. Neher and S.E. Forbush, Phys. Rev., **87**, 889 (1952).

(25) S.E. Forbush, Terr. Mag., **43**, 203 (1938).

(26) Attempts have been made by various authors to explain the diurnal variation of cosmic ray intensity by the electric field. See for example;
H. Elliot and D.W.N. Dolbear, J. Atmos. Terr. Phys., **1**, 205 (1951).
Y. Sekido, S. Yoshida and Y. Kamiya, Rep. of Ionos. Res. in Japan, Vol. VI, No. 4, 195 (1952).

(27) Strictly speaking, if the electric field which is derived from potential is not symmetrical to the earth's magnetic dipole axis, the cut-off energy E_λ varies with local time and then we may expect the diurnal variation of cosmic rays by such a field. As such a diurnal variation has the character similar to that expected from the static magnetic field hypothesis,[7] we will consider later the former variation with the latter.

(28) L. Jànossy, "Cosmic Rays," Oxford, Clarendon Press, p. 268 (1950).

(29) W.F.G. Swann, Phys. Rev., **44**, 224 (1933).

(30) The expression of D in Ref. (28) is not correct. D must be constant in the electro-magnetic field.[29]

(31) This problem will be treated quantitatively in the near future.

(32) D.I. Dawton and H. Elliot, J. Atmos. Terr. Phys., 3, 217 (1953).
J.A. Bergstralh and C.A. Schroeder, Phys. Rev., **81**, 244 (1951).

(33) See for example, M.S. Vallarta, "On the Allowed Cone of Cosmic Radiation," Toronto Univ. Press (1938).

(34) Eqs. (A, 8) and (A, 9) are the expansion of the Störmer transformation in case of the existence of the static electric field.

(35) T. Nagata, J. Geophys. Res., **55**, 127 (1950).
S. Hayakawa, J. Nishimura, T. Nagata and M. Sugiura, J. of Scien. Res. Inst. in Japan, **44**, 121 (1950).
S.B. Treiman, Phys. Rev., **89**, 130 (1953).

(36) J.A. Alpher, J. Geophys. Res., **55**, 437 (1950).

(37) J.A. Simpson, Phys. Rev., **83**, 1175 (1951).

(38) J.A. Simpson, W. Fonger and S.B. Treiman, Phys. Rev., **90**, 934 (1953).

(39) S.B. Treiman, Phys. Rev., **86**, 917 (1952).

The Meeting of the Society of Terrestrial Magnetism and Electricity:
The 14th General Meeeting was held at the Kyoto University on Oct. 30–Nov. 1, 1953. 43 Reports were read, about 60 Members assembled.

The Tanakadate-Prize was awarded at the meeting for the following excellent worker:
The 14th, Mr. K. Nagashima, World-Wide Variation of Cosmic Ray Intensity by the Electro-Magnetic Field.

Self-Reversal of Thermo-Remanent Magnetism of Igneous Rocks (III)*†

By T. NAGATA, S. AKIMOTO and S. UYEDA

(Geophysical Institute, Tokyo University)

Abstract

Besides the dacitic pumice of Mt. Haruna, an igneous rock having the tendency of self-reversal of thermo-remanent magnetization has been found in a pitchstone of Mt. Asio. Although the self-reversal property of the Asio ferromagnetic minerals is weaker than that of the Haruna ferromagnetic minerals, the magnetic and crystallographic properties of the former are fundamentally same as those of the latter.

By thermo-magnetic separation, an ensemble of ferromagnetic grains in both the Haruna and the Asio rocks were divided into A, B and AB groups. The results of thermo-magnetic measurement, chemical analysis, and X-ray analysis of these three groups showed that the A-constituent is a titanomagnetite of the crystal structure of inverse spinel type having the Curie-point at 430°–510°C, and the B-constituent is an ilmenite-hematite solid-solution of the rhombohedral crystal structure having the Curie-point at about 230°C, while the AB grains are composed of both A- and the B-constituents.

The measurement of thermo-remanent magnetization of a large number of single grain gave the result that only the AB grains can have the reverse thermo-remanent magnetization, the A- and the B-grains getting the ordinary normal thermo-remanent magnetization.

§ 1. Iutroduction

In the previous papers [1, 2], experimental evidence of the self-reversal of thermo-remanent magnetism of a dacitic rock of Mt. Haruna was reported: that is, the Haruna rock and the ferromagnetic minerals separated from it have the thermo-remanent magnetization, the direction of which is opposite to that of the magnetic field applied during their cooling from the Curie-point. It was also found out that the ferromagnetic minerals in the Haruna rock are composed of the group of ferromagnetics similar to magnetite having the Curie-point at about 500°C and another

---

* Contribution to Geophysical Papers dedicated to Prof. M. Hasegawa on his sixtieth birthday, January 2, 1954.

† Contribution from the Division of Geomagnetism and Geoelectricity, Geophysical Institute, Tokyo University, Series II, No. 42.

group of ferromagnetics having the Curie-point at about 230°C; the former was called the A-constituent and the latter the B-constituent. The saturation magnetization of the B-constituent increases so linearly with decrease in temperature that this could not be identified to some of titanomagnetites which are usual sources of ferromagnetism of rocks.

Each grain of ferromagnetic minerals in that rock is composed of the A- and the B-constituents with their various ratios, the most grains being almost the A-constituent, while some of them are either the B-constituent or mixtures of A and B. It was suggested that only the grains consisting of both the A- and the B-constituents are responsible for the self-reversal of thermo-remanent magnetization; pure A-grains and B-grain can have the normal thermo-remanent magnetization.

Thus it seems likely that the self-reversal of thermo-remanent magnetism of the Haruna rock is due to the mechanism proposed by Néel [3]; *i.e.* during a process of cooling in a weak magnetic field, the magnetic domains of the B-constituent are fixed in the direction of the strong demagnetizing field owing to the A-constituent magnetization which is parallel to the applied field, the intensities of both of the fixed A and B domains increasing with decrease in temperature; the direction of the resultant magnetization of the sum of these two kinds of magnetization becomes opposite to that of the applied magnetic field below a certain temperature, since the rate of increase in the spontaneous magnetization with decrease in temperature is much larger for the B-constituent than for the A-constituent. Each of the above processes was experimentally verified for the case of the Haruna rock. We may therefore say that the Néel's two-constituent hypothesis is valid for the reversed remanent magnetization of this rock.

On the other hand, a large number of reversely magnetized igneous rock-bodies have been found hitherto at various localities over the world, and characteristics of thermo-remanent magnetism of some of these rocks were examined. For example, many samples of reversely magnetized rocks in Auvergne of France were examined by Roche, [4, 5], and his result shows that the thermo-remanent magnetization of these rocks is normal, *i.e.* its direction is in agreement with that of the applied magnetic field. Similar studies were carried out by Hospers [6] for the basaltic lavas of Iceland which are reversely magnetized [7], and also by Vincenz [8] for the reversely magnetized dykes in England and Scotland.

All of their results show that the thermo-remanent magnetism of these rocks is normal. We have also continued to examine the thermo-magnetic properties of reversely magnetized rocks in Japan, but we have been able to find out only two examples of igneous rocks having the self-reversal properties of thermo-remanent magnetism.

The above facts would suggest that the typical self-reversal of thermo-remanent magnetism, which is reproducible in laboratory experiments, may be not common property of the reversely magnetized rocks. This was pointed out also by a number of scientists at the joint meeting of Royal Astronomical Society and the Geological

Society for the geophysical discussion on the magnetization of rocks [9].

Under such a circumstance, main problems in the study of the reversed thermo-remanent magnetism of rocks will be as follows: What parts of a large number of reversely magnetized rocks *in situ* have the capability of the self-reversal of thermo-remanet magnetism: What are the exact conditions for the capability of the self-reversal in the physical, chemical and mineralogical properties of the ferromagnetic minerals in rocks.

It will be quite reasonable to assume that various properties of many igneous rocks at present may have been appreciably changed from the corresponding original properties which these rocks had when they were produced in old geologic times. In other words, the thermo-magnetic properties of rocks at present might be appreciably different from those of the same rocks at their original fresh stage. As pointed out by Graham [10], the magnetic properties of rocks are not always reproducible, even in the sense of rough approximation; that is, the magnetic properties of some rocks are so changed by heating only once up to a certain temperature that the reproduction experiment of their thermo-remanent magnetism is hardly possible. This fact has long been noticed since it was found that the change in magnetization in some rocks is irreversible with respect to temperature [11, 12].

These facts may indicate that knowledge of the exact requirements for the capability of the self-reversal of thermo-remanent magnetism as well as the physical nature of general thermo-remanent magnetism itself will be able to lead us to the reliable conclusion about the cause of reversed magnetization of igneous rocks *in situ*.

In this report, therefore, the result of experimental studies carried out as in detail as possible along the above-mentioned line will be summarized.

§ 2. Properties of Thermo-Remanent Magnetism of Dacitic Pitchstone of Mt. Asio

It has already been reported [1, 2] that, among a large number of the rock samples examined so far in our laboratory, the dacitic pumice of Mt. Haruna shows the typical capability of self-reversal of thermo-remanent magnetism. Similar studies have been extended in order to find other examples of the rocks having the same characteristic.

What we have found so far is only one example of the dacitic pitchstone of Mt. Asio in Japan. The total thermo-remanent magnetization of this rock is by no means the reversed one, but a certain part of its partial thermo-remanent magnetism has the property of the self-reversal just similar to that of the Haruna rock.

Fig. 1 illustrates the partial thermo-remanent magnetism (P.T.R.M.) of the ferromagnetic minerals separated out from the Asio dacitic pitchstone, where the temperature range ΔT is kept 100°C. As clearly seen in this figure, P.T.R.M. produced by cooling from 300°C to 200°C in a magnetic field H, $J^{200}_{300,H}$, is reversed. The dependency of this $J^{200}_{300,H}$ upon H is illustrated in Fig. 2, where it is noticed that P.T.R.M. is reversed provided that H is less than the critical value 3.5 *Oe.*, while it becomes normal if H exceeds this critical value. The general tendency of the curve $J^{200}_{300,H}-H$ of the Asio rock is similar to that of the Haruna rock described in the

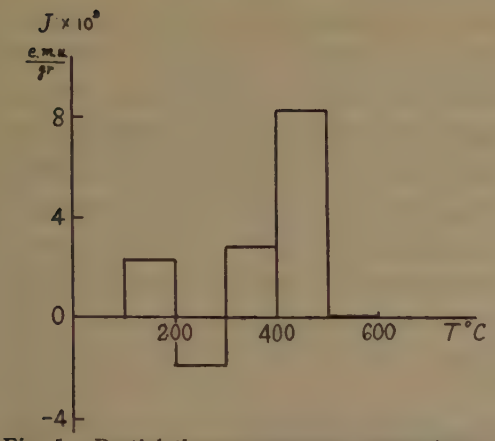

Fig. 1. Partial thermo-remanent magnetism of the ferromagnetic minerals in the Asio rock. (H=2.03*Oe.*)

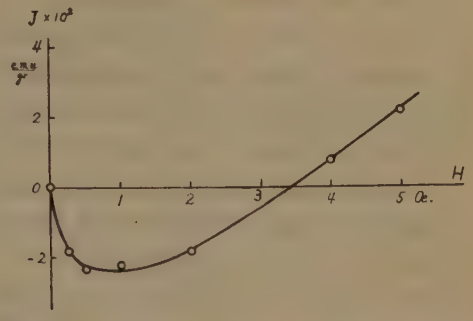

Fig. 2. Dependency of the partial thermo-remanent magnetization, $J^{200}_{300,H}$ upon the external magnetic force, H.

first report [1], except the critical value of H which is about 7.0 *Oe.* in the latter.

In both the Haruna and the Asio rocks, the thermo-remanent magnetism of their ferromagnetic minerals is composed of the normal P.T.R.Ms. for the high (>400°C) and low (<200°C) temperatures and the reverse P.T.R.M. for the intermediate temperatures, the reversed component of the thermo-remanent magnetism taking place mainly during the temperature range from 300°C to 200°C. The remarkable discrepancy of the Asio sample from the Haruna sample is the magnitude of the reverse P.T.R.M.; *i.e.* in the former, the reverse P.T.R.M. is so small in comparison with the normal P.T.R.M., that the total thermo-remanent magnetism is normal.

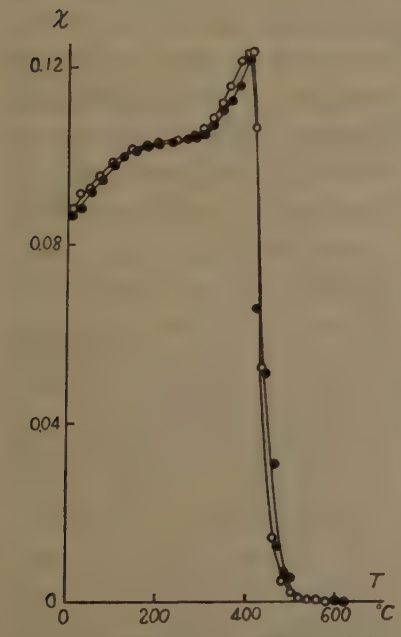

Fig. 3. Specific susceptibility of the ferromagnetic minerals in the Asio rock. (H=1.35*Oe.*)

Thus, it seems likely that the fundamental properties of thermo-remanent magnetism of the ferromagnetic minerals of the Asio rock are mostly similar to those of the Haruna samples; the degree of the self-reversal is weakened in the former.

Fig. 3 shows the change in specific magnetic susceptibility with temperature of the Asio sample. This $\chi-T$ curve, forming the stepwise change, resembles that of the Haruna sample. In both cases, the $\chi-T$ curves have two Curie-points, *i.e.* at about 540°C and about 280°C. This fact may also suggest that the ferromagnetic mineals of the Asio rock have the constitution nearly similar to that of the Haruna ferromagnetic minerals.

§ 3. Thermo-Magnetic Separation of Ferromagnetic Minerals

It was decribed in the second report [2] that the preliminary trial to classify the ferromagnetic

minerals with respect to their Curie-points was fairly successful. The experimental procedure to separate ferromagnetic and non-ferromagnetic minerals at various temperatures will be called the thermo-magnetic separation. If the group of the ferromagnetic grains in a rock-sample is composed of various kinds of grains having different Curie-points, (Θ), we could find the spectrum $f(\Theta)$ of this group of grains with respect to their Curie-points with the aid of the thermo-magnetic separation.

Let us assume that a grain is sufficiently ferromagnetic below Θ and completely non-magnetic above Θ. Then the mass of ferromagnetic minerals which are non-magnetic at T_j and ferromagnetic at T_i ($\Delta T = T_j - T_i > 0$), is given by

$$M\int_{T_i}^{T_j} f(\Theta)\,d\Theta, \qquad (1)$$

where M denotes the total mass of the whole ensemble of grains. If $\Delta T = T_j - T_i$ is made sufficiently small, we can put that the mean value of $f(\Theta)$ for the range of ΔT is nearly equal to $f(\Theta)$ at $\Theta = (T_j + T_i)/2$.

In the practical experiment, all ferromagnetic grains at a temperature T are separated out, and then the temperature is decreased to $T - \Delta T$, at which the same procedure of separating out the ferromagnetic grains is carried out. Repeating the same procedure at successively lower temperatures, we can get $M\int_{T}^{\infty} f(\Theta d\Theta,)$ $M\int_{T-\Delta T}^{T} f(\Theta)d\Theta$, $M\int_{T-2\Delta T}^{T-\Delta T} f(\Theta)\,d\Theta$,.....

If we take $T = 600°C$, $\int_{T}^{\infty} f(\Theta)\,d\Theta$ is practically zero in most cases. This may indicate that the most igneous rocks contain magnetite and the other ferromagnetic minerals having the Curie-point less than that of magnetite.

The principal parts of a thermo-magnetic separator are schematically shown in Fig. 4. As shown in this figure, the separation of ferromagnetic minerals is done in a N_2-gas electric furnace in order to avoid the oxidation of samples. The grains to be separated are spread over in the form of single layer on a brass plate (B.P.); the laterally movable electro-magnet (E.M.) sweeps over the plate and pulls up the ferromagnetic grains at T; the pulled up grains fall down into the trap by cutting off the electric current through the magnet; this process is repeated until no grain is pulled up by the magnet at the fixed temperature T.

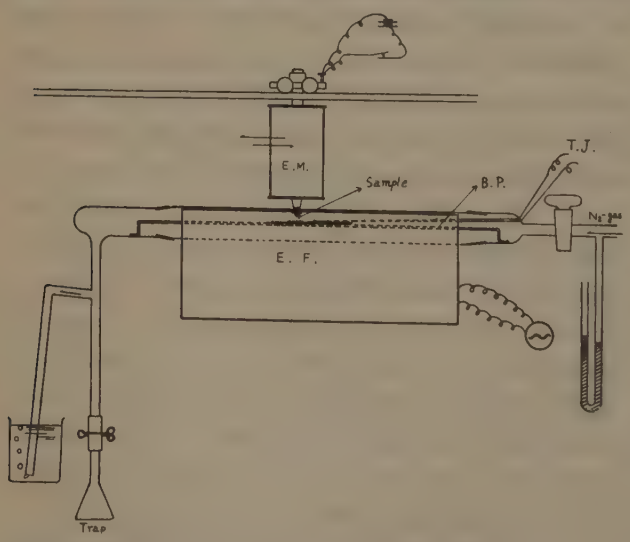

Fig. 4. Schematic view of thermo-magnetic separator.
B.P..... brass plate
E.M.....electro-magnet
E.F..... electric furnace
T.J..... thermo-junction

The temperature of the

specimens is kept uniform within the error of 5°. However, the magnetic separation by means of the above method is subject to the uncertainty due to the intensity of magnetization and mass of the grains to be separated out. Let mass and the specific intensity of magnetization of a grain at temperature T under the magnetic force H of the magnet be denoted by m and $J(H, T)$. Then, the necessary condition for pulling up the grain by the magnet is

$$mJ(H, T)\frac{\partial H}{\partial z} \geqq mg, \tag{2}$$

where $\partial H/\partial z$ is the vertical gradient of magnetic force H on the plate on which the grain lies. If we put,

$$g/\frac{\partial H}{\partial z} = C, \tag{3}$$

the critical condition for (2) is written as

$$J(H, T_C) = C, \tag{4}$$

where T_C denotes the critical temperature for the magnetic separation. Since $H=$ 1600 *Oe.* in the actual equipment. $J(H, T_C)$ may be nearly equal to the saturation magnetization $J_s(T_C)$ of the same sample at T_C. Hence (4) can be written as

$$J_s(T_C) = C. \tag{4'}$$

The magnitude of C defined by (3) is an instrumental constant, and it may rule the resolving power of the equipment for the thermo-magnetic spectrum $f(\Theta)$. By using the small grains of pure nickel, the constant C was calibrated to be about 2.1 in the writers' equipment. This means that the critical temperature T_C of the magnetic separation is more or less lower than the Curie-point, since a grain is pulled up by the magnet only when its magnetization exceeds 2.1 e.m.u. per gram.

Provided that $dJ(T)/dT$ near the Curie-point is sufficiently large, the difference $\Delta\Theta$ between Θ and T_C is approximately given by

$$\Delta\Theta = \Theta - T_C = -C/\left(\frac{\partial J_s}{\partial T}\right)_{T=\Theta}. \tag{5}$$

For the case of pure nickel grains $\Delta\Theta$ is about 4°. Since $(\partial J_s/\partial T)_{T=\Theta}$ of most ferromagnetic minerals in rocks is of nearly the same order as that of nickel, $\Delta\Theta$ for them will be generally less than 5° degrees. It must be noticed however that T_C becomes appreciably different from Θ for such specimens as hematite whose J_s and $|\partial J_s/\partial T|$ are very small.

Figs. 5 and 6 illustrate the thermo-magnetic spectra of the ferromagnetic minerals of the Haruna and the Asio rocks respectively. In these diagrams, the area of each rectangle represents $M\int_{T_i}^{T_j} f(T_C)\,dT_c = Mf(T_C)\Delta T$, where $\Delta T = T_j - T_i$ is not always constant in Fig. 6. In both spectra, there is a sharp increase of $f(T_C)$ at about $T_C = 450$°C, and another small peak is seen at about 230°C. Hence we may conclude that the ferromagnetic minerals in the Haruna and the Asio rocks are

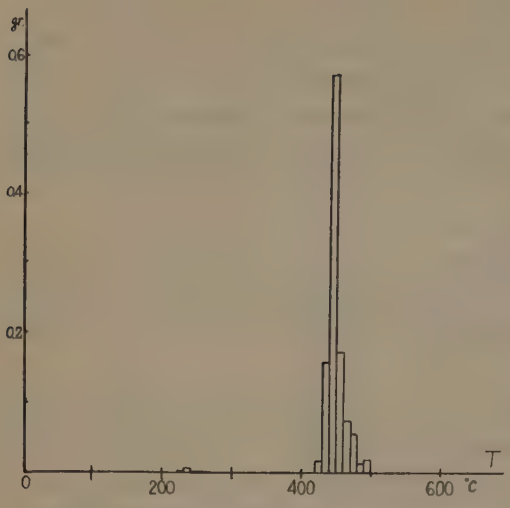

Fig. 5. Spectrum $Mf(T_c)$ of thermo-magnetic separation temperature of ferromagnetic minerals of the Haruna rock. Total mass $M=1.015$ g.

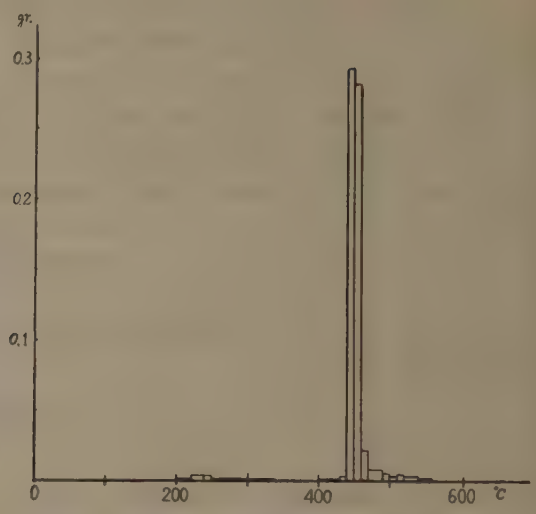

Fig. 6. Spectrum $Mf(T_c)$ of thermo-magnetic separation temperature of ferromagnetic minerals of the Asio rock. Total mass $M=0.787$ g.

classified either to the group having Curie-point around 450°C or to the group of Curie-point of about 230°C. The former will be tentatively called the A-constituent group and the latter the B-constituent group.

Strictly speaking, however, there may arise a question whether T_C really represents an approximate value of Θ, if some non-magnetic substances are contained in the grain of ferromagnetics.

Let the mass of non-magnetic substance at temperature T be denoted by m_B. Then the necessary condition for pulling up a grain composed of m_B of non-magnetic substance and m_A of magnetic one whose magnetization is $J_A(T)$ at T is given by

$$m_A J_A(T)\frac{\partial H}{\partial z}-(m_A+m_B)g\geqq 0\,. \tag{6}$$

Putting $m_B/m_A=x$, we get from (3), (4) and (6) that

$$J_A(T_c)=(1+x)C. \tag{7}$$

This indicates that T_c is lowered by x. If x is not large, $\Delta\Theta=\Theta-T_c$ for this case is approximately expressed by

$$\Delta\Theta=-(1+x)C/\left(\frac{\partial J_A}{\partial T}\right)_{T=\Theta}. \tag{8}$$

Since it is practically difficult to separate exactly the ferromagnetic minerals alone from their mother rock, the above mentioned effect may probably take place in the results illustrated in Figs. 5 and 6. In other words, it may be ambiguous whether the spread of the spectral lines in those T_C diagrams represents the real spread of the Curie-points or the spread of $\Delta\Theta$ owing to various different amounts of x for different grains.

§ 4. Change with Temperature of Magnetization of A, B, and AB-Grains

The magnetization of each single ferromagnetic grain, which was separated out by the thermo-magnetic separation method, was measured in a fairly strong magnetic field at continual temperatures from 20°C to 600°C by a magnetic balance [13].

The magnetic field for measuring the magnetization was about 2400 *Oe.* According to the measurement of the magnetization curve of these specimens, the intensity of magnetization observed in $H=2400$ *Oe.* is not much less than that of the saturation magnetization.

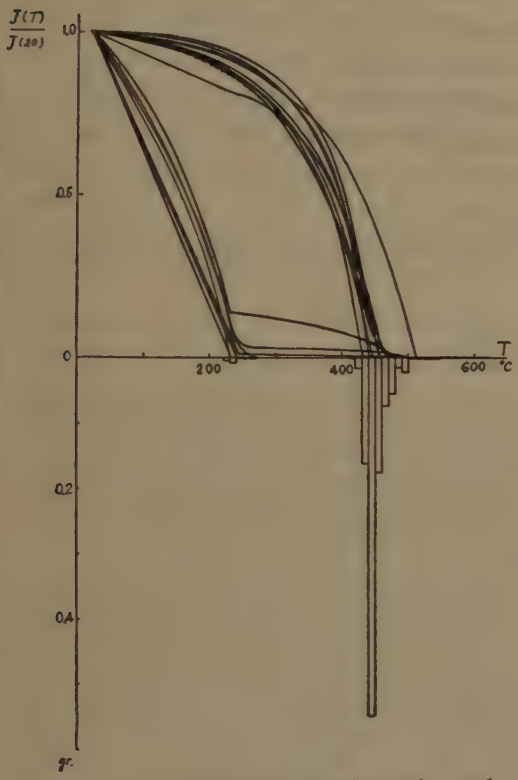

Fig. 7. $J(T)$-T curve of single grain and thermo-magnetic separation spectrum of the Haruna rock.

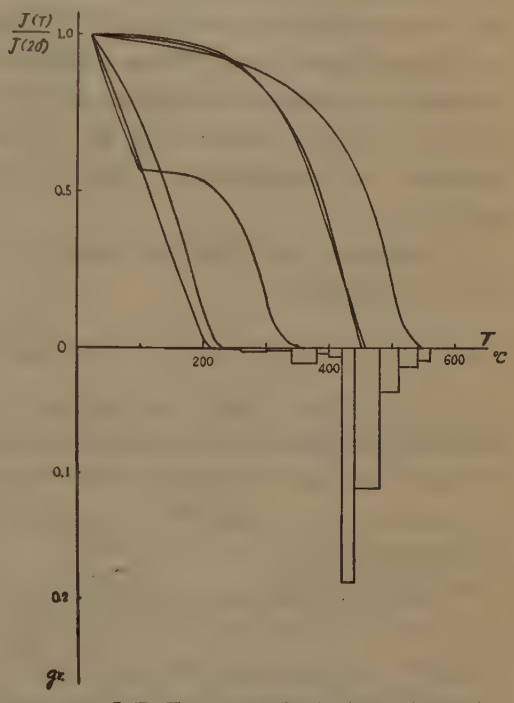

Fig. 8. $J(T)$-T curve of single grain and thermo-magnetic separation spectrum of the Asio rock.

The dependency of the nearly saturated magnetization ($J(T)$) upon temperature for single grains having various values of magnetic separation temperature (T_C) of the Haruna and the Asio rocks are illustrated in Figs. 7 and 8 respectively, where the abscissa represents the ratio of the intensity of magnetization $J(T)$ of a single grain at T to that of the same grain at 20°C. Throughout results obtained, the curves $J(T)$-T are reversible with respect to temperature; *i.e.* the $J(T)$-T curve in the cooling process is practically coincident with that in the heating process.

As clearly seen in Fig. 7, the $J(T)$-T curves in one group have their Curie-point at temperatures from 430°C to 510°C, taking the forms of the Curie curves. The $J(T)$-T curves of another group have the Curie-point at about 230°C, their form

being almost a straight line representing a linear relation between $J(T)$ and T. Generally speaking, the former group of $J(T)$-T curves corresponds to the A-constituent group defined in the preceding section, and the latter group to the B-constituent group. The specific intensity of magnetization of the A-constituent at 0°C is about 80 *e.m.u.*, while that of the B-constituent is about 20 *e.m.u.*. These values do not differ much from their respective saturation values.

There are also several cases that the $J(T)$-T curve seems to consist of the straight line in the temperature range below 230°C and the Curie curve for the temperatures above 230°C. There will be no room for doubt that the grains having the above properties of their $J(T)$-T curves consist of the A-constituent phase and the B-constituent phase. These grains which are composed of both the A- and B-phases will be called the AB-grains. The general tendency of the $J(T)$-T curve of the Asio grains illustrated in Fig. 8 is almost the same as that of the Haruna samples; *i.e.* these grains may also be devided into the three main classes: A, B, and AB.

It seems likely that the magnetization J_{AB} of the AB-grain in a strong magnetic field is expressed as

$$J_{AB}=\frac{m_A}{m}J_A+\frac{m_B}{m}J_B, \tag{9}$$

were $m=m_A+m_B$. Then, judging from the $J(T)$-T curves of the AB-grains, we may say that the ratio m_B/m_A can take various values from zero to infinity in both the Haruna and the Asio rocks. For example, with the aid of (9), the ratio m_B/m_A is estimated to be about 0.7, 31 and 235 for the three typical curves of the AB type illustrated in Fig. 7.

However there is practically a limit for the value of the ratio which could be detected by measuring the $J(T)$-T curve. The detectable value of m_B/m_A in the authors' equipment is in the range from about 0.5 to about 300. That is to say, a very small content of the A-constituent within the AB-grain can rather easily be detected, but the B-constituent in an AB-grain can be detected only if its content exceeds a half of the whole grain.

It will be concluded from the diagram in Fig. 7 that the Curie-point Θ of the A-constituent spreads over the temperature range from 430°C to 510°C and that of the B-constituent over the range from 230°C to 240°C. This spread of the Curie-point may indicate that neither the A- nor the B-constituent group is composed of ferromagnetic grains having a common constant structure, but each of them has a finite width spectrum with respect to the Curie-point. Let us now compare these groups of $J(T)$-T curves with the result of the thermo-magnetic separations of the same samples. The lower half in Figs. 7 and 8 represents the frequency distribution $f(T_C)$ of the Haruna and the Asio grains respectively with respect to their temperature T_C of the thermo-magnetic separation. Then it may be said that the spectrum $f(T_C)$ can approximately represent the spectrum of Curie-point $f(\Theta)$ except for the case of the AB- grains.

Since $J_B(T)$ is practically zero when T exceeds Θ_B, the discussions summarized by (6), (7) and (8) can be applied to the case of the AB-grains provided that $T>\Theta_B$. Therefore, when m_B/m_A in the AB-grains is larger, T_C for these grains will be the more lowered from Θ_A. When T_C becomes less than Θ_B, the critical condition for the thermo-magnetic separation must be given by

$$J_{AB}(T_C)=\frac{m_A}{m}J_A(T_C)+\frac{m_B}{m}J_B(T_C)=C \qquad (10)$$

For example, the grain of $\Theta_A=470°C$, $\Theta_B=220°C$ and $m_B/m_A=0.7$, which is shown in Fig. 7, was separated out by the thermo-magnetic separator in the temperature range of 450°C–460°C. That the AB-grains are the aggregates of the A-constituent and the B-constituent was more directly proved as follows. The group of ferromagnetic minerals of $440°C<T_C<450°C$ was separated out by the thermo-magnetic separator from the Haruna rock; the grain-size is on average about $0.3mm$ in diameter: then this group of grains was pulvurized into the small grains of $3\sim5\,\mu$ in the mean diameter; these small grains were again thermo-magnetically separated. The result showed that these small grains could be divided into the three groups: *i.e.* 75.5% for $500°C<T_C<525°C$, 13.8% for $200°C<T<250°C$, and the remaining 8.6% for non-magnetic minerals. The first and the second groups correspond to the A- and the B-constituents respectively. Thus, it will be clear that any ferromagnetic grain in the Haruna and the Asio rocks is composed of the A- and the B-constituents, which are distinctly separated out from each other in regard to their Curie-point. The above argument includes the special case that a grain consists of the A- or the B-constituent alone.

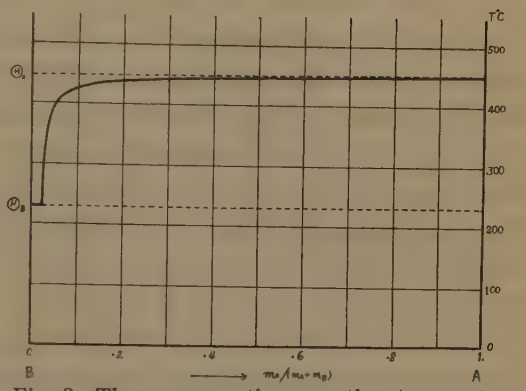

Fig. 9. Thermo-magnetic separation temperature (represented by a full thick line) with the ratio of the content of A- and B-phases.

It seems difficult to define uniquely the A- and the B-constituents, since the both constituents may have a finite range of their Curie-point. But the conception of the presence of the two constituents, A and B, in the ferromagnetic minerals of the Haruna and the Asio rocks will be acceptable.

§ 5. Thermo-Remanent Magnetization of Single Grains

The total thermo-remanent magnetization (TRM) of each single grain produced by cooling from 600°C in the geomagnetic field was measured by an astatic magnetometer. The purpose of this experiment is to look for the source of the reverse thermo-remanent magnetization of the Haruna and the Asio rocks. This experiment was first done for 16 Haruna grains whose $J(T)$-T curves were obtained.

Each grain of the A-constituent having the Curie-point at 430°–510°C has weak normal TRM and also each single grain of the B-constituent having the Curie-point at 230°–240°C has weak normal TRM. The AB-grains which consist, as proved in their $J(T)$-T curves, of both the A- and the B-constituents have generally a strong reverse TRM. Some grains which have the Curie-point at 230°–250°C and so look like the B-constituent grains could have also a fairly strong reverse TRM. It seems likely therefore that these B-like-grains contain a small amount of the A-constituent which has effective influence upon the fixing of the magnetization of B-constituent, and so these will be called the aB grains.

Thus it may be said that the ferromagnetic mineral which contains both the A- and the B-constituents within each single grain is mainly responsible for the reverse TRM. This result will indicate positive evidence of the two-constituent theory proposed by Néel [3] and a little modified by the authors [1].

In order to confirm the above argument, it will be desirable to carry out the similar examination of a large number of ferromagnetic grains in the Haruna and the Asio rocks. Since the exact measurement of the $J(T)$-T curves of many grains are too laborious, it was assumed that the procedure of thermo-magnetic separation is able to indentify approximately the A-, the B- and the AB-grains. As illustrated in Figs. 5 and 6, the $f(T_C)$ spectrum can be divided into two main classes; the group A at temperature higher than 400°C consists of the A-constituent and the AB-constituent of $m_B/m_A<20$, the latter being denoted here by Ab; the group B at temperature lower than 230°C consists of the B-constituent and the AB-constituent of $m_B/m_A>30$, the latter being denoted by aB. The grains having T_C at temperaturs between 230°C and 400°C will be denoted by ab, in which $30>m_B/m_A>20$, as estimated in the diagram shown in Fig. 9.

There is no ab grain in the Haruna rock, as shown in Fig. 5. The grains of the group A have either the normal TRM of weak intensity or the reverse TRM of moderate or weak intensity; the first and the second cases may correspond practically to the A grain and the Ab grain respectively, where the AB grains containing rather small amount of the B-constituent will be practically considered to belong to the A-grains. The grains of the group B have either the normal TRM of weak intensity or the reverse TRM of strong intensity; the first may correspond to the B-grain and the latter to the aB grain. Among 89 grains of the group A, 67 are of the A type and 22 are of the Ab type; and among 17 grains of the group B there are 15 of the aB type and 2 of the B type.

A similar examination was done for the Asio grains; 9 among 10 grains of the group A are of the A type, the remaining one having the type of Ab, while 3 of 5 grains of the group B is of the aB type and the remaining two are of the B type.

It may therefore be concluded that each single grain of the AB-constituent can generally have the reverse TRM, and that the thermo-remanent magnetization of a rock sample as a whole can be reverse when the sum of the reverse magnetization of these grains exceeds that of the normal magnetization of the other grains.

§ 6. Chemical Composition and Crystallographic Structure of A- and B-Grains

Our problem will now be concerned with what minerals are the A- and the B-constituents in the Haruna and the Asio rocks. The result of chemical analysis of the A- and the B-constituents of the Haruna sample, made by courtesy of J. Ossaka, is given in Table I, and they are represented by the points A and B on the diagram of the ternary system of FeO-Fe_2O_3-TiO_2 in Mol percentage shown in Fig. 10. In this diagram, the points Fe_2O_3, $TiFeO_3$ and Fe_3O_4 represent respectively hematite, ilmenite, and magnetite, and the line connecting Fe_3O_4 and $TiFe_2O_4$ represents the complete solid solution between Fe_3O_4 and $TiFe_2O_4$, being usually called the titanomagnetite. According to Pouillard [14], the solid solution of hematite and ilmenite is possible only in the two limited ranges of $Fe_2O_3 : TiFeO_3$, which are represented by two limited lines in Fig. 10.

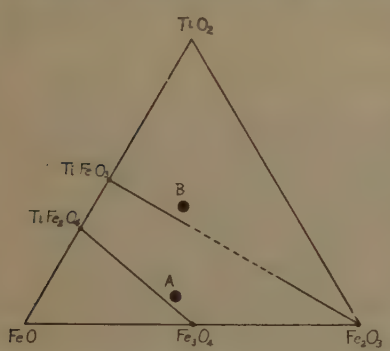

Fig. 10. Chemical composition of A- and B-constituents in the Haruna rock, represented on a FeO-Fe_2O_3-TiO_2 diagram in Mol. percentage.

Then it will be obvious in Fig. 10 that the chemical composition of the A-constituent is nearly a titanomagnetite, which is not much different from the pure magnetite, and that the chemical composition of the B-constituent is nearly that of a solid solution of $TiFeO_3$ with Fe_2O_3; *i.e.* an ilmenite-rich ilmenite-hematite solid-solution.

In the last column of Table I, the chemical composition of the whole ferromagnetic minerals of the Haruna rock is given for comparison. Comparing this chemical conposition with that of the A- and the B-constituents, we may say that the largest parts of the Haruna ferromagnetic minerals are the A-constituent, the ratio of content of B to that of A being of the order of 1/100. This is in good agreement with the result of the thermo-magnetic separation dealt with in § 4.

Table I. Chemical Composition of "A" and "B" Constituents of the Ferromagnetic Minerals of the Haruna Rock.
(By J. Ossaka and T. Katura)

	A		B		Total	
	Weight %	Mol %	Weight %	Mol %	Weight %	Mol %
Fe_2O_3	58.7	39.4	43.5	26.9	57.9	38.7
FeO	34.2	51.1	24.2	33.2	34.7	51.5
TiO_2	7.0	9.4	32.3	39.9	7.4	9.8

For the purpose of determining the crystal structure of these A- and B-constituents, their X-ray analysis was carried out with the aid of a "NORELCO" X-ray spectrometer. Examples of the X-ray spectrograms of the A-, the B- and the AB- grains of the Haruna rock are illustrated in Fig. 11. Here the grains of $Tc > 500°C$, those of $Tc < 250°C$, and those of $250°C < Tc < 400°C$ were assumed to represent the A-, the B-, and the AB-grains respectively.

It was found that the A-constituent has the cubic crystal structure of inverse spinel type which is the same as that of magnetite, while the B-constituent has a rhombohedral crystal structure, *i.e.* the same structure as that of hematite and ilmenite. The crystal structure and the lattice parameters of the A-, the B-, and the AB- constituents of both the Haruna and the Asio rocks are summarized in Table II, where those of almost pure magnetite and ilmenite, observed with the same apparatus, are also given for comparison.

It will be evident that the A-constituent chiefly consist of a magnetite-rich titanomagnetite, since the lattice constant of the first is nearly the same as that of the second. This is in good agreement with the results of both chemical analysis and the thermo-magnetic separation.

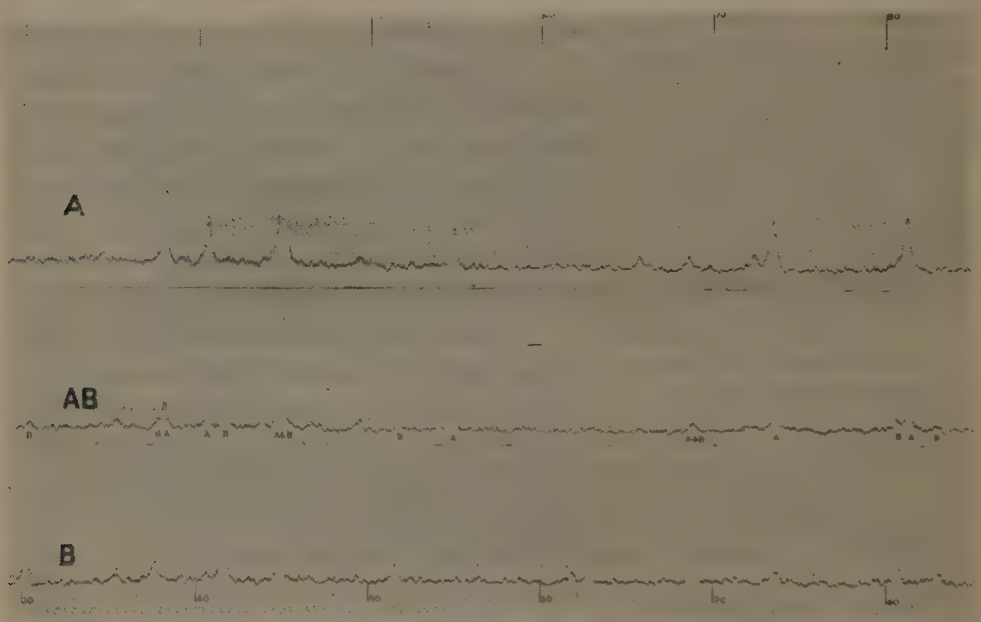

Fig. 11. Examples of X-ray spectrogram of A-, AB-, and B- constituents by "Norelco" with Fe K radiation.

Table II. Crystal Structure and Lattice Parameters of A, B, and AB Constituents of the Haruna and the Asio Rocks.

Source	Grain	Crystal Structure	Lattice Parameters
Haruna	A	Cubic (Inverse spinel)	$a_c = 8.403 \pm 0.002$ Å
	B	Rhombohedral	$a_{rh} = 5.480 \pm 0.002$ Å, $\alpha_{rh} = 55°08' \pm 01'$
	AB	Cubic + Rhombohedral	$a_c = 8.401 \pm 0.001$ Å, $a_{rh} = 5.473 \pm 0.008$ Å, $\alpha_{rh} = 55°08' \pm 05'$
Asio	A	Cubic (Inverse spinel)	$a_c = 8.397 \pm 0.004$ Å
	B	Rhombohedral	$a_{rh} = 5.483 \pm 0.004$ Å, $\alpha_{rh} = 55°01' \pm 03'$
	AB	Cubic + Trace of Rhombohedral	$a_c = 8.405 \pm 0.003$ Å

Magnetite	Cubic (Inverse spinel)	$a_c = 8.397 \pm 0.003$ Å
Ilmenite	Rhombohedral	$\begin{cases} a_{rh} = 5.540 \pm 0.002 \text{ Å} \\ \alpha_{rh} = 54°44' \pm 02' \end{cases}$

The crystal structure of the B-constituent is rhombohedral, but its lattice parameters are appreciably different from those of pure ilmenite; that is, they are shifted towards those of hematite. Taking the chemical composition into consideration, we may conclude therefore that the B-constituent is chiefly composed of a solid-solution of ilmenite with hematite.

It will be seen in Fig. 11 and Table II that the X-ray spectrogram of the AB-grains is composed of both the cubic structure lines of the A-constituent and the rhombohedral structure lines of the B-constituent. This result indicates that the AB-grains are mixtures of the A- and the B-grains.

It may be safely said therefore that all of thermo-magnetic, chemical, and crystallographic analyses of the structure of the A-, B-, and AB-constituents have shown the consistent result.

§ 7. The Ferromagnetic Mineral of B-Constituent

It has already been shown in the previous papers [1, 2] that the reverse TRM of the Haruna rock at the atmospheric temperature is caused by the marked increase of the reverse magnetization with decrease in temperature of the B-constituent, which overcomes the normal magnetization of the A-constituent. It has further been found in the present study that this B-constituent is a kind of the ilmenite-hematite solid-solution.

On the other hand, it has been believed that both hematite and ilmenite are by no means the ferromagnetic minerals, and it was proved [15] that at least hematite has the antiferromagnetic arrangement of the spins within the crystal. Then we may presume that a particular solid-solution of these two non-ferromagnetic minerals, ilmenite and hematite, might be able to have such a strong ferromagnetic property as that of the B-constituent. Hence the magnetic properties of the B-constituent may deserve some detailed investigation.

As already shown in Figs. 7 and 8, the Curie-point of the B-constituent is about 230°C and its saturation magnetization at 0°C was determined to be about 20 *emu/gr.* This saturation magnetization of this B-constituent changes almost linearly with temperature between the Curie-point and 0°C. The measurement of the magnetization was extended down to the temperature of the boiling liquid air (about −180°C), the result showing that its linear relation with temperature holds almost perfectly between 230°C and −180°C.

By courtesy of Néel and Pauthenet, the saturation magnetization (J_s) of the B-constituent in the Haruna rock was measured by them for a wide range of temperature from the Curie-point to the temperature of the liquid helium. Their result is

reproduced in Fig. 12. As clearly seen in this diagram, the saturation magnetization J_s increases linearly with decrease in temperature down to about $70°K$, becoming about 54 *e.m.u./gr.* at $0°K$. This intensity of J_s at $0°K$ is more than a half that of magnetite at the same temperature. The above mentioned linear change of J_s with temperature may suggest that the B-constituent is a kind of the ferrimagnetic material.

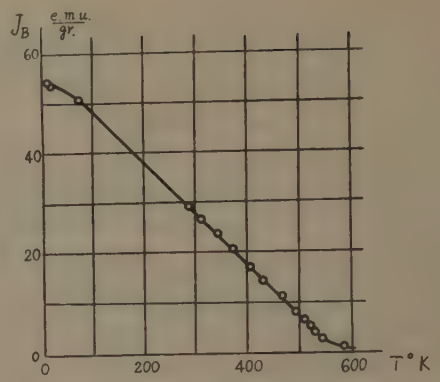

Fig. 12. Saturation magnetization I_B of the B-constituent of the Haruna rock, $H=19{,}500$ *Oe.* (After Néel and Pauthenet)

On the other hand, the fact that hematite has usually feeble ferromagnetic properties has often been reported [16], and Néel [17] attempted with a successful result to explain the origin of this feeble ferromagnetism by assuming the presence of some deviation of the arrangement of spins from their perfect antiferromagnetic order. It might therefore be possible to assume that the fairly strong ferromagnetic property of the B-constituent is due to a kind of ferrimagnetism caused by a certain disturbance in the antiferromagnetic arrangement of spins in the ilmenite-hematite crystal. If so, it seems likely that this ferrimagnetism is due to the substitution

$$2\,Fe^{+++} \rightleftarrows Fe^{++} + Ti^{++++},$$

where Fe^{+++} and Fe^{++} have the magnetic moment of 5 and 4 in Bohr magneton number while Ti^{++++} has no magnetic moment.

In the case of the B-constituent, its chemical composition can be expressed approximately by $Ti_{\frac{2}{3}}Fe_{\frac{4}{3}}O_3$ and the intensity of its saturation magnetization is represented by about 5/3 Bohr magnetons per Mol. Then taking into consideration the condition that ilmenite and hematite may have the perfect antiferromagnetic arrangements such as $(Ti_{\frac{1}{2}}{}^{++++}\ Fe_{\frac{1}{2}}{}^{++})\ (Ti_{\frac{1}{2}}{}^{++++}\ Fe_{\frac{1}{2}}{}^{++})\ O_3{}^{--}$ and $(Fe^{+++})\ (Fe^{+++})\ O_3{}^{--}$ respectively, we might be able to presume a suitable ferrimagnetic arrangement of Fe^{+++}, Fe^{++} and Ti^{++++} ions in the two sites of the crystal so that the arrangement fulfils the observed coditions for J_s and the chemical composition. The simple nearest arrangement will be $(Fe_{\frac{1}{6}}{}^{++}\ Fe_{\frac{2}{3}}{}^{+++}\ Ti_{\frac{1}{6}}{}^{++++})\ (Fe_{\frac{1}{2}}{}^{++}\ Ti_{\frac{1}{2}}{}^{++++})\ O_3{}^{--}$, which gives $Ti_{\frac{2}{3}}Fe_{\frac{4}{3}}O_3$, in chemical comsosition and 2 Bohr magnetons in spontaneous magnetization.

The above argument may still be somewhat ambiguous, since the accuracy of both the chemical composition and the spontaneous magnetization of the substance may be not sufficient enough. It will be desirable therefore to study systematically the magnetic properties of the $TiFeO_3$-Fe_2O_3 series.

§ 8. Conclusion and Unsolved Problems

A phenomenological mechanism of self-revercal of remanent magnetization of the AB-grains has already been proposed in the previous paper and summarized in § 1 of this article. In the present study, it has been confirmed that the A-constituent

is a titanomagnetite having the Curie-point at 430°C–510°C and the B-constituent is a ferrimagnetic solid solution of ilmenite and hematite, having a rhombohedral crystal structure and the Curie-point of about 230°C. The observed large value of the temperature coefficient of J_B below Θ_B in comparison with that of J_A seems to be sufficiently large to verify the two-constituent theory of reverse TRM.

However there still remains problem concerning detailed mechanism of the assumed magnetic coupling between the A- and the B-phases within each AB-grain. This is by no means self-evident. According to the result of microscopic observation of the surface of the AB-grains, the B-phase of ilmenite type of the form of a thin band sometimes intergrows within the A-phase. It seems that this behaviour of the B-phase is favourable to the assumption of strong anti-parallel coupling between J_A and J_B. From the geophysical stand point of view, it will be desirable to know how often the necessary condition for the anti-parallel coupling between J_A and J_B can takes place within the actual ferromagnetic minerals. In other words, the possibility of the said coupling will be a significant problem in relation to the generality of the phenomenon of self-reversal of thermo-remanent magnetization. It seems therefore that this problem well deserves the further detailed study.

Another important problem will be the degree of petrological commonness of the ilminite-like B-constituent in rocks. As clearly shown in this study, the amount of the B-costituent is only about one per cent of that of the A-constituent even in the Haruna rock which shows the remarkable reverse thermo-remanent magnetization. The presence of this particular ferrimagnetic phase in this rock had been overlooked even in the authors' own study of the general magnetic properties of rocks until its characteristics of themo-remanent magnetism were revealed.

On the other hand, the crystals of ilmenite, so-called in petrology, appear in almost all igneous rocks and further they are usually associated with magnetite crystals, as observed under a microscope. But very little work has been done with respect to the detailed magnetic properties of ilmenite in rocks. It might be possible therefore to assume that some ilmenites have the ferrimagnetic properties such as those of the B-constituent. If the remanent magnetization of this ilmenite-like ferrimagnetic phase is stabler than that of the ordinary titanomagnetite, we may expect that the former magnetization alone has survived at present after a long life of rocks since they were formed in geologic time. If further there was the strong anti-parallel coupling between the ilmenit-like ferrimagnetics and the titanomagnetites, we may find that the rocks show the reverse magnetization *in situ*, but we may not be able to reproduce the reverse magnetization by a simple laboratory experiment of thermo-remanent magnetism, except for the special case that J_B of the ilmenite-like ferrimagnetics is stronger than J_A of the titanomagnetites at the initial stage of the creation of thermo-remanent magnetization.

The above-mentioned is merely an example of hypothetical possibility, just for emphasizing a significance of presence of the ilmenite-like ferrimagnetics in rocks. This problem must be examined in detail in future.

Acknowledgment

The authors' work on rock-magnetism has been continuously supported and encouraged during the past seventeen years by Prof. M. Hasegawa of Kyoto University. At the occation of his sixtieth birthday anniversary, the authors wish to express their hearty thanks to him. The authors wish to mention their sincere thanks to Prof. L. Néel and Dr. M. Pauthenet for their kindness of measuring the magnetization of the B-constituent in low temperature, to Dr. H. Kuno for his continuous help and useful advice from the petrological side, to Mr. S. Iida for his advice from the side of the physics of solid matters, and to Mr. J. Ossaka for his chemical analysis of the Haruna samples.

The outline of the present work was discussed with Prof. P.M.S. Blackett, Dr. J.A. Clegg, Dr. M. Pickering, Dr. H. Manley and Dr. J. Hospers in England and with Prof. E. Thellier and Dr. J. Roquet in France. The authors' indebtness is also due to these scientists for their fruitful discussions and comments.

References

(1) T. Nagata, S. Uyeda and S. Akimoto; Journ. Geomag. Geoele., **4**, 22 (1952).
(2) T. Nagata, S. Uyeda and S. Akimoto; Journ. Geomag. Geoele., **4**, 102 (1952).
(3) L. Néel; Ann. de Géophys., **7**, 90 (1951).
(4) A. Roche; C.R. Acad. Sci., **233**, 1132 (1951).
(5) A. Roche; C.R. Acad. Sci., **236**, 107 (1953).
(6) Private communications from J. Hospers.
(7) J. Hospers; Nature, **168**, 1111 (1951).
(8) Private communication from S.A. Vincenz.
(9) Nature, **171**, 500 (1953).
(10) J.W. Graham; Journ. Geophys. Res., **58**, 243 (1953).
(11) R. Chevallier et J. Pierre; Ann. de Phys., (10) **18**, 383 (1932).
(12) T. Nagata; ROCK-MAGNETISM, pp. 39 and 109, Tokyo (1953).
(13) S. Akimoto; Journ. Geomag. Geoele., under press.
(14) E. Pouillard; Ann. de Chimie **5**, 164 (1950).
(15) C.G. Shull, W.A. Strauser and E.O. Wollan; Phys. Rev., **83**, 333 (1951).
(16) J. Roquet; C.R. Acad. Sci., **224**, 1418 (1947).
(17) L. Néel; Rev. Mod. Phys., **25**, 58 (1953).

昭和29年1月15日　印刷
昭和29年1月30日　發行
第5卷　第4號

編輯兼發行者　日本地球電氣磁氣學會
代表者　長谷川万吉

印刷者　京都市下京區上鳥羽學校前
田中幾治郎

賣捌所　丸善株式會社京都支店
丸善株式會社 東京・大阪・名古屋・仙台・福岡

JOURNAL OF GEOMAGNETISM AND GEOELECTRICITY

Vol. V No. 4

1953

CONTENTS

Ionospheric Variations Associated with Geomagnetic Disturbances

I. Variations at Moderate Latitudes and the Equatorial Zone, and the Current System for the S_D Field ..... S. MATSUSHITA 109

Latitude Effect of the Intensity Decrease in the Cosmic-Ray Storm.....

.....S. YOSHIDA and Y. KAMIYA 136

The World-Wide Variation of Cosmic Ray Intensity by the Electro-Magnetic Field. ..... K. NAGASHIMA 141

Self-Reversal of Thermo-Remanent Magnetism of Igneous Rocks (III).....

.....T. NAGATA, S. AKIMOTO and S. UYEDA 168